九州大学学術情報リポジトリ
Kyushu University Institutional Repository

Development of Hydrogel Films Consisting of Thermal Responsive Amine-Functionalized Microgel Particles and Linear Polymers as CO2 Absorbent in Wet Environment

岳, 梦晨

https://doi.org/10.15017/1543973

出版情報：九州大学, 2015, 博士（工学）, 課程博士
バージョン：
権利関係：全文ファイル公表済

Development of Hydrogel Films Consisting of Thermal Responsive Amine-Functionalized Microgel Particles and Linear Polymers as CO_2 Absorbent in Wet Environment

2015-09

Kyushu University,
Department of Chemical Engineering

Mengchen Yue

Supervisor: Yoshiko Miura, Yu Hoshino

Contents

Chapter 1. Introduction 1

1.1. Background of CO_2 capture and separation 3
1.1.1. Greenhouse effect 3
1.1.2. Industrial CO_2 capture technologies 7
1.1.3. CO_2 separation techniques 12
1.1.3.1. Absorption 14
1.1.3.2. Adsorption 19
1.1.3.3. Membrane separation 26
1.2. Temperature responsive hydrogel 31
1.2.1. Temperature responsive polymers and gels 31
1.2.2. pH responsibility of the thermal responsive polymers and hydrogels 35
1.2.3. Adjustment of the LCST of the thermal responsive polymers 36
1.2.3.1. Control LCST via copolymerization with other monomers 36
1.2.3.2. Control LCST via additional compounds 36
1.2.3.3. Influence of pressure on the LCST of thermal responsive polymers 39
1.2.4. Swelling kinetics of the thermal responsive hydrogel 41
1.2.5. Thermal responsive hydrogels with different structures 42
1.2.5.1. Microgel particles (GPs) 43
1.2.5.2. Macroporous gels 50
1.2.5.3. “plum-pudding” gel 56
1.2.5.4. Other structures of hydrogel 63
1.3. About this study 64
1.4. References 70

Chapter 2. Development of Temperature Responsive Microgel Particle Films as Reversible CO_2 Absorbents in Wet Environment 81

2.1 Introduction 83
2.2. Materials and experiments 86
2.2.1. Materials 86
2.2.2. Synthesis of 4-Acrylamidofluorescein Monomer (Fluorescein monomer) 87
2.2.3. Preparation of GPs 87
2.2.4. Preparation of GP Films 89
2.2.5. Preparation of Fluorescent-labeled GP30 Film (GP30F film) 90
2.2.6. Preparation of Monolithic Film (M30) 90

2.2.7. Preparation of Fluorescent-labeled Monolithic Film (M30F) 91
2.2.8. Quantification of hydrodynamic diameters 91
2.2.9. Quantification of amine content in GPs 92
2.2.10. Observation of surface structure of GP film and monolithic film by SEM... 92
2.2.11. Observation of inner structure of GP film and monolithic film by LSCSM . 92
2.2.12. Measurement of reversible CO_2 absorption/desorption of GP films and monolithic films 92
2.3. Results and Discussion 93
2.3.1. Structure of GP film and homogeneous monolith film 93
2.3.2. Effect of added water amount on the CO_2 capture capacity of the GP films . 95
2.3.3. Effect of film thickness on the CO_2 capture capacity 97
2.3.4. The reversibility of CO_2 capture by GP film and homogeneous monolith film 98
2.4. Conclusion 100
2.5. References 100

Chapter 3. Design Rationale of Thermally Responsive Microgel Particle Films That Reversibly Absorb Large Amounts of CO_2 and Maximization of CO_2 capture capacity 103

3.1. Introduction 105
3.2. Experiments 108
3.2.1 Materials 108
3.2.2 Preparation of GPs 109
3.2.3. Quantification of hydrodynamic diameter, VPTT, swelling ratio of GPs 112
3.2.4. Quantification of amine content in GPs. 112
3.2.5. Measurement of pK_a shift curve in heating process. 112
3.2.6. Preparation of GP films 113
3.2.7. Measurement of CO_2 absorption capacity of GP films 113
3.3. Results and Discussion 114
3.3.1. Effect of pK_a values of GPs on the reversible CO_2 capture stoichiometry of GP films. 114
3.3.2 Effect of ΔpK_a of GPs on the reversible CO_2 capture stoichiometry of GP films. 121
3.3.3. Effect of VPTT of GPs on the reversible CO_2 capture stoichiometry of GP films. 123
3.3.4. Effect of Size of GPs on the reversible CO_2 capture stoichiometry of GP films. 127

3.3.5. Effect of swelling ratio of GPs on the reversible CO_2 capture stoichiometry of GP films. 130
3.3.6. Rational design of GP film with large reversible CO_2 capture stoichiometry. 133
3.3.7. Maximization of reversible CO_2 capture capacity of GPs films. 135
3.3. Conclusion 137
3.4. References 138

Chapter 4. Effect of Hydrophobic Modification of Polyvinylamine Films on the CO_2 Capture and Release Behavior: Comparison between Copolymers and Polymer Blends 143

4.1. Introduction 145
4.2. Materials and experiments 148
4.2.1. Materials. 148
4.2.2. PVAm preparation 149
4.2.3. Hydrophobic modification of PVAm 150
4.2.4. ^{1}H NMR measurement 152
4.2.5. Quantification of LCST of the polymers 152
4.2.6. Polymer film preparation 153
4.2.7. Quantification of reversible CO_2 absorption/desorption of polymer films ... 153
4.3. Results and discussion 154
4.3.1. Preparation of the PVAm 154
4.3.2. Preparation and Modification of the PVAm 155
4.3.3. LCST of the hydrophobically modified PVAm 156
4.3.4. Effect of modification ratio on the reversible CO_2 capture stoichiometry of the polymer films 158
4.3.5. Effect of LCST on the reversible CO_2 capture stoichiometry of the polymer films 159
4.3.6. CO_2 capture stoichiometry of blended polymer films 164
4.4. Conclusions 166
4.5. References 167

Chapter 5. Effect of Film Inner Structure on the CO_2 Release and Capture Kinetics 171

5.1. Introduction 173
5.2. Materials and experiments 176

5.2.1. Materials 176
5.2.2. Preparation of GPs with different size 177
5.2.3. Preparation of fluorescent GPs 178
5.2.4. Preparation of GP films 178
5.2.5. Preparation of 2-layer GP films consisting D5-L-AFA0.01 and D5-L-MTRh0.01 179
5.2.6. Preparation of homogeneous monolith gel films 180
5.2.7. Preparation of plum-pudding gel films 181
5.2.8. Preparation of macroporous gel films 182
5.2.9. GP mobility in GP films observation by LSCM 183
5.2.10. CO_2 release/capture rate measurement 184
5.3. Results and discussion 184
5.3.1. Preparation of GPs with different size 184
5.3.2. Preparation of fluorescent GPs 185
5.3.3. Mobility of GPs in GP film after moisture absorption 186
5.3.4. Homogeneous gel and pudding gel film preparation 187
5.3.5. Effect of flow rate of 10% CO_2 gas and void volume of quantification system on CO_2 release/capture rate 188
5.3.6. Effect of inner structure of gels on the CO_2 release rate of the gel film 189
5.3.7. Effect of inner structure of gels on the CO_2 capture rate of the gel film 191
5.4. Conclusion 193
5.5. References 193

Chapter 6. Summary 195

Acknowledgement 201

Chapter 1. Introduction

1.1. Background of CO_2 capture and separation

1.1.1. Greenhouse effect

As it can be seen, the greenhouse gases emissions represent the biggest market failure. The greenhouse gases are the gases that capture and emit radiation with in the thermal infrared range. [1]

The Sun powers Earth's climate, radiating energy at very short wavelengths, predominately in the visible or near-visible (e.g., ultraviolet) part of the spectrum. About 1/3 of the solar energy that reaches the Earth's atmosphere is reflected directly back to space. The remaining 2/3 is absorbed by the surface.[1] As a result of the energy absorption, the Earth have to radiate the same amount of energy back to space. The Earth radiates at much longer wavelengths to the space, primarily in the infrared part of the spectrum, because it is much colder than the Sun (see Figure 1-1). Most of this thermal radiation emitted by the land and ocean is absorbed by the atmosphere, and subsequently reradiated back to Earth. This phenomenon is called the greenhouse effect. The greenhouse effect warms the surface of the Earth. Without the natural greenhouse effect of the Earth, the temperature of the planet's surface would be about 33 °C colder on average, which is below the freezing point of water[2],[3]. Thus, the natural greenhouse effect of Earth makes life possible.

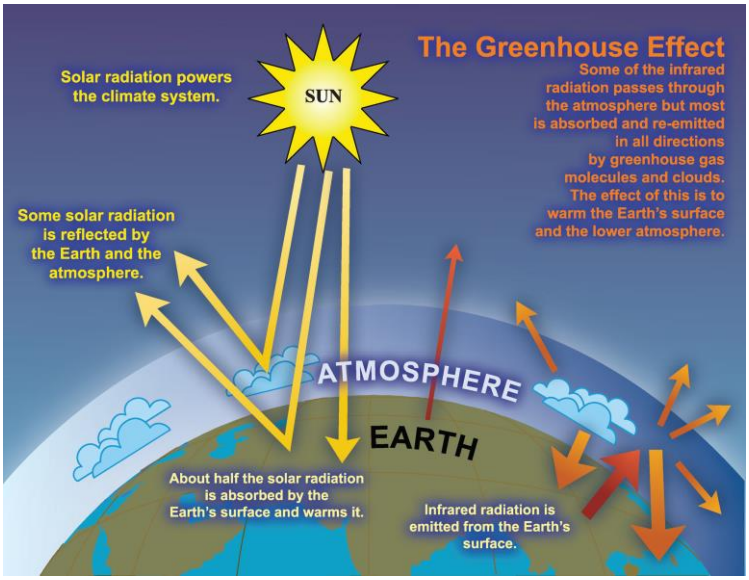

Figure 1-1. Illustration of greenhouse effect.

However, human activities, mainly the burning of fossil fuels and the destroying of forests, have significantly intensified the natural greenhouse effect of the Earth, leading to global warming. The two most abundant gases in the atmosphere, nitrogen (accounting for 78% of the dry atmosphere) and oxygen (21%), do not show greenhouse effect. Instead, the greenhouse effect comes from more complex molecules.[1], [2] Water vapor is the most important greenhouse gas, and carbon dioxide (CO_2) is the second-most important one. Methane, nitrous oxide, ozone and several other gases present in the atmosphere in small amounts also contribute to the greenhouse effect.[2] The contribution of the main greenhouse gases to the global warming is shown in figure 1-2a.[2] The Intergovernmental Panel on Climate Change (IPCC) showed the CO_2 concentration in atmosphere increased dramatically since industrial revolution (figure 1-2b), and the largest growth in CO_2 emissions has come from power generation, industrial processes and road transport (figure 1-2c).[4],[5] Because these gases have very long atmospheric lifetimes (decades to centuries), they are accumulated in the atmosphere with

increasing concentrations. The greenhouse gases trap outgoing radiation from the Earth to space, warming up the Earth.[3]

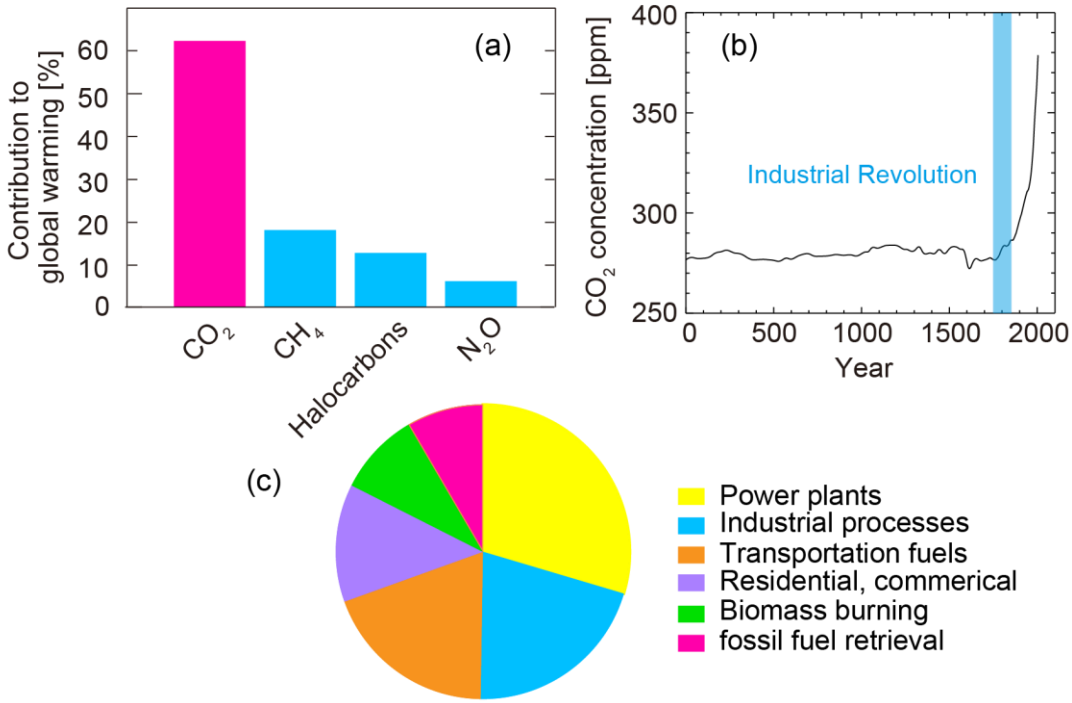

Figure 1-2. Contribution of the main greenhouse gases to the global warming.

The IPCC predictes that, by the year 2100, the CO_2 concentration may build up to 570 ppm in the atmosphere, increasing the global temperature of around 1.9 °C and the sea level of about 3.8 m on average.[6] It is estimated by the IPCC that CO_2 emitted to the atmosphere could be reduced by 80–90% for a modern conventional power plant by equipping CO_2 capture and storage system.[7]

Reduction of human activities caused CO_2 emissions into the atmosphere can be achieved by variety of methods, which has been summarized by Professor Yoichi Kaya:[8]

$$CO_2^{\uparrow} = POP * \frac{GDP}{POP} * \frac{BTU}{GDP} * \frac{CO_2^{\uparrow\uparrow}}{BTU} - CO_2^{\downarrow}$$

where $CO_2^{\uparrow}$ is the total CO_2 released to the atmosphere, POP is population of

human beings, GDP/POP is per capita gross domestic product and is a measure of the level of living, BTU/GDP is energy consumption per unit of GDP and is a judgement of energy intensity; $CO_2^{\uparrow\uparrow}$/BTU is the amount of CO_2 released per unit of energy consumption and represents the carbon intensity; $CO_2^{\downarrow}$ is the amount of CO_2 stored or sequestered in biosphere or geosphere sinks.

As for the first two measures, reducing the population or decreasing the level of living is not likely to be considered. Therefore, the only three remaining options to reduce total CO_2 emission into the atmosphere are: (1) reducing energy intensity, for example, use the fuel efficiently; (2) reducing carbon intensity, for instance, use of carbon-free fuel such as hydrogen and renewable energy; and (3) enhancing the sorption of CO_2, including the development of technologies to capture and sequester more CO_2.

It is clear that all the three above-mentioned options will be necessary if CO_2 emission reduction becomes a serious global priority. However, at the current state of development, the non-fossil fuel energy alternatives such as nuclear, solar energy, biomass, cannot meet our need due to the high risks and cost. Thus to meet mid-to long-term CO_2 reduction requirements, low cost CO_2 capture options from fossil fuel burning and subsequent sequestration options need to be evaluated, in view of the growing world demand for energy.

To enhance the sorption and sequestration of CO_2, carbon dioxide capture and storage (CCS) technologies must be improved with development of new CO_2 separation and capture approaches.

1.1.2. Industrial CO_2 capture technologies

Capturing CO_2 from flue gas streams is essential for the abatement of CO_2 concentration in the atmosphere. CO_2 emissions can be reduced for industrial power generation by three capture technologies: post-combustion, pre-combustion and oxyfuel combustion, as illustrated in figure 1-3.

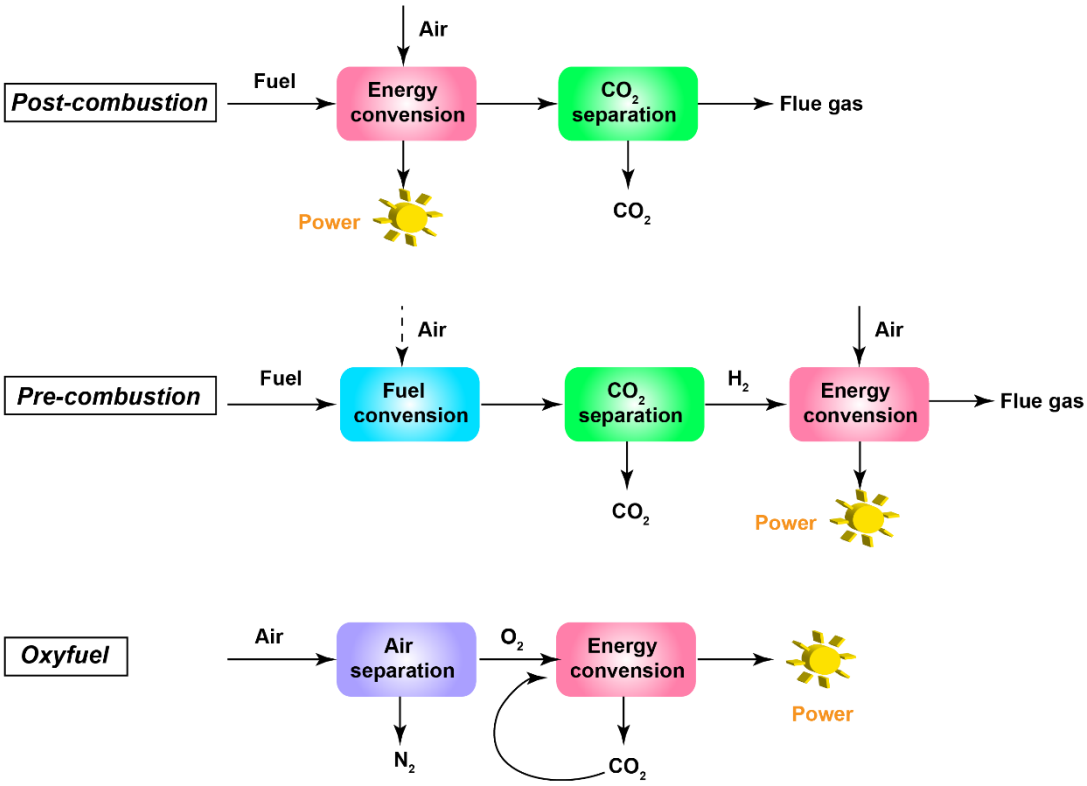

Figure 1-3. Illustration of post-combustion, pre-combustion, and oxyfuel.

Post-combustion carbon capture is the most common and widely used process. In this method, CO_2 is separated from other gases after combustion of the fossil fuel. , The major obstacle for post-combustion capture from flue gas is the low pressure of the flue gas (1 atm, see Table 1-1).[9] The low concentration of CO_2 in power-plant flue gas means a large volume of gas that has to be handled, leading to the large

equipment sizes and high costs. In addition, the CO_2 concentration is low (15%), the regeneration temperature is high, and capture requires separation from a high volume stream of flue gas containing other component gases, predominantly N_2.[9] A further demerit of the low CO_2 concentration is that powerful chemical solvents have to be used, and thus the regeneration of the solvents to release CO_2 will require large amount of energy. However this process is still the most well developed and has been used for several decades.

Table 1-1. Benchmark parameters showing typical compositions of gases (by weight) in post-combustion and pre-combustion processes, and the kinetic diameter of the gas molecules. [9]

	Post-combustion	Pre-combustion	Kinetic diameter (Å)
Composition			
CO_2	15-16%	35.5%	3.30
H_2O	5-7%	0.2%	2.65
H_2		61.5%	2.89
O_2	3-4%		3.45
CO	20 ppm	1.1%	3.75
N_2	70-75%	0.25%	3.64
SO_x	< 800 ppm		
NO_x	500 ppm		
H_2S		1.1%	
Temperature	50-75 °C	40 °C	
Pressure	1 bar	30 bar	

The alternative technologies, the pre-combustion capture and oxyfuel processes, are aimed to achieve higher efficiencies for CO_2 separation and capture, which will mitigate the extensive capital investments in the longer term.

Pre-combustion methods are employed in natural gas plants where CO_2 capture occurs at high partial pressures.[10],[11],[12] The pre-combustion process for converting a methane rich fuel into hydrogen, for example, the Integrated Gasification Combined Cycle (IGCC) plants, involve three stages (Figure 1-3). First, a fuel (natural gas in the case IGCC) is reacted at high pressure and temperature to form a synthesis gas (syngas) containing CO, CO_2, and H_2 [Eq. (1-1)]. Then, the CO is converted in to H_2 using a water-gas shift reactor, in which the CO_2 and H_2 are separated prior to combustion [Eq. (1-2)]. [10],[11],[12]

$$H_2O + CH_4 \rightarrow 3H_2 + CO \qquad \text{Eq.}\,(1-1)$$

$$H_2O + CO \rightarrow H_2 + CO_2 \qquad \text{Eq.}\,(1-2)$$

The significant advantage of pre-combustion capture is the reduction of the energy consumption penalty to 10–16%, roughly half that for post-combustion CO_2 capture, as a result of the higher CO_2 concentrations and pressures of this process (Table 1-1).[12] Although the initial fuel conversion steps are more elaborate and costly than in post-combustion systems, the resulting high concentrations of CO_2 and the high pressures are more favorable for CO_2 separation.[12] A further advantage is that pre-combustion technology generates a hydrogen-rich fuel, which can be used as a chemical feedstock, in a fuel cell for power generation, or in the development of a hydrogen economy.[10]

In contrast to post- and pre-combustion methods, oxyfuel combustion takes place

in a pressurized CO_2-rich recirculating stream in which N_2 is completely excluded from the combustion process through a preliminary air separation step (Figure 1-3).[11] Suitable fuels include coal, natural gas, hydrocarbons or syngas. The product of combustion is a concentrated stream of CO_2 (in high, sequestration ready concentrations of 80-98%), which is circulated back into the energy conversion system. [11] [11] The water product is removed from the flue gas by condensation. Oxyfuel technology forms the basis for "zero emission cycle" plants which are considered more promising compared with post-combustion CO_2 capture.[13] One shortcoming of the process is the significant energy requirements of the air separation step. However, this cost should be compensated by the elimination of the need for CO_2 capture. By reducing the volume of inert gas (mainly) in the furnace, the thermal efficiency of the boiler is also increased.[13] Since the separation of interest in this case is air separation (O_2 from N_2), reducing the cost of oxygen generation is key. As an alternative to cryogenic air separation, oxygen selective membranes offer a promising new technology in this regard.[14]

The concentration of CO_2 in the gas stream, the pressure of the gas stream and the fuel type (solid or gas) are the important factors in selecting the capture system.[8] The status and characteristics of these technologies are summarized in Tables1-2.

Table 1-2. Characteristics of the CO_2 capture technologies

Post-combustion capture	Pre-combustion capture	Oxyfuel combustion
Applicable to most coal-fired plants	Gas turbines must be capable of using H_2-rich fuel	Need to recycle large amount of flue gas to avoid excessively high combustion temperature
Low CO_2 partial pressure	Higher CO_2 partial pressure	Very high CO_2 concentration in flue gas.
Solvent degradation is a problem	High driving force for CO_2 separation	Large cryogenic oxygen production requirement may be cost prohibitive.
Efficiency and cost penalties for coal-fired power plants (IGCC) with conventional MEA scrubbing are well known	Efficiency and cost penalties for coal fired power plants are lower	CO_2 is recycled to the compressor to provide the expansion medium, instead of air.
Improved solvents may reduce energy losses	Barriers to commercial application of gasification are common	Potential for advanced oxygen separation membranes with lower energy consumption.
Significant cost saving are possible	Potential for reduction in compression cost	Decreased process efficiency.

1.1.3. CO_2 separation techniques

A wide range of technologies currently exist for separation of CO_2 from gas streams (Figure 1-4). They are based on different physical and chemical processes including absorption, adsorption, cryogenics and membranes. The choice of a suitable technology depends on the characteristics of the flue gas stream, which depend mainly on the power-plant technology. The conditions for CO_2 separation in pre-combustion capture processes will be quite different from those in post-combustion capture.[8] The regenerated CO_2 can be used for various industrial and commercial processes such as urea production, fertilizer production, foam blowing, carbonation of beverages and dry ice production.[8]

The absorption/stripping process, using amine solutions such as monoethanolamine (MEA), is a commercialized technology used in natural gas industry for 60 years and is regarded as the most mature process.[15] The stability of the amines and the energy consumption of the stripping process have large room of further improvement.[16]

The adsorption process is based on the same principle but using porous solid adsorbents such as zeolites and activated carbon. Chemical reactions between the adsorbent and CO_2 may or may not occur during the separation process. Both pressure swing adsorption and temperature swing processes are widely used. [15]

The large-scale membrane separation process has an advantage over other processes. Membrane materials with high selectivity for CO_2 over O_2 or N_2 have been developed, including polymeric materials and inorganic materials. Porous membranes with supporting amine solutions could be effective for the separation of CO_2 [15]. Currently, a sufficiently high selectivity with a large flux has not been achieved for membrane separation process.

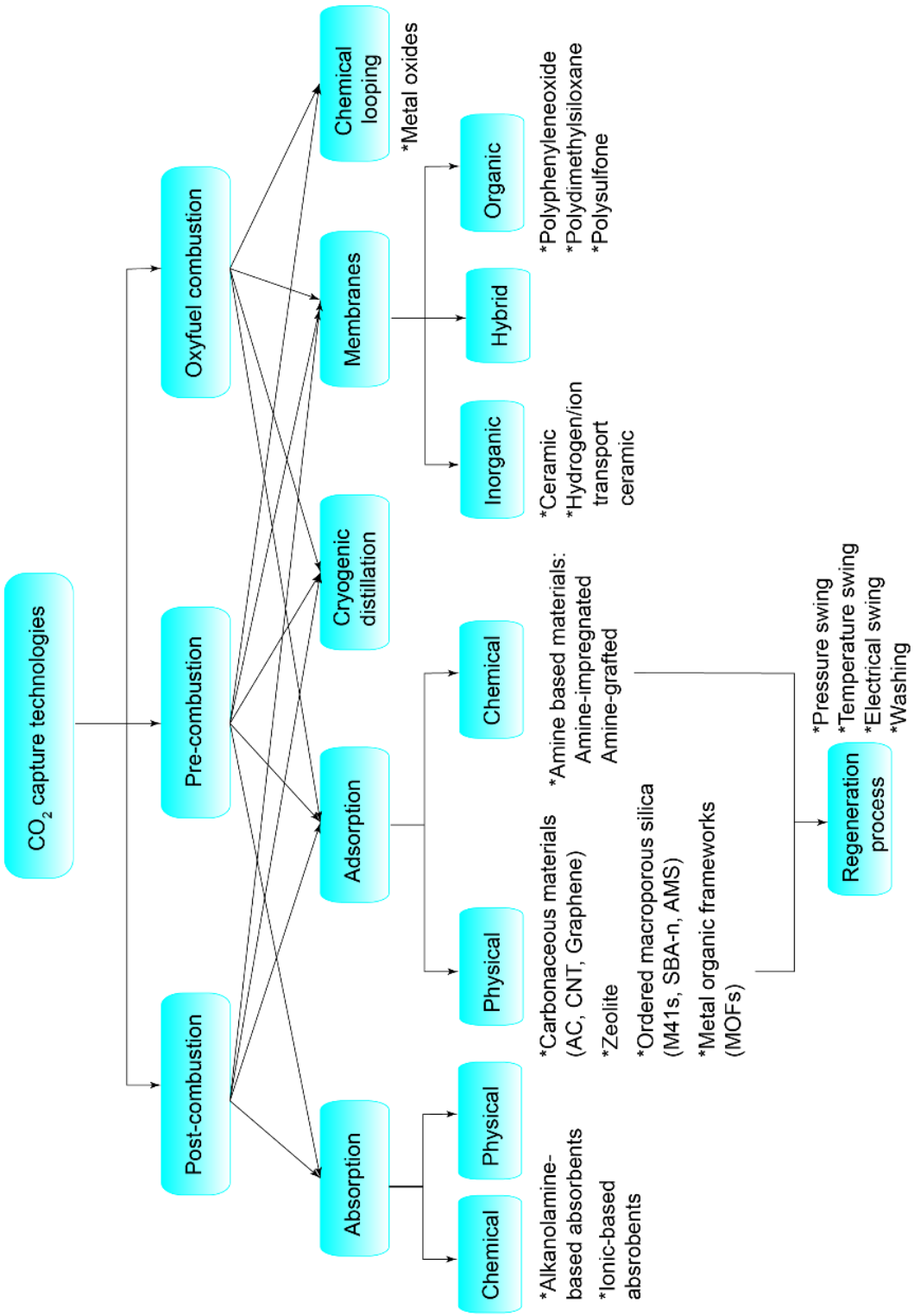

Figure 1-4: Technology options for CO_2 separation.

1.1.3.1. Absorption

1.1.3.1.1. Absorption by aqueous amine solution

Chemical absorption is preferred for low CO_2 partial pressures. Since CO_2 is an acid gas, chemical absorption of CO_2 from gaseous streams such as flue gases depends on acid-base neutralization reactions using basic solvents.[8] The CO_2 reacts with chemical solvents to form a weakly bonded intermediate compound in the absorption process. In the desorption process, the compound is then broken down by the application of heat, regenerating the original solvent and producing a pure CO_2 stream.[8] Specialized solvents were developed more than 60 years ago to remove CO_2 from impure natural gas.

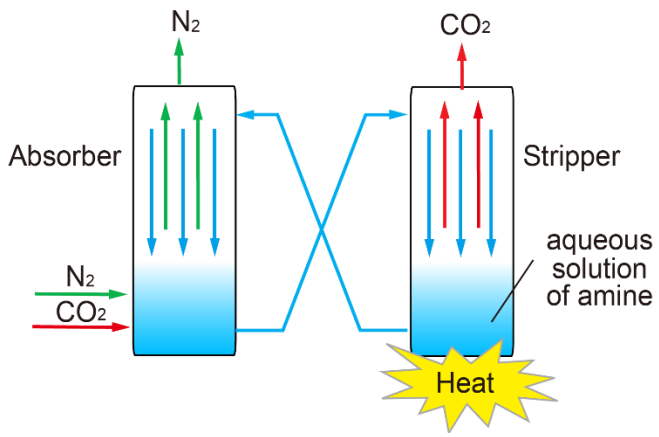

Figure 1-5. Schematic illustration of typical chemical absorption system for CO2 recovery from flue gas.

As depicted in figure 1-5, a typical chemical absorption process consists of an absorber and a stripper in which absorbent is regenerated at elevated temperature. In a chemical absorption process, the flue gas containing CO_2 enters a packed bed absorber from the bottom and contacts with the CO_2-lean absorbent. After absorption, the CO_2-absorbed absorbent flows into a stripper for thermal regeneration. After regeneration, the CO_2-lean absorbent is cycled back to the

absorber for reuse. The operation pressure is around 1.0 bar and the temperatures in the absorber and stripper are generally in the ranges of 40–60°C and 120–140°C, respectively.[17] The pure CO_2 regenerated from the stripper is compressed for the subsequent transportation and storage. According to the US DOE CO_2 capture goal, a 90% CO_2 capture efficiency with a cost increase less than 35% is needed to be achieved for post-combustion, therefore the improvements on absorbent efficiency, absorption operation, and thermal regeneration are necessary. [17]

The advantage of a chemical absorption is that it is the most matured technology for CO_2 capture and it has been commercialized for many decades. Another advantage of this technology is that it is suitable for retrofitting of the existing power plants. [10] However, there are also several drawbacks including (1) low CO_2 loading capacity; (2) high equipment corrosion rate; (3) amine degradation by SO_2, NO_2, and O_2 in the flue gases; (4) high energy consumption during high temperature absorbent regeneration; (5) large equipment size.[10] The possible remedies to these drawbacks such as the improvement of absorbents and operations are addressed below.

Alkanolamines are widely used as the absorbents for CO_2 capture. The structures of alkanolamines include primary, secondary, ternary amines containing at least one OH and amine group such as monoethanolamine (MEA), diethanolamine (DEA) and N-methyldiethanolamine (MDEA). The reactivity of amines to CO_2 follows the order primary, secondary and tertiary amines, for example, the reaction constants with CO_2 are 7,000, 1,200 and 3.5 m^3/s/kmol for MEA, DEA and MDEA at 25°C, respectively[18],[19],[20]. On the contrary, the CO_2 loading capacity for tertiary amine is 1.0 mol CO_2/mol amine, higher than that of primary and secondary amines where the CO_2 loading capacity lies between 1.0

mol CO_2/mol amine, as can be seen from figure 1-6. Zwitterion is first formed for the reaction of primary and secondary amine with CO_2, and then carbamate is formed. [21],[22],[23],[24] In the presence of water, some carbamate react with water to form bicarbonate and free amine is released. For the reaction of a tertiary amine with CO_2, bicarbonate is formed instead of carbamate (Figure 1-6).[21],[22],[23],[24]. Because of different properties and advantages of different amines, mixed amines have been proposed to enhance CO_2 capture efficiency and to reduce regeneration cost.

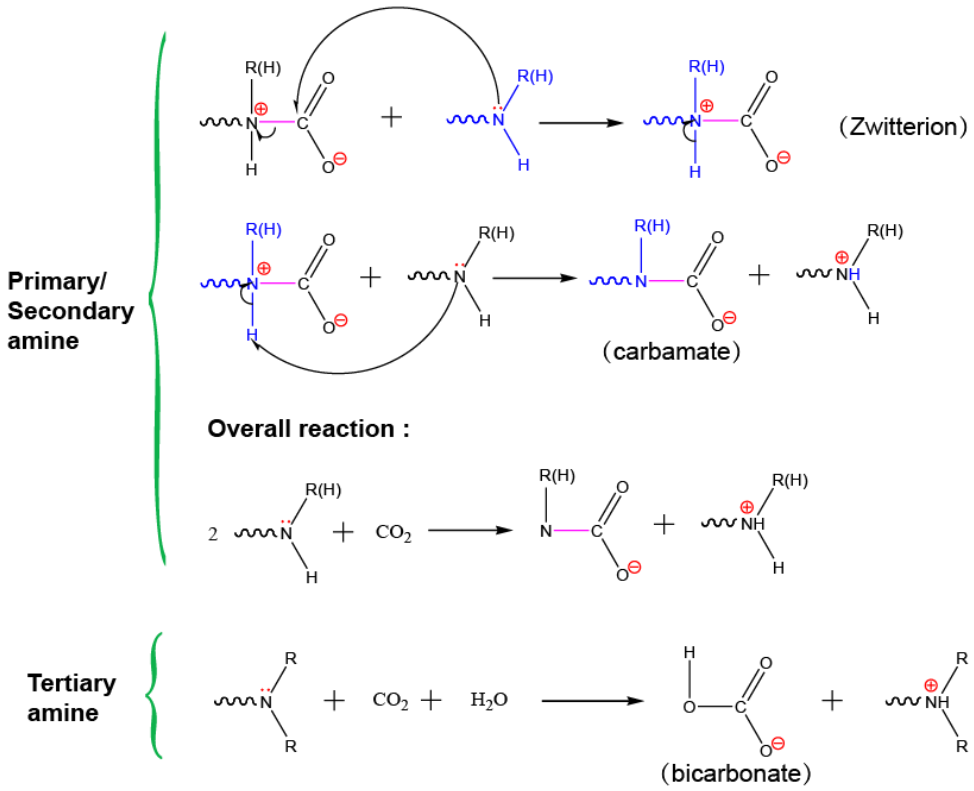

Figure 1-6. Reaction mechanism of primary amine, secondary amine and tertiary amine with CO_2.

In addition to the primary, secondary and tertiary alkanolamines, the steric hindrance amines such as 2-amino-2-methyl-1-propanol (AMP) were also used. Due to the steric hindered structure, the stability of the formed carbamate is

obviously reduced. Therefore, carbamate can undergo hydrolysis to form bicarbonate, and in the meanwhile, release free amines for further reaction with CO_2. As a result, the CO_2 equilibrium loading capacity is enhanced to 1.0 mol CO_2 /mol amine, as high as that of tertiary amine.[21] For example, piperazine (PZ) is a cyclic diamine which has been used as the promoter for CO_2 capture because of its rapid formation of carbamate with CO_2 [25],[26] The thermodynamic properties of some reported amines, such as solubility, CO_2 absorption constant, and heat capacity are listed in Table 1-3. [27], [28]

Table 1-3. Thermodynamic properties of the amines.

	Structural formula	Solubility in water at 293 K	Pseudo first-order rate constant (298 K)	Activation energy	CO_2 absorption capacity
			m^3/kmol/s	kJ/mol	mol CO_2 /mol absorbent
MEA		Free	7,000	46.7	0.5
AEEA	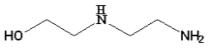	Free	12,100	N/A	1.0
PZ	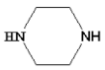	14 wt%	53,700	35	1.0
MDEA	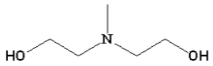	Free	3.5	44.3	1.0
AMP	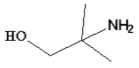	Free	681	41.7	1.0
DETA	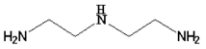	Free	49,740	--	1.0

1.1.3.1.2. Absorption by ionic liquid

Because the physical and chemical properties of room-temperature Ionic liquids (ILs) could be enhanced and modified by both their cationic and anionic moieties,

they serve a broad range of applications, such as solvents, sensors, solid-state photocells, and several analytical techniques, including separation techniques, and electrochemistry.[29],[30],[31],[32],

Therefore, considering that the properties of ILs can be tailor-designed to satisfy the specific application requirements, the use of ILs for CO_2 capture has received interest in the last few years because of their unique characteristics such as very low vapor pressure, good thermal stability, high polarity, and non-toxicity and high solubility of CO_2 in some of the studied ILs. [33], [34],[17]

For CO_2 capture, ILs can be applied to absorb CO_2 by either physical absorption or chemical absorption. For physical absorption, the free volume and size of ILs as well as cation and anion influence CO_2 solubility in ILs. In general, anion has more influence on CO_2 solubility than cation.[35], For use of ILs as chemical absorbents, amino-function group containing ILs that can react with CO_2 can be selected. This kind of IL is called task-specific ionic liquid (TSIL), because IL is synthesized with the desired properties. [35] It is found that the CO_2 absorption capacity of TSIL was three times higher than that of the IL in physical absorption.[36] However, there is a limitation of TSIL for CO_2 absorption that is high viscosity possessed by TSIL which is due to the formation of hydrogen bond between cation and anion.[17]

To enhance CO_2 capture capacity of IL, it is proposed to use the supported ILs.[37] The viscosity of an IL [aP4443][AA] was found to increase markedly with CO_2 absorption, leading to the highest CO_2 capture capacity as only 0.2 mol CO_2/mol IL. However, the CO_2 capture capacity could be improved to 1.2 mol CO_2/mol IL when the IL was loaded onto the support silica gel. [37] To reduce the drawback of high viscosity of ILs, the blended solutions containing IL and alkanolamine are also proposed for CO_2 capture,[38], [17]

1.1.3.2. Adsorption

There are some shortcomings accompanying the aqueous amine absorption processes, such as low contact area between gas and liquid, low CO_2 loading, and severe absorbent corrosion. Therefore solid adsorption process may be an alternative to achieve the CO_2 capture purpose. A variety of solid adsorbents have been developed to take into account of their structures, compositions and adsorption mechanisms. Figure 1-7 schematically shows the typical CO_2 adsorption system by porous solid materials. CO_2 molecules are selectively adsorbed on the surface of the pores and capillaries via chemical or physical interaction. By increasing temperature, or decreasing pressure, the CO_2 can be released and the adsorbents can be regenerated.

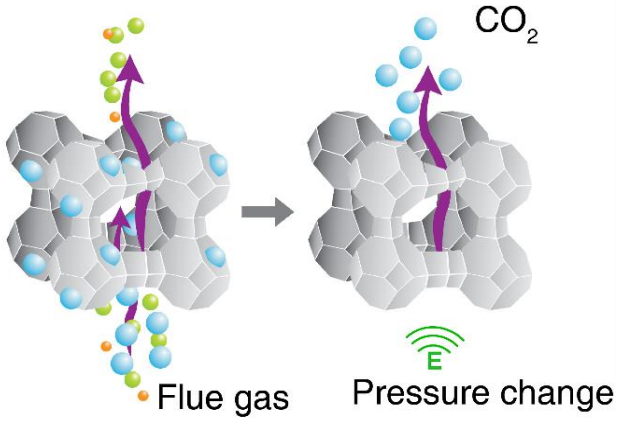

Figure 1-7. Schematic illustration of typical CO_2 adsorption system by porous solid materials.

1.1.3.2.1. Physical adsorbents[17],[39],[16]

Carbonaceous adsorbents such as activated carbon[40] have been widely used for CO_2 capture due to their wide availability, low cost, high thermal stability and low sensitivity to moisture, however, their application is limited to treat high pressure gases. As a consequence, current research focuses on how to improve the CO_2 adsorption capacity and selectivity by two means: (1) to prompt surface area and

pore structure of the adsorbents by creating different structures such as ordered mesoporous carbon[41], graphene[42], multi-walled carbon nanotube[43]; (2) to increase alkalinity by chemical modification on surface. [17],[39],[16]

Zeolites, a class of porous crystalline aluminosilicates built of a periodic array of TO_4 tetrahedra (T=Si or Al) (Figure 1-8), have been widely used in separation applications mainly because of their unique ability of molecular sieving.[44]. Zeolites as the physical adsorbents for CO_2 capture have been widely reported. The adsorption efficiencies of zeolites are largely affected by the porous structures, such as size, charge density, and chemical composition of cations [45]. Accordingly, a number of zeolites with highly crystalline structure, high surface area, and 3-dimensional pore structures have been developed by altering their composition such as Si/Al ratio. Though CO_2 adsorption can be increased by these methods, there are also some several drawbacks. The CO_2 adsorption capacity and the CO_2/N_2 selectivity are relatively low[46]. Besides, the CO_2 adsorption capacity greatly drops in the presence of water moisture in gas, because the water molecules will compete with CO_2 to be adsorbed on the pore surface, and the liquefied water will block the small pores and capillaries. Thus a high regeneration temperature (often above 300 °C) is needed.

Ordered mesoporous silica may be a candidate because of its high surface area, high pore volume, tunable pore size and good thermal and mechanical stability. [47],[48],[49] So far mesoporous silicas such as the families of MCM-41s, Santa Barbara Amorphous type material (SBA-n), anionicsurfactant- templated mesoporous silica (AMS) (Figure 1-8), have been reported. However, they do not show high enough the CO_2 adsorption capacities, especially, at atmospheric pressure.[47],[48],[49]

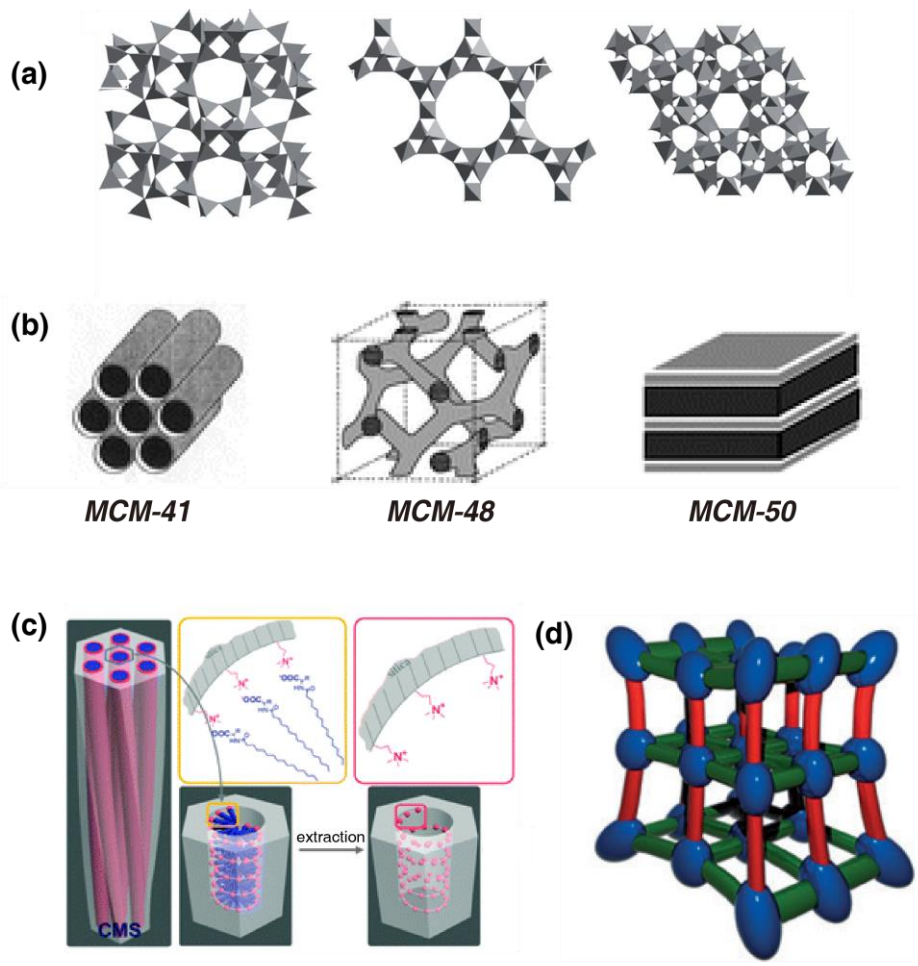

Figure 1-8. Structure of (a) Zeolites[50], (b) MCM[51],(c) AMS[52] and (d) MOF[53].

Metal-organic frameworks (MOFs) (Figure 1-8) as CO_2 adsorbents have attracted significant interest due to their significantly high surface area, controllable pore structures and tunable pore surface properties, which can be easily tuned by changing either the metallic clusters or the organic ligands. It is reported that MOFs exhibit exceptional CO_2 adsorption capacity to deal with pure CO_2 at high pressures. However, their adsorption capacities significatly decrease when they are exposed to gas mixture.[54],[55] Though MOFs have shown promising CO_2 capture capacity in laboratory, more studies are needed to ensure their practical applications.

1.1.3.2.2. Chemical adsorbents

Many efforts have been made to improve CO_2 adsorption capacity and selectivity by chemical modification of the surface of the porous solid materials. The alkalic organic group (amine) and inorganic metal oxide (alkali metal or alkali-earth metal) are of great importance. The interaction between the acidic CO_2 molecules and modified basic active sites on the pore surface facilitates CO_2 adsorption through the chemical reaction.

Recently, the improvement of amine-based adsorbents was proposed by the approaches: (1) the preparation of supports with high amine loading, (2) the use of amine with high nitrogen content, and (3) the effective methods for amine introduction. [45]

According to the type of the interactions between amines and supports, the amine-based adsorbents can be categorized as amine-impregnated materials via weaker interactions and amine-tethered materials via stronger covalent bonding [46].

(a) Amine-impregnated adsorbents

The structure of amine-impregnated adsorbents is schematically illustrated in figure 1-9. The amines are loading in the porous solids by easily impregnation. polyethylenimine (PEI) is the most studied polymer amines due to the high amine content. The effects of PEI loading, gas conditions, temperature, moisture and supports on CO_2 adsorption capacity for the PEI-impregnated mesoporous silica and carbonaceous materials have been reported previously[56], [57]. A higher PEI loading dramatically improved CO_2 adsorption capacity, though the surface area, pore size and pore volume of the PEI-impregnated supports decreases. The largest

CO_2 adsorption capacity (3.02 mmol/g) for the PEI-impregnated MCM-41 (PEI/MCM-41) with 75 wt% of PEI loading was observed under 100% CO_2 at 75°C. [56], [57] The amine loading is not directly related to the amines for CO_2 adsorption because the formation of amine aggregation on supports decreases the amine accessible to CO_2. When the PEI/MCM-41 with 50 wt% PEI loading was used to treat an anhydrous gas containing 15% CO_2 (85%bN_2) at 75°C, the adsorption capacity decreased to 2.03 mmol/g. At a lower temperature of 25°C, the CO_2 adsorption capacity decreased as well. It is known that CO_2 adsorption is an exothermic process, the increasing temperature is unfavorable for CO_2 adsorption capacity. However, at low temperature, the formation of bulk-like viscous PEI inside the pore leads to CO_2 adsorption as a diffusion-limited process[46]. At high temperature, the high CO_2 adsorption capacity is possibly due to the high diffusion rate of CO_2 into less viscous PEI.

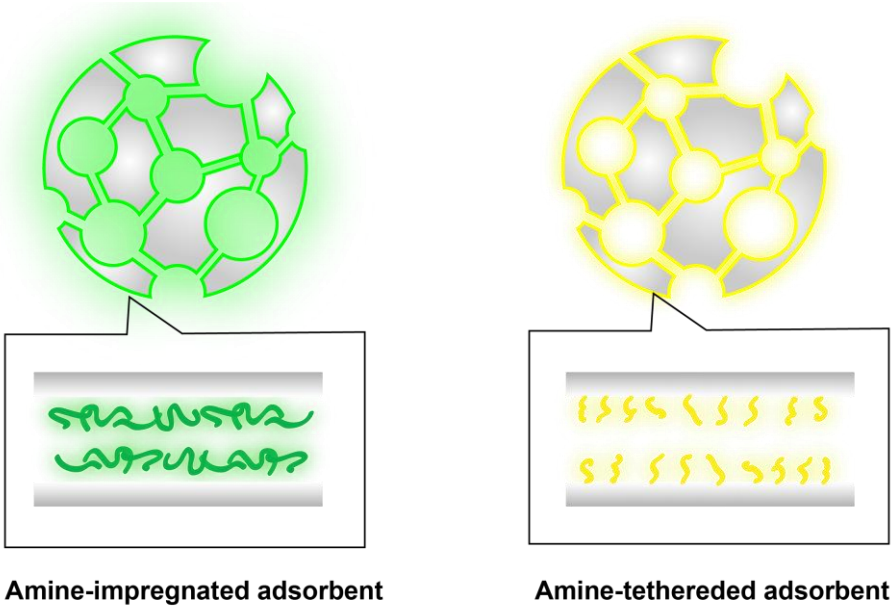

Figure 1-9. Schematic illustration of amine-impregnated adsorbents and amine-tethered adsorbents.

The effect of moisture on CO_2 capture capacity of PEI/MCM-41was also studied. [58] The CO_2 adsorption capacity increased from 2.03 mmol/g for an anhydrous flow to 2.84 mmol/g for a flow containing 10% of moisture. The improvement of CO_2 adsorption capacity was interpreted in terms of adsorption mechanisms, i.e., the formation of carbamate and bicarbonate under anhydrous and hydrous conditions, respectively[58]. The positive effect of moisture was only observed for the molar concentration of moisture not higher than that of CO_2.

The effect of support was also reported. The CO_2 adsorption capacity and kinetics were mainly influenced by pore size and followed an order of hexagonal mesoporous silica (HMS) > KIT-6 > SBA-16 ≈ SBA-15 > MCM-48 > MCM-41. [59],[60]

Except for PEI, the tetraethylenepentamine (TEPA), mixture of TEPA and diethanolamine (DEA), pentaethylenehexamine (PEHA) diisopropanolamine (DIPA), hindered 2-amino-2-methyl-1,3-propanediol (AMPD), and triethanolamine (TEA) were also studied. [61],[62] ,[63],[64]

(b) Amine-tethered adsorbents

Though high CO_2 adsorption capacity was observed in amine-impregnated materials, the interaction between the support and the supported species is weak, since the amine is loaded by simple impregnation (see figure 1-9). Therefore, the material could be operated only at relatively low temperature. To overcome this limitation, aminosilanes were used to be covalently grafted onto the intra-channel surface of the mesoporous silicas through silylation.

Sayari's group comprehensively investigated amine-grafted MCM-41 and pore-expanded MCM-41 (PE-MCM-41) for CO_2 capture. It is concluded that the larger pore diameter and pore volume of PE-MCM-41 enhanced CO_2 adsorption. They

further demonstrated the formation of urea groups, which was stable in desorption, would cause deactivation of the amine-tethered adsorbents. Therefore it is suggested the stability of amine-based adsorbents can be improved by using humid streams to prevent the deactivation. [65],[58], [66],[67],[68].

Generally, the amine-tethered adsorbents exhibit higher adsorption rate and higher stability in cyclic runs than the amine-impregnated ones. However, the grafted amount of amine depends on surface silanol groups, sometimes resulting in a lower amine loading as compared with the impregnated amount. Although the higher amine loadings may be achieved by impregnation, a large diffusion resistance also occurs. [65],[58], [66],[67],[68]

1.1.3.3. Membrane separation

Compared with CO_2 absorption and adsorption processes, membrane separation have several advantages, such as the relatively small footprint that reduces the capital costs; no regeneration requirements, thereby the complexity in designing heat-exchange systems is reduced; no solvent requirements, making them more environmentally friendly; and higher efficiency of separation due to a lack of phase change.[69]

Membranes are semi-permeable barriers capable of separating substances by various mechanisms (solution/diffusion, adsorption/ diffusion, molecular sieve and ionic transport).[8] They are available in different material types, such as organic (polymeric) or inorganic (carbon, zeolite, ceramic or metallic), and in different structure forms, for example porous or non-porous. Membranes act as filters to separate one gas from a feed gas mixture and generate a specific gas rich permeate as shown in figure 1-10.

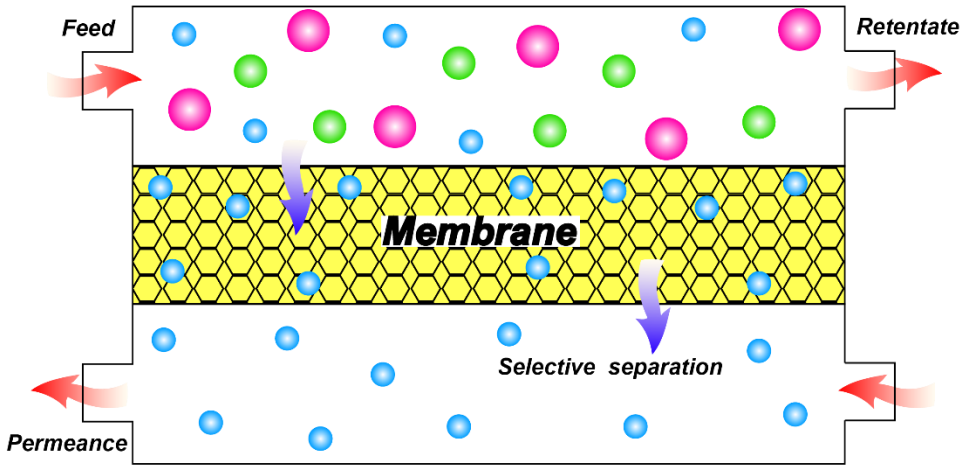

Figure 1-10. Schematic of gas separation memebrane

There are two characteristics to evaluate the membrane performance: (1) permeability, which is defined as the flux of a specific gas through the membrane,

and (2) selectivity, the membrane's preference to pass one gas species over the other.

Molecular sieving and solution-diffusion are the two main mechanisms for almost all the gas separating membranes[8] (see figure 1-11). For the solution-diffusion type gas separation membrane, the relationship between permeability, diffusivity and solubility can be described by:

$$P = D*S \qquad \text{Eq. (1-3)}$$

where P is the permeability coefficient, a measure of the flux of the membrane, D is the diffusivity coefficient, a measure of the mobility of molecules within the membrane, and S is the solubility coefficient, which measures the solubility of gas molecules within the membrane. [8]

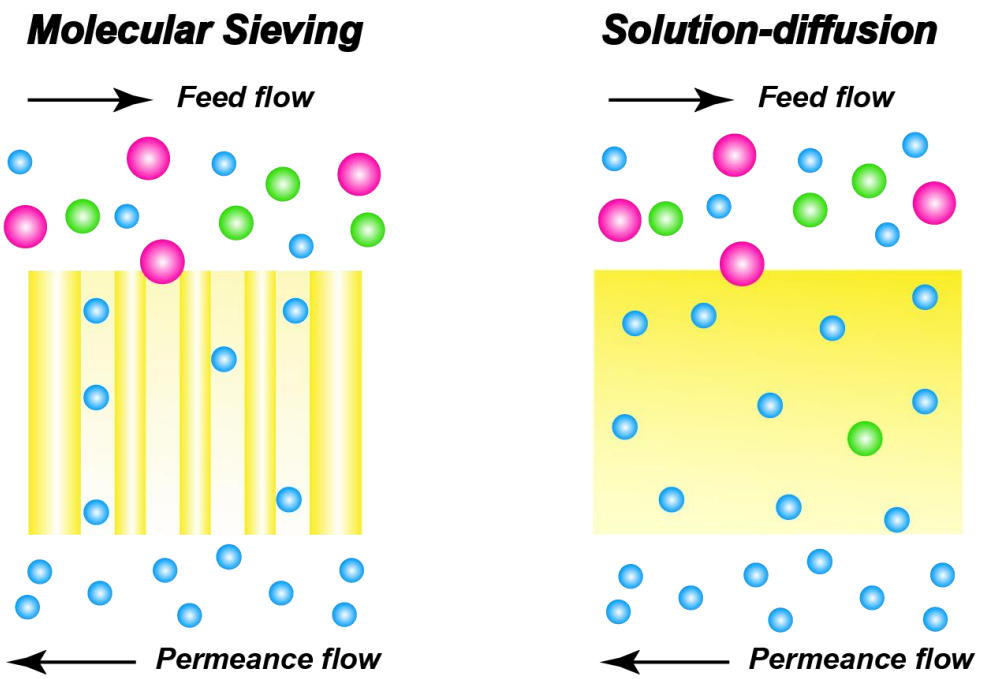

Figure 1-11. Mechanism of molecular sieving and solution-diffusion.

There appears to be a trade-off between selectivity and permeability of gas separation polymeric membranes. As described by Eq. (1-3), materials for effective CO_2 separation can follow one of two overall strategies: increasing the rate of diffusion of CO_2 through the polymeric structure and increasing the solubility of CO_2 in the membrane. [16]

As an alternative to conventional polymeric membranes, facilitated transport membranes have attracted attention because of the potential of achieving both high permeabilities and high selectivities.[70] Facilitated transport membranes may selectively permeate CO_2 by means of a reversible reaction of CO_2 with an incorporated complexing agent (carrier) in the membrane, whereas gases such as H_2, N_2, and CH_4 will permeate exclusively by the solution- diffusion mechanism.[70]

Facilitated transport membranes for gas separation was first developed by impregnating the pores of a microporous support with a carrier solution.[71] However, serious degradation problems usually accompany these membranes or supported liquid membranes (SLMs), such as the loss of carrier solution and the deactivation of the complexing agent (carrier). The application of fixed-site–carrier (FSC) membranes was proposed as a method to overcome the problems of SLMs. These FSC membranes have carriers covalently bonded to the polymer backbone, therefore, the mobility of carriers is restricted. However, the decreased mobility of carriers is favorable when stability is considered. It is obvious that the diffusivity (and thus permeability) in an FSC membrane is lower than that of a mobile carrier membrane. The diffusivity of a swollen FSC membrane should, however, show diffusivities between that of a mobile and a fixed carrier. [70] [71]

It was assumed that tertiary amino groups acted only as weak base catalysts for the CO_2 hydration reaction in water swollen membranes.[72],[73] Therefore, CO_2 does

not interact directly with the fixed amino groups. Instead, CO_2 is carrier-transported in the form of HCO_3^- , which possesses mobility comparable to that in the mobile carrier membranes. The mechanism of CO_2 separation from N_2 by a FSC membrane with polyvinylamine fixed on polysulfone membrane is schematically illustrated in figure 1-12. This mechanism gives a possibility of enhanced permeability and selectivity in favor of CO_2 for the aminated fixed-site-carrier membranes comparable to those of the mobile carrier membranes.

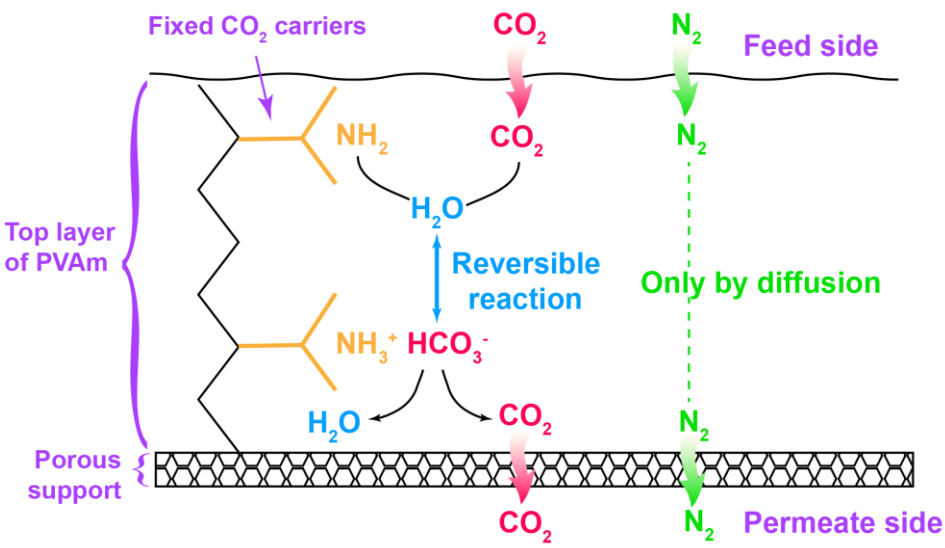

Figure 1-12: Schematic illustration of the mechanism of facilitated transport of CO_2 in a fixed-site-carrier membrane (PVAm on PSf membrane).

May-Britt Hägg's group has extensively studied the polyvinylamine (PVAm) FSC membranes prepared by crosslinking the PVAm in porous membrane supports.[70],[74],[75],[76] The performance of the PVAm FSC membrane and some other polymeric membranes are summarized in table 1-4, mainly separating post-combustion flue gas with CO_2/N_2 being the main components[77].

Table 1-4. The performance of polymeric membranes[77] and PVAm FSC membrane[76] separating CO_2/N_2.

	Permeance ($m^3/(m^2*Pa*s)$)	Selectivity ($\alpha CO_2/N_2$)
Polyimide	735	43
Polydimethylphenylene oxide	2750	19
Polysulfone	450	31
Polyethersulfone	665	24.7
Poly(4-vinylpyridine) / polyetherimide	52.5	20
Polyacrylonitrile / poly(ethylene glycol)	91	27.9
Poly(amide-6-b-ethylene oxide)	608	61
PVAm/PVA blends supported in polysulfone (FSC)	2088	174-194

1.2. Temperature responsive hydrogel

A gel is a type of 3-dimensional soft matter composed of crosslinked polymers that are swollen with a medium. The gels combine the properties of solids and fluids: on the one hand, they have structural integrity and do not flow appreciably when removed from their container. On the other hand, for molecules that are significantly smaller than the gel pore size, the transport of molecules/ions through a gel is similar to mass transport in a fluid. [78]

Hydrogels are gels that swell strongly in aqueous media, and are typically composed of a hydrophilic organic polymer component that is cross-linked into a network by either physical or chemical interactions. The crosslinking provides for dimensional stability, while the high solvent content gives rise to the fluid-like transport properties. The particular physical properties that result from this unusual state of matter make hydrogels ideal candidates for a number of applications.[78]

The stimuli-responsive gels are also called "smart" materials, because they not only swell upon water absorption, but also response to subtle changes in the environment by changing the swelling.[79], These hydrogels can be made responsive to temperature,[80] pH value,[81] ionic strength,[82],[83] light,[84] electric field,[85] and biomolecules.[86], [87] The responsive behavior of the hydrogels is inherited from the chemical composition and microstructure of the gels. [78]

1.2.1. Temperature responsive polymers and gels

Poly(*N*-isopropylacrylamide) (pNIPAm) is the most widely studied stimuli-sensitive polymer. pNIPAm can be easily synthesized by a variety of methods: redox initiation, free radical initiation, ionic initiation, and photo-initiation.[88]

Various functional groups can also be introduced to the polymers by copolymerization or post polymerization modification, thereby giving multi-responsive and multifunctional polymers. [78]

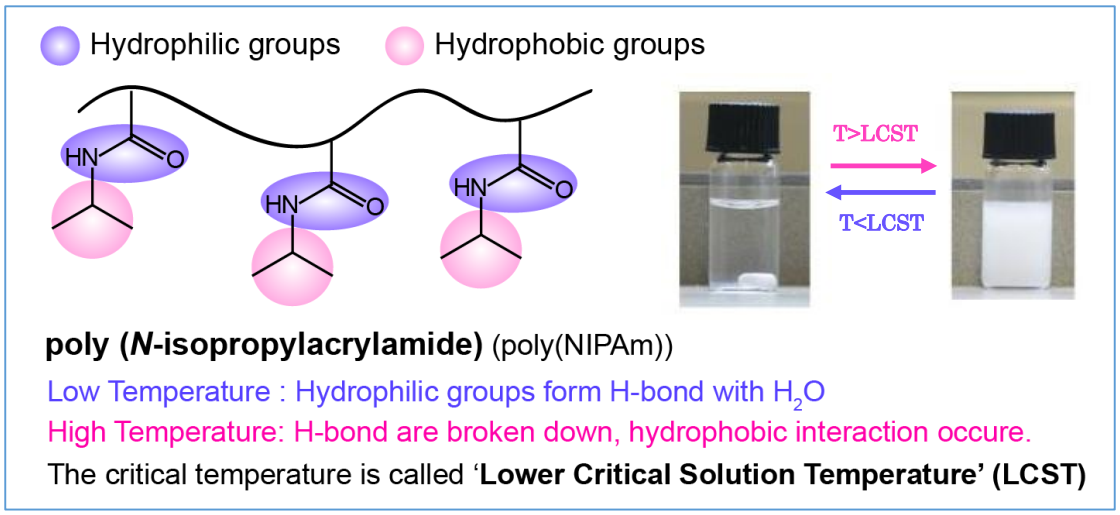

Figure 1-13. Illustration of structure and phase transition of pNIPAm.

One of the earliest studies on the solution properties of pNIPAm carried out by Heskins et al. reported that the phase transition of pNIPAm is endothermically entropy driven.[89] The dissolve behavior of any polymer in a solvent is related to the balance between solvent–solvent, solvent–polymer, and polymer–polymer interactions. For stimuli-sensitive polymers, the polymer solvation can be "switched" by strengthening one of these interactions or by weakening another. In the case of aqueous solution of pNIPAm, the hydrogen of amide side chains of the polymer and water form hydrogen bond, as described in figure 1-13. However, the isopropyl group on the side chain induces hydrophobic structuring of the water. This structured water leads to entropically driven polymer–polymer interactions by the hydrophobic effect.[88] Under the conditions where pNIPAm has a random-coil structure, the solvent–polymer interactions are stronger than the polymer–

polymer interactions. At higher temperatures, the hydrogen bonds between amide hydrogens the water molecules are broken and there is an entropically favored release of structured water, resulting in the formation of a globular polymer conformation. As a result, the polymer–polymer hydrophobic interactions become stronger than the polymer–solvent interactions, and the polymer phase separation occurs. The temperature at which this phase separation occurs is called the lower critical solution temperature (LCST).

However, it should be noticed that, other than hydrophilicity and hydrophobicity of the side-chains that contribution to polymer solvation, more factors must be considered when describing LCST behavior. For example, the polymers formed from *N*-isopropylmethacrylamide,[90],[91],[92],[93] which differs from NIPAm by only a single methyl group, has a higher LCST in water, indicating it is more hydrophilic than pNIPAm despite having one more methyl group. Apparently, this "increased hydrophilicity" does not come from an increase in polymer polarity, instead, it is caused by the decrease in chain flexibility after adding more methyl groups in the backbone. This feature changes the entropic contribution to the free energy of mixing, and thus increases the LCST. [78]

Contrary to the LCST behavior, there are other classes of thermo-responsive polymers that show an upper critical solution temperature (UCST). In this case the polymer is phase separated at low temperatures owing to inter- or intra-molecular interactions, while at high temperatures these interactions break and the polymer dissolves or swells. Most often these interactions are hydrogen bonding or electrostatic. [78]

Table 1-5 lists the transition temperatures of some thermal responsive polymers in aqueous solution. [94]

Table 1-5. Structures and LCSTs of some thermal responsive polymers in aqueous solution.

Polymer	Formula	LCST (°C)	Ref
Poly(N-isopropylacrylamide) (PNIPAm)		32	
Poly(N-n-propylacrylamide) (PNNPAm)		10	[95]
Poly(N-cyclopropylacrylamide) (PNCPAm)		53	[96]
Poly(N,N-diethylacrylamide) (PDEAm)		33	[97]
Poly(N-vinylisobutyramide) (PNVIBA)		39	[98], [99]
Poly(N-vinyl-n-butyramide) (PNVBA)		32	[100]
Poly(N-vinylcaprolactam) (PVCa)		32	[101]
Poly(N-ethylpyrrolidine methacrylate) (PEPyM)		15	[102]
Poly(N-acryloylpyrrolidine) (PAPR)		51	[103]
Poly(dimethylaminoethyl methacrylate) (PDMAEMA)		14-50	[104]

Poly(ethylene oxide) (PEO)	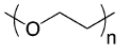	85	[105]
Poly(ethylene glycol) (PEG)			
Poly(propylene oxide) (PPO)	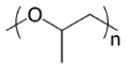	0-50	[106]
Poly(propylene glycol) (PPG)			

Due to this attractive LCST behavior in aqueous media, thermal responsive polymers such as pNIPAm have been widely used to make responsive hydrogels. A hydrogel comprising of thermal responsive polymers is called thermal responsive hydrogel. Instead of the reversible solubility change of thermal responsive polymers observed at the temperature LCST, a reversible volume change of the thermal responsive hydrogel occurs at the volume phase transition temperature (VPTT). Basically, the VPTT of the hydrogel is same to the LCST of the constituent polymer.

1.2.2. pH responsibility of the thermal responsive polymers and hydrogels

Researchers have copolymerized ionic monomers with pNIPAm to create pH-responsive polymers and hydrogels.[81],[107],[108],[109]

The swelling of a pH-sensitive hydrogel is the result of the interplay of the pH and the ionic strength of the solution which the hydrogel is exposed to. The ionizable monomers inside the hydrogel will dissociate as a function of the pH. The resulted free counter ions in the hydrogel exchange with salt ions from the solution, generating a certain c osmotic pressure difference between the gel and the solution. Consequently the hydrogel will swell until the elastic forces inside the hydrogel are in equilibrium with the osmotic force.[110]

1.2.3. Adjustment of the LCST of the thermal responsive polymers

1.2.3.1. Control LCST via copolymerization with other monomers

LCST of the thermos-responsive polymers can be controlled by incorporation of co-monomers with different hydrophobicity, because LCST of the thermal responsive polymers mainly depends on the balance between hydrophobic groups and hydrophilic groups. General speaking, as shown in figure 1-14, LCST will increase by incorporating monomers with higher hydrophilicity, due to the increased tendency of H-bonding formation. On the contrary, incorporation of more hydrophobic monomers will decrease the LCST. [111] [112]

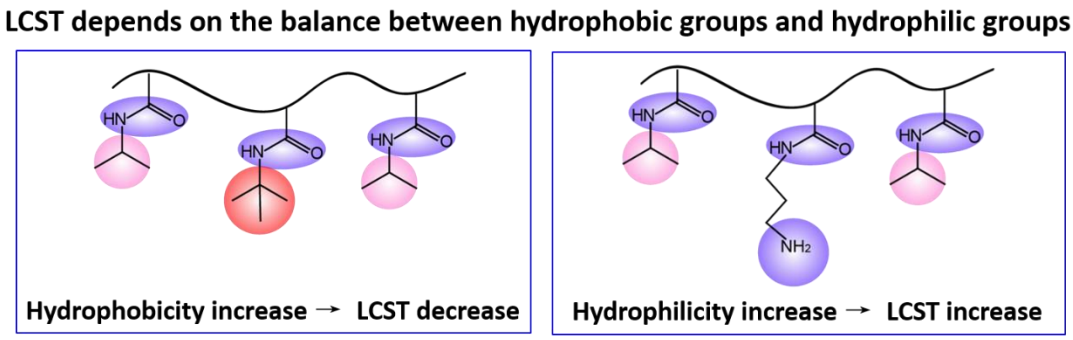

Figure 1-14. Illustration showing the control of LCST via copolymerization of other monomers of different hydrophobicity/hydrophilicity.

1.2.3.2. Control LCST via additional compounds

The LCST of the thermal responsive polymers can also be tuned by adding various additives into the solvent, which interact with the polymer.

Figure 1-15 shows that high temperature and high ionic strength leads to the aggregation of the thermal responsive polymer pNIPAm. The blue arrow represents the temperature dependent stability. pNIPAm disperse stably as free

coil below the transition temperature, but become globule and sometimes aggregation when the temperature exceeds the transition temperature, and forms stable dispersions again upon cooling below the transition temperature. The red arrow indicates that the addition of salts decreases the inter-particle electro-repulsive force due to screening effect and causes the formation of aggregates. In contrast, the desalting process decreases ionic strength, increases the electro-repulsive force and stabilize the dispersion. [113]

This salting-out effect can be explained by the water-structuring ability of salt ions, hence decreasing the phase separation temperature.[114],[115] These principles enable the control of dispersion stability using temperature and/or salt concentration.[116] , [117], [118]

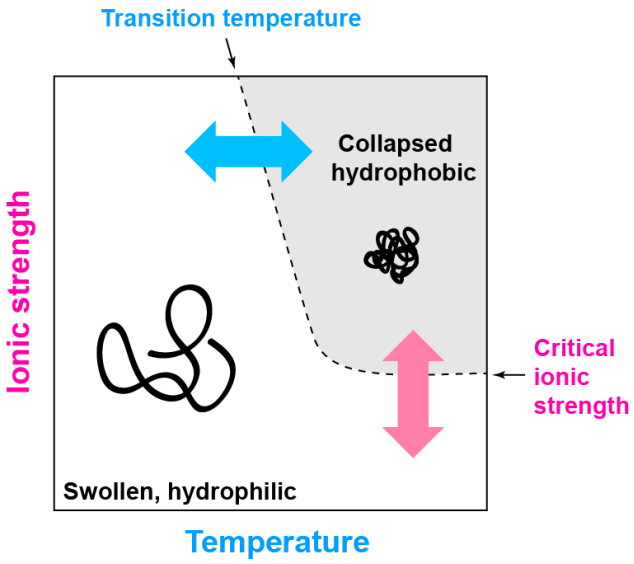

Figure 1-15. Schematic representation of the dependence of thermal responsive polymer stability pNIPAm on temperature and ionic strength.

In additional to salt, the addition of a saccharide to pNIPAm solutions decreases the LCST.[119] The presence of saccharides increased the hydrophobic interactions between the polymer chains, by increasing the number of non-polar polymer

conformations while stabilizing them. It was also supposed that the hydrophobic interaction was increased by ordering of water molecules around the polymer. [119]

Conversely, the LCST will increase when adding more anionic or cationic surfactant such as sodium dodecyl sulfate or cetylpyridinium chloride into the aqueous solution of pNIPAm.[120] The surfactant contributes to better solubilize the pNIPAm chains in water and thus increases the phase separation temperature.

Furthermore, a supplementary amount of a solvent different from water can vary the LCST of pNIPAm. For instance, it was showed that the LCST of pNIPAm is closely related to the amount of methanol (MeOH) added to an aqueous solution of the polymer, as shown in figure 1-16.[121] The LCST changes drastically up to a methanol molar fraction of 0.45 and is not detectable after this value.

Methanol is a better solvent for pNIPAm. In this solvent the polymer behaves as a flexible coil. In pure water, on the other hand, the polymer is elongated and stiffer than in methanol. Hydrogen bonding occurs between water molecules and the amide groups of the polymer, causing the formation of a layer of highly structured water molecules around the polymer. Such polymer - water interactions contribute favorably to the free energy of dissolving but unfavorably to the entropy of dissolving. As the solution temperature is increased, polymer bound water is released. The relative values of the thermodynamic functions change: the entropic term becomes dominant, resulting in a positive free energy of mixing, as a result a two-phase system is favored. [121]

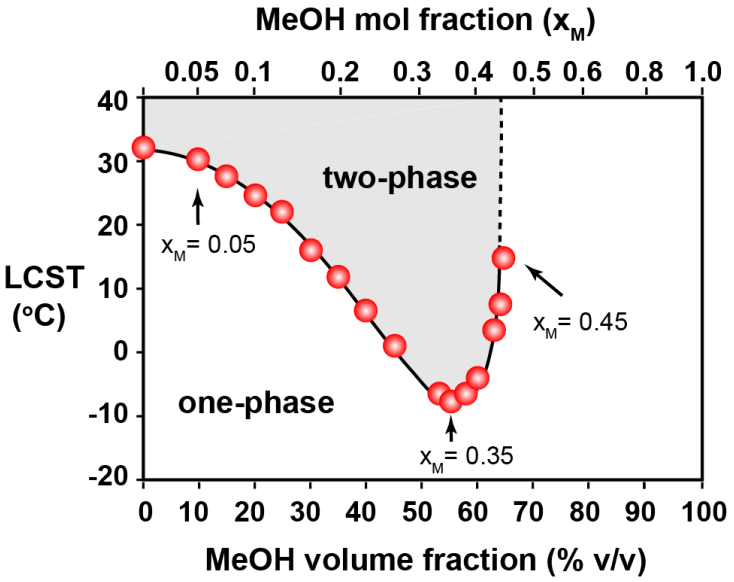

Figure 1-16. Phase diagram of a pNIPAm solution of 1.0g/L in co-solvent of water/MeOH. [121]

The nature of solvent structure of methanol-water mixtures has been studied extensively. For solvent compositions of $x_M < 0.05$, the methanol molecules are kept apart from each other by the formation of hydration cages around each molecule. Under these circumstances the polymer-solvent interactions are essentially undisturbed by the presence of methanol molecules. As the methanol mole fraction increases, there is no longer sufficient water to provide clathrate cavities for all the methanol molecules. These are now free to interact with polymer segments. Changes in LCST observed for $0.05 < x_M < 0.45$ reveal on a macroscopic scale the changes in the relative importance of the free energy of association in methanol-polymer, water-polymer, and methanol-water. In solutions of higher methanol content the methanol-polymer interactions become predominant. [121]

1.2.3.3. Influence of pressure on the LCST of thermal responsive polymers

Not only do the chemical parameters play an important role in shifting the LCST

of a polymer, but also the physical parameters such as pressure.[122] As shown in figure 1-17, at low pressure range, the transition temperature increases with increasing pressure for both poly(*N*-vinyl isobutylamide) and pNIPAm. However, at pressures higher than 150 MPa, it decreased with increasing pressure. Hence, there appeared to be a turning point in the LCST-Pressure curve for both polymers. [111]

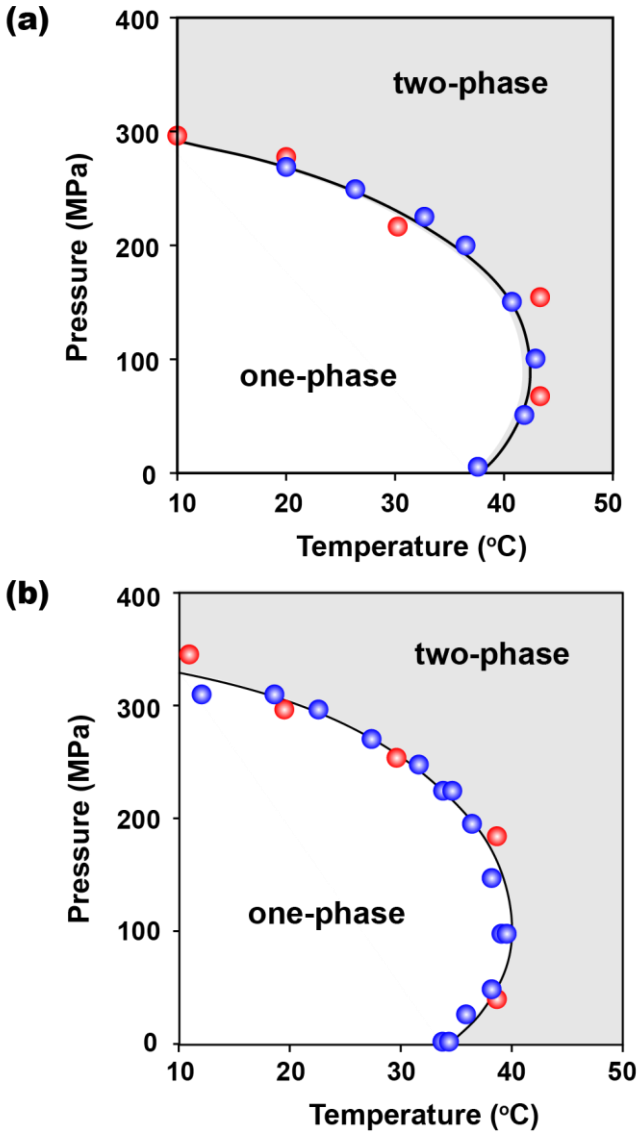

Figure 1-17. T-P diagrams for the cloud point of solutions of (a) poly(*N*-vinyl isobutylamide) (0.1 wt/vol.%) and (b) pNIPAm (0.5 wt/vol.%). Blue cycle: T scanning and red cycle: P scanning. [122]

1.2.4. Swelling kinetics of the thermal responsive hydrogel

In a temperature jump experiment, the relaxation time τ of the swelling process of a thermal responsive hydrogel is determined experimentally from the single-exponential region of the time dependent volume change.

The radius of a gel changes rapidly for times smaller than τ, then later more slowly and single-exponentially: [123],[124]

$$\Delta R(t) \sim \left(\frac{6\Delta R_0}{\pi^2}\right)\exp\left(\frac{-t}{\tau}\right) \qquad \text{Eq. (1-4)}$$

Where R is the final equilibrium radius and ΔR_0 is the total radius change.

The relaxation time τ of the volume change of a spherical gel is defined as the decay time appearing in the single-exponential region: [123],[124]

$$\tau = \frac{R^2}{\pi^2 D} \qquad \text{Eq. (1-5)}$$

Where D is the collective diffusion coefficient defined as the ratio of the osmotic bulk modulus K and the friction coefficient f between the gel network and water.

The Eq. (1-5) shows that the relaxation time is proportional to the square of the gel radius and inversely proportional to the collective diffusion coefficient of the hydrogel, which is dependent on the inner structure of the polymer network.[123],[124]

1.2.5. Thermal responsive hydrogels with different structures

The pNIPAm based gels are used for drug delivery systems, separation operation in biotechnology, processing of agriculture products, sensors and actuator. However the pore size of a conventional pNIPAm hydrogel (homogeneous gel) is relatively small and its response to thermal cycling is relatively slow. In these applications, a fast response rate of the hydrogel to the external stimuli is needed. In order to increase the response rate of pNIPAm gels, several techniques were proposed:

1. Submicrometer-sized particles[125],[124]:as described by equation (1-5) that the rate of response is inversely proportional to the square of the size of the gel, small pNIPAm particles will repond to the external stimuli more quickly than bulk gels.
2. Macroporous pNIPAm gels: the kinetics of gel volume change involves absorbing or desorbing solvent by the polymer network, which is diffusive process. As described by equation (1-5) that the rate of response is proportional to the diffusion coefficient, the macroporous gel with larger diffusion coefficient will show faster response rate, because for a network having an interconnected pore structure, absorption or desorption occurs through the pores by convection, which is much faster than the diffusion process that dominated the non-porous gels.
3. Gels with microgel particles (GPs) embedded (plum-pudding gel): The structure of plum-pudding gel, with the chains of the network passing through the pores of the GPs, combined with the sponginess and rapid shrinking properties of the pNIPAm GPs seemed like a possible mechanism for speeding up the shrinking process of bulk gels, which are often hampered by the formation of a dense layer

of collapsed polymer on the gel surface which slows down the subsequent shrinking dramatically.

1.2.5.1. Microgel particles (GPs)

A micron- or submicron-sized water swellable gel is referred to as a micro hydrogel particles (GPs). To be classified as a microgel, the size of the swollen particles must reside within the generally accepted colloid range of 1 nm to 10 µm.[78] The overall dimensions of GPs are comparable to the high molecular weight polymers, but their internal structure resembles a typical network.[126],[127] Below the transition temperature, the GPs have sponge-like structures, with the interstitial spaces filled with water. However, when the temperature is increased above the transition temperature, the GPs reversibly shrink and become hard and sphere shaped.[128],[127]

A number of applications of pNIPAm GPs have been developed, benefiting from the fact that their response time to environmental change of GPs is many times faster than that of bulk gels, as well as the much larger surface area-to-volume ratio of GPs, which leads to increased accessibility and higher loading of solutes.[127]

1.2.5.1.1. Preparation of GPs

Mono-disperse GPs of controllable size and crosslink density can be prepared using several methods including (surfactant-free) emulsion polymerization, pseudo-precipitation polymerization or inverse emulsion polymerization.[129]

In the case of pNIPAm GPs preparation by pseudo-precipitation polymerization, the monomers is water soluble but the polymer is less soluble over the

polymerization temperature range usually used. There are good reasons for carrying out the polymerization at high temperature: the radicals, which initiate the polymerization need to be formed. After initiation, the NIPAm monomer is attacked by the radical, there then follows radical propagation and chain growth. Once the chain reaches a critical length, it collapses upon itself producing precursor particles. The chain collapses because the polymerization temperature is higher than the LCST of the polymer, hence the name precipitation polymerization. The precursor particles grow by aggregation with the other precursor particles, by being captured by existing particles, by capturing growing oligoradicals, and by monomer addition. The charge imparted by the initiator or the surfactant stabilizes the microgels once they have reached a critical size. Figure 1-18 shows the proposed mechanism for precipitation polymerization. This method is extremely versatile from the standpoint of particle size control. For example, to synthesize smaller microgels, the precursor particles must be stabilized earlier in the reaction. Since there is not enough charge available from initiator fragments to stabilize small precursor particles, an ionic surfactant can be added to impart colloidal stability earlier in the reaction. Similarly, larger particles can be obtained by decreasing the surfactant concentration. The temperature at which the reversible swell-shrink of hydrogel occurs is called volume phase transition temperature (VPTT), which is consistent with the LCST of the polymers. [129]

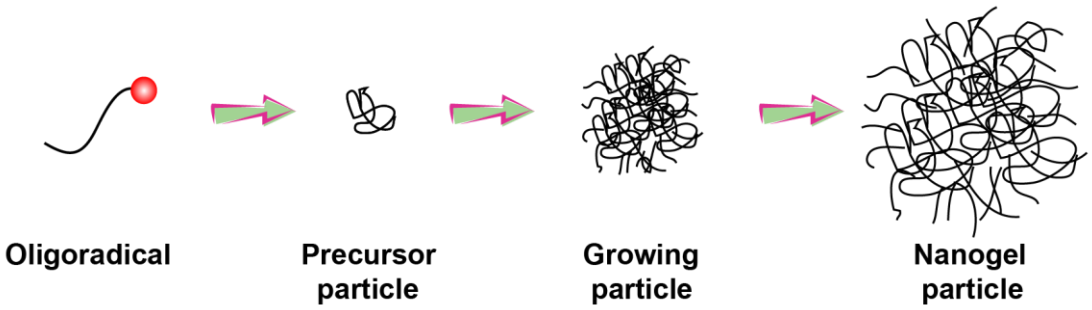

Figure 1-18. Precipitation polymerization of colloidal micro or nanogels from phase separating polymers.

The polymerization is termed surfactant-free precipitation polymerization when the polymerization is carried out in the absence of surfactant. The precursor particles are stabilized by the charged initiator fragments that reside at the particle surface. In this case, an aggregation step occurs during particle growth and this results in a larger average particle size than the GPs prepared in the presence of surfactant. The GPs of lowest dispersity are usually prepared by surfactant-free precipitation polymerization.[129]

Precipitation polymerization can also be used to incorporate comonomers in the GPs. For example, to copolymerize ionic monomers with pNIPAm to create pH-responsive GPs,[81],[107],[108],[109] to copolymerize a hydrophobic comonomer *N*-tert-butylacrylamide (TBAm) to give pH and temperature responsive GPs; these particles exhibit phase transitions at lower temperatures owing to the increase in hydrophobicity of the gel while retaining a pH-tunable VPTT.[109] Similarly, other functionalities can also be copolymerized into these GPs by this method.[78]

Precipitation polymerization has a few drawbacks. First, the method is useful only for materials that are stable at high temperatures and therefore cannot be used to incorporate biological macromolecules. Also the method is suitable for hydrophobic materials so that they can attach to the collapsed precursor particle

easily. Therefore, if a hydrophilic comonomer is to be copolymerized, only a certain percentage can be incorporated. Beyond that low incorporation percentage, the growing oligomer will be too hydrophilic to undergo efficient chain collapse, thereby resulting in a relatively polydisperse GP dispersion, or the complete failure to form GPs.[78]

To overcome these hurdles, researchers have developed the inverse micro-emulsion polymerization. In this method, aqueous solution of all the monomers is added to an appropriate amount of oil and surfactant and is stirred to form thermodynamically stable micro-emulsions. Polymerization can be initiated by having the initiator in the aqueous phase or in the oil phase. This method has been used to synthesize GPs with high content of ionic monomers and/or zwitterions.[78], [130], [131]

One other method for preparing GPs, which is similar to micro-emulsion polymerization, utilizes lipids to form liposomes inside which the GP is formed. [132],[78]

1.2.5.1.2. Structure of GPs

A concerted effort has been made in the literature to determine the structure of pNIPAm GPs crosslinked with *N,N'*-methylenebis(acrylamide) (Bis). It is reported that these crosslinked pNIPAm GPs typically show a radial distribution of cross-links in the GPs, with the highest cross-linker concentrations residing at the GP interior (see figure 1-19). [133]-[137] Heterogeneities in GP structures are often caused by the mismatched reactivity ratios for monomer and crosslinker during precipitation polymerization, where the reactivity ratio is a measure of the propensity of a monomer to propagate by reacting with itself or a different

monomer in the synthetic mixture.[135] It is found that during the GP formation, the crosslinker Bis was consumed faster than NIPAm and therefore preferentially incorporated into the particles.[133],[134],[135],[136] Because pNIPAm GPs are prepared at above their VPTT, it is reasonable to expect the central regions of the final GPs to contain a relatively high percentage of the monomers consumed in the early stages of the polymerization. Thereby, there is considerable opportunity for the development of an inhomogeneous structure within the interior of pNIPAm GPs.

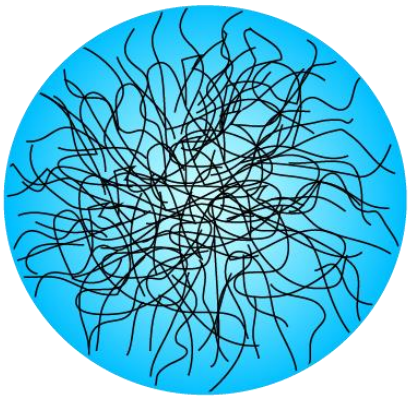

Figure 1-19. Schematic of heterogeneous hairy structure of p(NIPAm/Bis) GPs.

1.2.5.1.3. Thermal responsive kinetics of GPs

$$\tau = \frac{R^2}{\pi^2 D} \qquad \text{Eq. (1-5)}$$

The equation shows that the relaxation time of phase transition process of a thermal responsive gel is proportional to the square of the gel radius and inversely proportional to the diffusion coefficient of the polymer network.[123],[124] Therefore the GPs are expected to show a much shorter relaxation time due to the small dimension.

Lyon's group have studied the swelling kinetics of the GPs after temperature

jump (T-jump).[138] To induce a T-jump in a solution of pNIPAm particles on nanosecond time scale, a heating pulse centered at 1.9 μm (an energy where the polymer is transparent but the solvent D_2O is absorptive) was employed. The initial temperature was thermos-stated at 30 ℃, just below the VPTT (~34 ℃) of the GP. Upon introduction of the infrared laser pulse, a temperature jump of about 10 ℃ is induced within the first 20 ns, thereby causing the local temperature to rise above the LCST of the GPs. Figure 1-20 shows a typical time-dependence of the T-jump-induced transmittance change of pNIPAm GPs. A decrease in the solution transmittance is apparent approximately 600 ns after the introduction of the laser pulse.

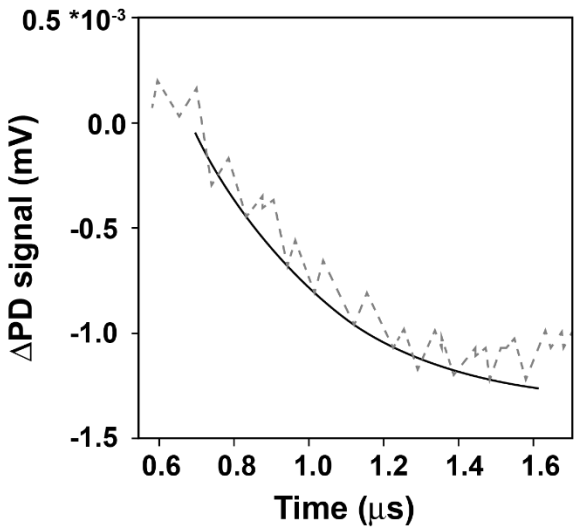

Figure 1-20. Representative time-dependence of the T-jump-induced transmittance change observed at 633 nm of pNIPAm GPs in D_2O. The particle collapse process can be fit to a single-exponential decay, with a formation time τ, of 0.39 μm. [138]

The clear transmittance change was not observed neither when the T-jump did not traverse the VPTT, nor from the pure solvent without GPs, suggesting the

observed decrease in the transmittance can be attributed to an increase in the solution turbidity associated with the shrinking of the GPs. [138] Curve fitting of the transmittance change shows a single exponential process, with an apparent formation time (τ) of 0.39 μs. [138]

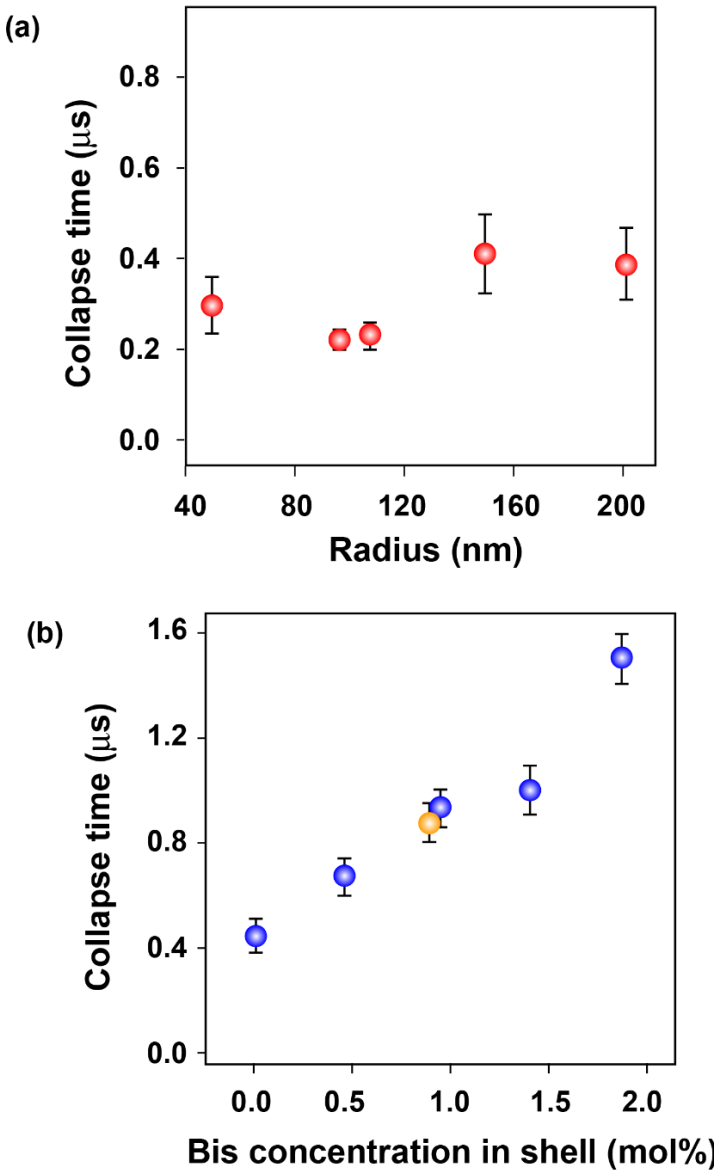

Figure 1-21. (a) Dependence of the collapse time, t, on the radius of the pNIPAm hydrogel nanoparticle. (b) Dependence of the collapse time on the Bis concentration in shell for a series of pNIPAm (core)/pNIPAm-co-Bis (shell). The orange data represents the particle with equal concentrations of Bis in both core and shell. [138]

To interrogate the influence of GP dimension on collapse rate, Lyon's group also prepared a series of pNIPAm GPs with various sizes (50 - 200 nm) containing a 5 mol % cross-linking density. Figure 1-21a shows the T-jump induced collapse time (τ) as a function of the GP size. The collapse time of the smaller GPs was shorter than the larger ones, though the difference is small (0.2 ~ 0.4 μs).

In addition, they found the collapse rate of the highly crosslinked GPs is slower than the slightly crosslinked ones (see figure 1-21b).

1.2.5.2. Macroporous gels

Hydrogels with pore sizes significantly larger than those of conventional hydrogels are referred to as "macroporous" hydrogels. They are characterized by large pore sizes, high pore volumes, and high specific surface area.[139]

1.2.5.2.1. Synthesis of macroporous gels

Currently the most well know method is to polymerize the macro-porous pNIPAm gel is to carry out the polymerization above LCST. The macroporous gels were also synthesized above their LCST in the presence of porogens such as hydroxypropyl cellulose (HPC)[139], poly(ethylene glycol) (PEG)[140], sucrose[141] to control the pore size and size distribution. The macroporous gel can also be prepared by polymerization of the monomer and crosslinker in the presence of a suitable quantity of silica particles with a polyhedral shape (particle size 3.3 μm) and the subsequent acid extraction of the silica. (Macromolecules, 2002, 35, 10). Macro-porous pNIPAm gel can also be prepared in NaCl solution at room temperature because LCST of pNIPAm will be decreased in the presence of

NaCl.[142]

It's now well understood that a phase separation during the polymer network formation process is mainly responsible for the formation of porous structures in a dried state. [143],[144],[145],[146] In order to obtain macroporous structures, a phase separation must occur during the course of the crosslinking process so that the two-phase structure is fixed by the formation of crosslinks. Depending on the synthesis conditions, phase separation can take place on a macroscale or on a microscale.[147]

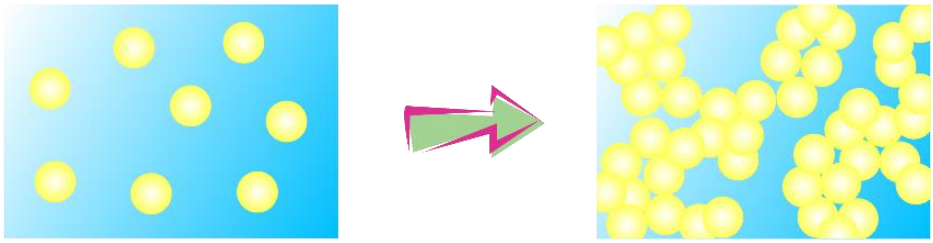

Figure 1-22. Schematic representation of phase separation during on macroscale crosslinking copolymerization of macroporous gels.

In the first case, the gel collapses at the critical point for phase separation and becomes a microsphere, whereas the separated liquid phase remains as a continuous phase in the reaction system[147] (figure 1-22 left). As the reaction proceeds, new microspheres are continuously generated due to the successive separation of the growing polymers. Agglomeration of microspheres leads to the formation of a macro-porous network consisting of two continuous phases (figure 1-22 right).[147]

The formation processes of macroporous networks derived from the monomers acrylamide[148], glycidyl methacrylate[149] and 2-hydroxyethyl methacrylate[150],[151] were also widely investigated.

1.2.5.2.2. Structure of macroporous gels

The structure of the pNIPAm-based conventional homogeneous gel and the macroporous gels prepared at higher temperature above LCST is schematically shown in figure 1-23.

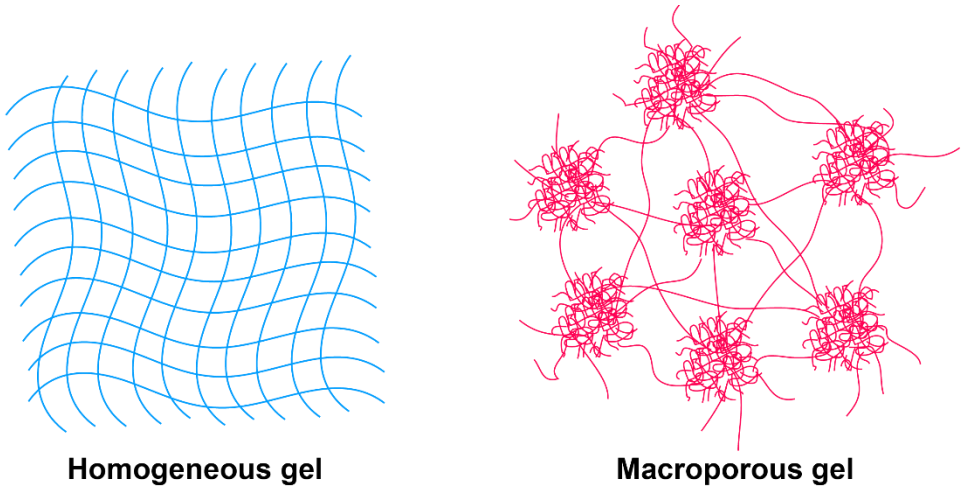

Figure 1-23. Structural illustration of homogeneous gel and macroporous gel.

The structure of pNIPAm macroporous hydrogels synthesized above their LCST (at 50°C) and homogeneous hydrogel synthesized from the same monomer solution at room temperature are compared. [139] The monomer concentration is 18 wt%, among which Bis crosslinker accounts for 2.5 mol%. After synthesis, the gels were cut into discs (20 mm in diameter and 2 mm in thickness). The gel discs were purified by sufficient washing by deionized water.

Pore size distribution of the gels were clarified by the permeation of FITC-dextran with different molecular weight into the gels. Clearly, figure-1-24 shows the macroporous pNIPAm hydrogel possesses a larger fraction of accessible pores than the homogeneous hydrogel does, especially for the larger probing molecules.[139]

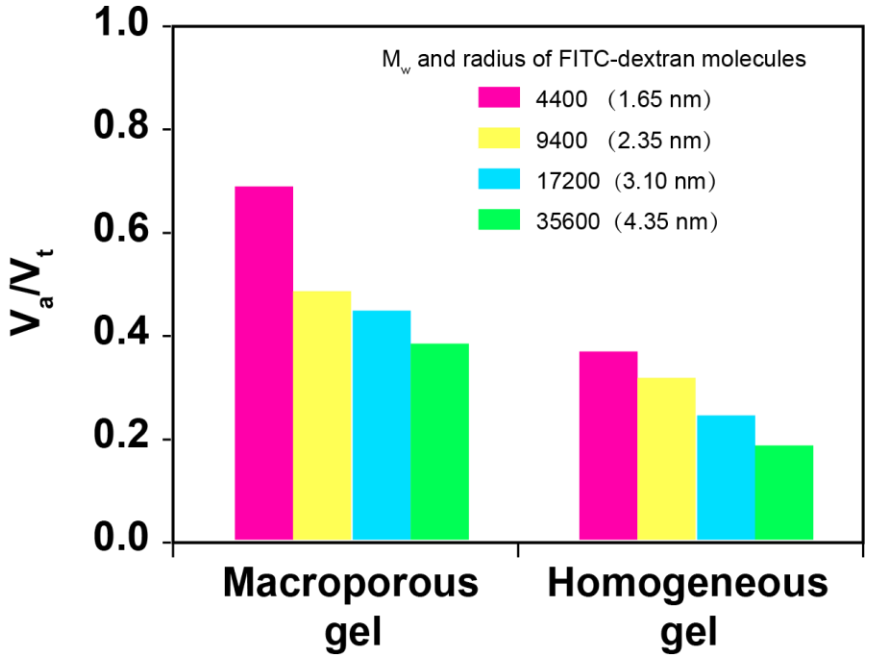

Figure 1-24. Pore size distribution in macroporous and homogeneous pNIPAm hydrogels. [139]

1.2.5.2.3. Thermal responsive kinetics of the macroporous gels

(a) Swelling ratio and LCST behavior

Figure 1-25 shows the equilibrium swelling ratio, which is defined as the swollen weight over the dry weight of a hydrogel as a function of temperature. The LCST of the macroporous pNIPAm hydrogel is almost the same as that of the homogeneous hydrogel. The larger pores in the macroporous hydrogels do not influence the LCST of the polymer network. The swelling ratio of macroporous hydrogel is apparently larger than that of the homogeneous hydrogel at temperatures below the LCST, due to their porous structure. [139]

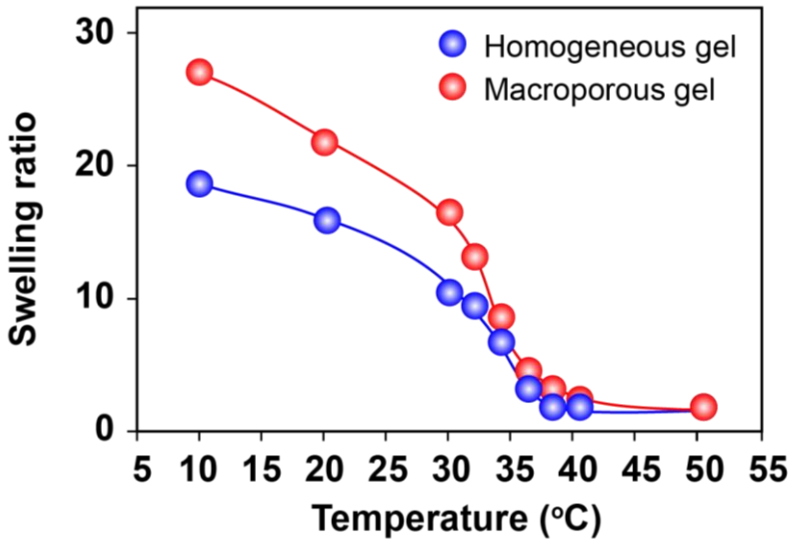

Figure 1-25. Temperature dependence of equilibrium swelling ratio of macroporous and homogeneous pNIPAm hydrogels. [139]

(b) Deswelling kinetics and reswelling kinetics

The deswelling kinetics of macroporous and homogeneous hydrogels are shown in figure 1-26a. The macroporous hydrogel shrinks to the equilibrated water content in only a few minutes, which is at least 10-fold faster than that of the homogeneous hydrogel. [139] The reason is still the presence of large pores and the highly open network mesh structure, which allows rapid collapse of the relatively few polymer "tie chains". When the homogeneous hydrogel shrinks, a dense skin forms at the hydrogel surface, which was observed as an opaque coating on the surface of homogeneous gel, but not on macroporous gel.[139] Highly porous hydrogels do not tend to form such a skin: during shrinking, the larger pores cannot close up, maintaining a channel to the center of the hydrogel that permits rapid mass transfer. This skin layer acts as a barrier to prevent the release of internal water. Therefore, when the macroporous hydrogel is heated above its LCST and collapses, the channels formed by the collapsed larger pores still allow

water to be squeezed out quickly without formation of a contiguous skin layer. [139]

The reswelling kinetics of macroporous and homogeneous pNIPAm hydrogels are shown in figure 1-26b. The macroporous hydrogel swells faster than the homogeneous hydrogel. The existence of large pores in the macroporous hydrogel increase the water-contacting area of the macroporous hydrogel, therefore, the water penetration into the interior of macroporous gel is faster than that of the homogeneous hydrogel. [139]

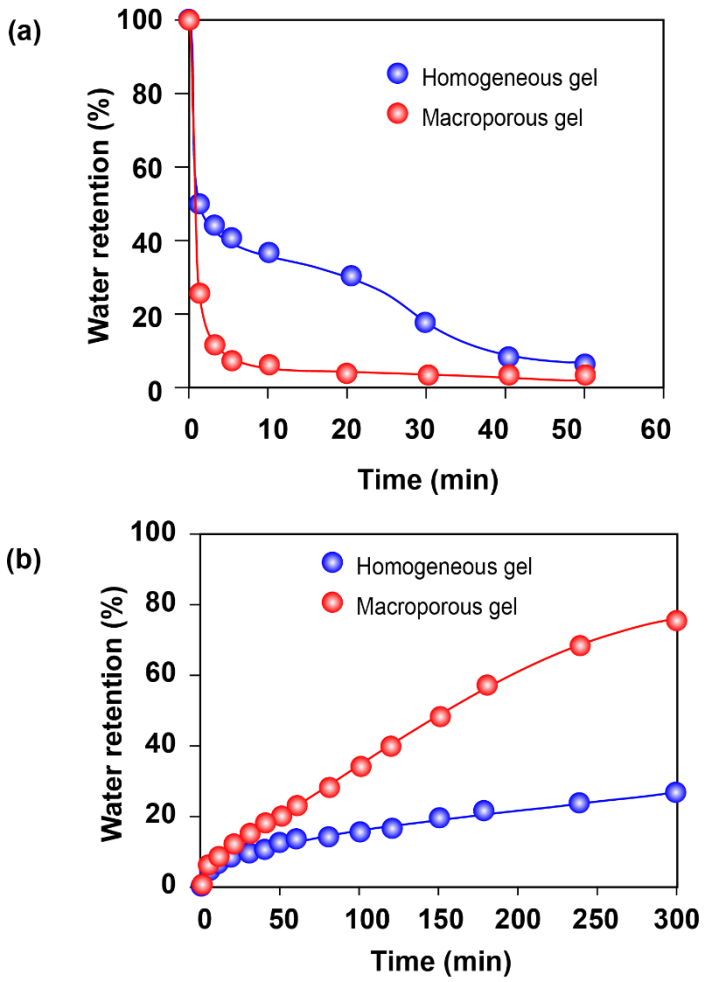

Figure 1-26. (a) Deswelling kinetics and (b) Reswelling kinetics of macroporous and homogeneous pNIPAm hydrogels. (gel dimension: 20 mm diameter, 2 mm thickness). [139]

By comparing the deswelling (figure 1-26a) and reswelling kinetics (figure 1-26b), it can be seen that the time scales are much faster for the collapse than the reswelling process. This is probably because, in the swelling process, the process for the aggregated chains to break their hydrophobic interactions and rehydrate is slower, compared to the collapse process where the free and hydrated chains are in a much more mobile state. [139]

In conclusion, the macroporous pNIPAm hydrogel have large pore volumes, large average pore sizes, and faster macromolecule permeation rates in comparison to homogeneous pNIPAm gels. The macroporous hydrogels have higher swelling ratios at temperatures below the LCST and exhibit faster deswelling and reswelling rates. The deswelling rates are especially rapid. [139]

1.2.5.3. "plum-pudding" gel

It has been realized that the pNIPAm GPs and macroporous gels provide useful properties for applications due to their rapid response to environmental change. Much scientific effort is currently being devoted to develop hydrogel systems for better applications.[127]

On the other hand, the current idea of using the same polymeric material to provide both functionality (fast responsibility) and simultaneously mechanical strength (durability, drag, compliance, etc.) is extremely limiting, as in general materials which response to their environment fast are mechanically poor, while materials with good mechanical properties do not provide the necessary functionality.[127] Thus, what appears to be missing to date is simple and cohesive structural motif that can be applied to an extensive range of applications, and which combines the concepts of functionality and mechanical strength.

Dawson's group has developed a simple composite gel structure, which is called the plum-pudding gel. [127] In this structure, pNIPAm GPs are incorporated into the network of a conventional bulk gel. The GPs were dispersed in the secondary monomer solution homogeneous and then initiate the gelation of the secondary network at temperature below VPTT.

The basic structural motif is to embed responsive GPs in a bulk gel medium. [127] Via varying the stimulus to which the GPs response, a vast range of materials can be designed and tailored to specific applications. By altering the nature of the bulk gel, materials with diverse mechanical properties can be prepared, and issues such as compliance can be considered.

1.2.5.3.1. Structure of plum-pudding gel

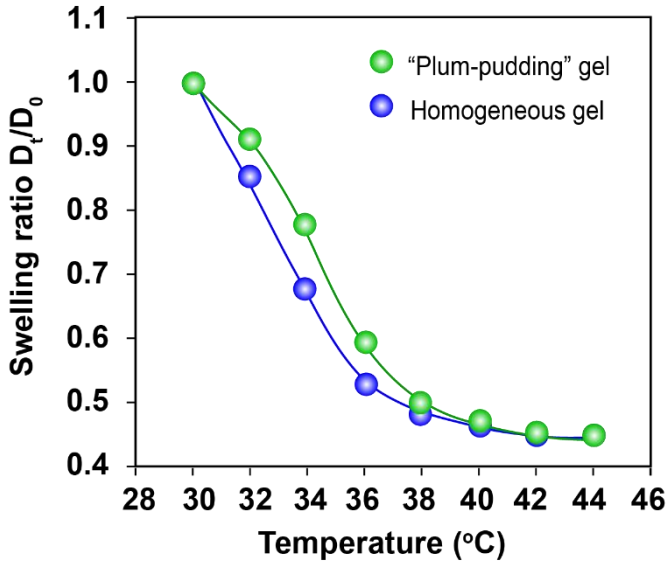

Figure 1-27. Comparison of the equilibrium shrinking curves of homogeneous gel and the "plum-pudding" gel containing 20 mol% of pNIPAm particles. [127]

Dawson's group has sufficiently studied the properties of plum-pudding gel. [127] The degree of swelling of the bulk gel and the plum-pudding gel as a function of

temperature is compared in figure 1-27. It is clear that there is no significant change in the swelling degree. Thus on the macroscopic scale, the presence of the GPs did not alter the network structure, as swelling is extremely closely related to network structure.

Due to the large swelling degree of the pNIPAm GPs at 20 °C (below the VPTT), it is supposed that the growing chains of the secondary network are essentially unaware of the presence of the GPs, and thus the GPs have essentially no effect on the gelation process, and therefore on the structure of the resulting gel. The structure of the composite plum-pudding gel is confirmed by laser scanning conforcal microscope (LSCM) and by dextran molecule exclude experiment, [127] that the network chains pass though the swollen GPs and thus the GPs become constrained within the gel. A schematic of this structure is given in figure 1-28a.

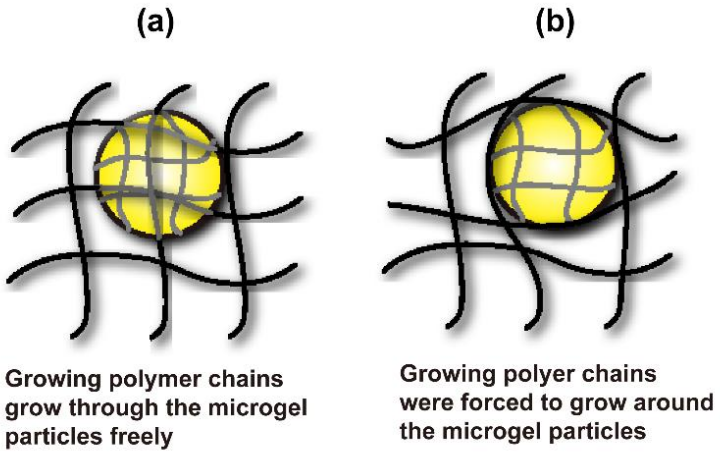

Figure 1-28. Schematic representation of the proposed internal structure of the "plum-pudding" gel.

1.2.5.3.2. Swelling kinetics of plum-pudding gel

Two distinct shrinking patterns were found, depending on the depth of the temperature jump.[127] T* was defined to be the temperature at which the gel first

reaches the fully collapsed state. The shrinking behavior was found to depend on whether the final temperature after the T-jump (T_f) was above or below T*.

In the case of $T_f < T^*$, the gel collapses exponentially with time, the shrinking process occurs simply by network diffusion, and the network has time to rearrange as it is never far out of equilibrium. Thus the shrinking occurs in a single step. There was no shape distortion, and no appearance of opacity. [127]

However, in the case of $T_f > T^*$, the gel collapses in two distinct steps. [127] The first step is a rapid initial shrinkage, which is also due to network diffusion. However, due to the fact that the gel is far from equilibrium, the outer gel layers respond faster than the internal gel, resulting in the formation of a dense layer of collapsed gel at the surface of the gel. This is evidenced by the appearance of opacity, and it prevents the internal water from being released and slows down the shrinking process. As the internal water tries to escape, there is a buildup of pressure inside the gel, which manifests itself as bubbles appearing on the gel surface. The second shrinkage stage is the slow relaxation of the gel to its equilibrium size, and is seen as the gradual disappearance of the opacity, which begins from the edges. [127] The shrinking process after T-jump to $T_f > T^*$ is shown in the photograph series in figure 1-29a-d.

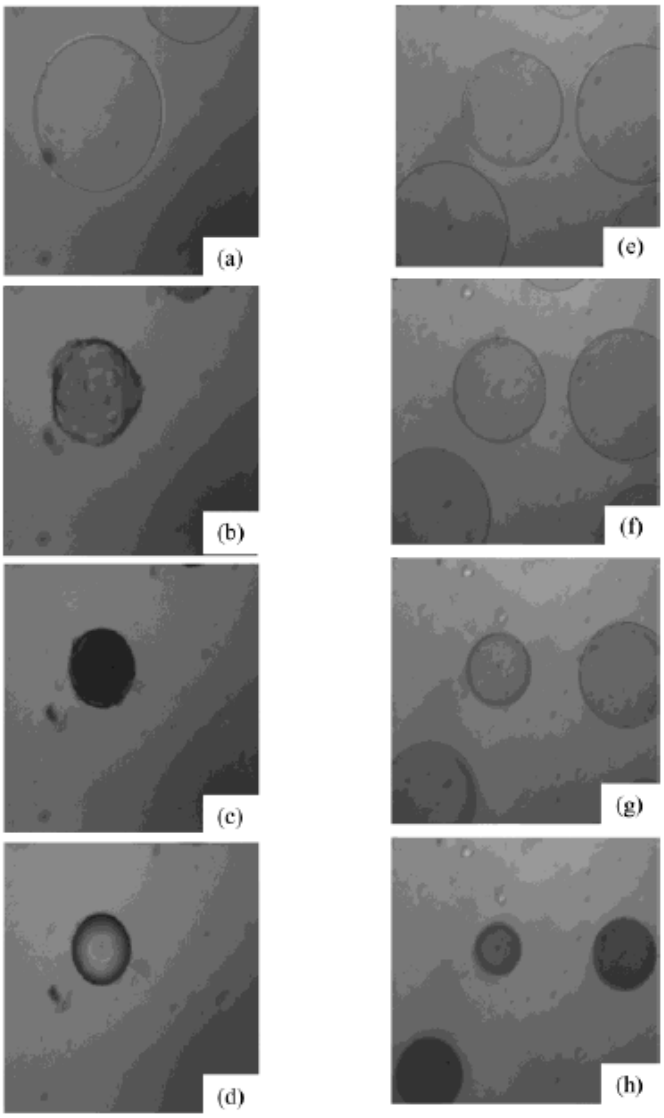

Figure 1-29. Photographs showing the shrinking for the gels following T-jumps from 30 to 38 °C. Bulk homogeneous gel: (a) 0, (b) 10, (c) 30 and (d) 850 s. Plum-pudding gel containing 20 mol% of pNIPAm GPs: (e) 0, (f) 5, (g) 20 and (h) 50 s. [127]

The exponential shrinking profile of the bulk gel and the plum-pudding gel comprising 20 mol % of pNIPAm GPs after T-jumps to 34 °C (< T*) are shown in figure 1-30. Clearly, the presence of the pNIPAm GPs enhances the shrinking rate, since the plum-pudding gel shrinks more than the bulk gel.

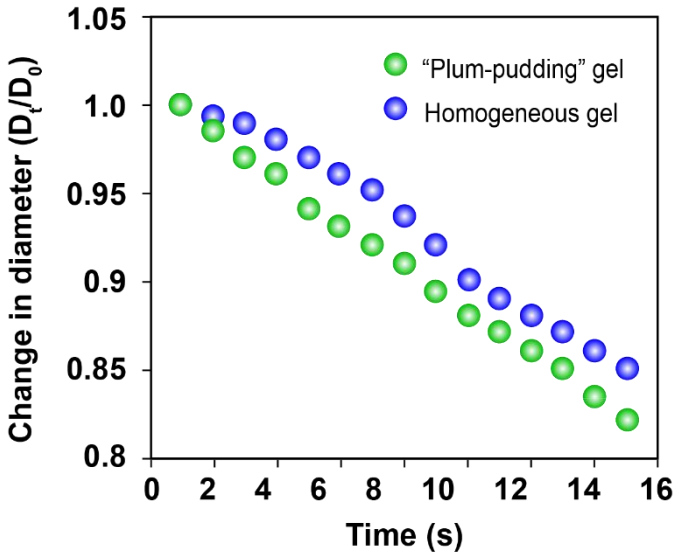

Figure 1-30. Initial rapid shrinking of the homogeneous gel and the "plum-pudding" gel with 20 mol% pNIPAm particles following T-jump from 30 to 34 °C. [127]

The shrinking data confirm that the presence of the responsive GPs reduces the impact of skin-layer formation on the shrinking of bulk gels, resulting in faster shrinking times.[127] Where $T_f < T^*$ the shrinking of the plum-pudding gel remained exponential but was slightly faster than that for the bulk gel. The reason for this is that the collapse transition temperature of the GPs has not been reached and so they do not undergo full collapse, but only shrink slightly. However, due to their extreme sponginess, they still responded to changes in their surroundings faster than the surrounding network, and due to the structure of the composite gel, where the network chains pass through the GPs, the rapid shrinking of the GPs pulled the associated network with them as they adjusted to the new temperature.

The shrinking profiles of the bulk gel and the plum-pudding gel containing 20 mol % of pNIPAm GPs after T-jumps to 38 °C (> T*) are shown in figure 1-31. Here, there is not much difference in the shrinking rate during the first initial burst of shrinking, but during the second slower shrinking stage the presence of the pNIPAm GPs clearly enhances the rate of shrinking. Thus, as well as achieving rapid, continuous collapse, addition of GPs prevents the formation of the dense layer of collapsed gel at the surface.

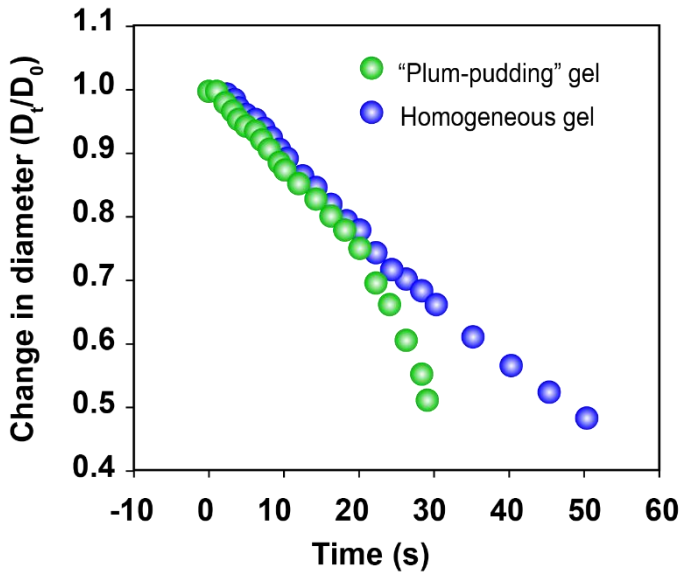

Figure 1-31. Shrinking profiles of the homogeneous gel and the "plum-pudding" gel with 20 mol% pNIPAm particles after T-jump from 30 to 38 °C.

The most dramatic increase in the shrinking time of the network resulted from T-jumps to temperatures above T*. Here, the entire network underwent dramatic and rapid shrinking. Again this was due to the sponginess of the GPs, which underwent a rapid phase transition, and the structure of the composite gels. The shrinking of the GPs results in local regions of collapsed hydrophobic polymer appearing throughout the gel (as opposed to just at the surface in the case of skin-layer formation). These hydrophobic regions cause the entire network to collapse

rapidly, as a result of the hydrophobic effect, in combination with the effect of the shrinking GPs pulling the associated network polymer with them as they collapse. Due to the fact that the plum-pudding gels shrink more rapidly than the model gel, more water is expelled during the initial shrinking stage, and thus the skin layer that forms is much less dense than that in the case of the model gel, and there is no appearance of bubbling during the shrinking process.

1.2.5.4. Other structures of hydrogel

Several other approaches to faster shrinking kinetics have also been reported in the literature, for example, gels having dangling chains[152],[153],[154]: Dangling chains in a gel easily collapsed or expand upon an external stimulus because one side of the dangling chain is free. pNIPAm gels incorporated with long chains of polyacrylamide[155] or poly(ethylene oxide) channels[156], which acted as water-release channels, have also been designed to speed up the shrinking process.

1.3. About this study

The accumulation of CO_2 in atmosphere caused by the burning of fossil fuels has caused serious climate change.[2] Meanwhile the CO_2 can be a carbon source to produce liquid fuels such as methanol and dimethyl ether. [157] Thus the sorption of CO_2 from the main emission sources such as fire power plants is essential to mitigate the greenhouse effect and to generate the carbon based energy.

Currently the most commercialized CO_2 recovery method from the humid exhaust gases of fire power plants is absorption by using aqueous solution of small molecule amines such as MEA. In this process, CO_2 in exhaust gas is selectively absorbed at low temperature, and desorbed by heating the solution to a high temperature, typically above 140 °C. [158],[159],[160] Though the aqueous amine solution showed large CO_2 capture capacity, the high energy consumption make them less attractive. [159],[160],[161],[162],[163]

As an alternative for the aqueous amine solution, the porous solid materials such as activated carbons, the metal-organic frameworks (MOFs) were developed. The CO_2 is selectively bounded on the surface of the adsorbents via physical or chemical interaction, and then can be released in a relatively mild condition. ,[164],[165],[166],[68] However the intrinsic property of porous materials make them negatively affected by the water gases, because the water gases will compete with the CO_2 to be adsorbed on the pore surface, and the liquefied water will block the small pores and the capillaries. [39],[165],[166]

Thus it's of great importance to develop a CO_2 sorbent that is capable of working in wet environment and being regenerated at a relatively lower temperature (< 100 °C).

In order to achieve this goal, we studied the efficient CO_2 transport in blood. In the case of reversible CO_2 absorption by the blood of animals, the pK_a value of the

Brønsted acid and base in the hemoglobin plays a crucial role for the control of CO_2 solution equilibrium (see figure 1-32): The pK_a value of the ammonium and imidazolium cations decreases due to the drastic conformational change of the hemoglobin caused by oxygen binding to the heme. The shift of the pK_a triggers the release of H^+ into the blood, leading to the release of CO_2 efficiently from lungs (Bohr effect).[167]

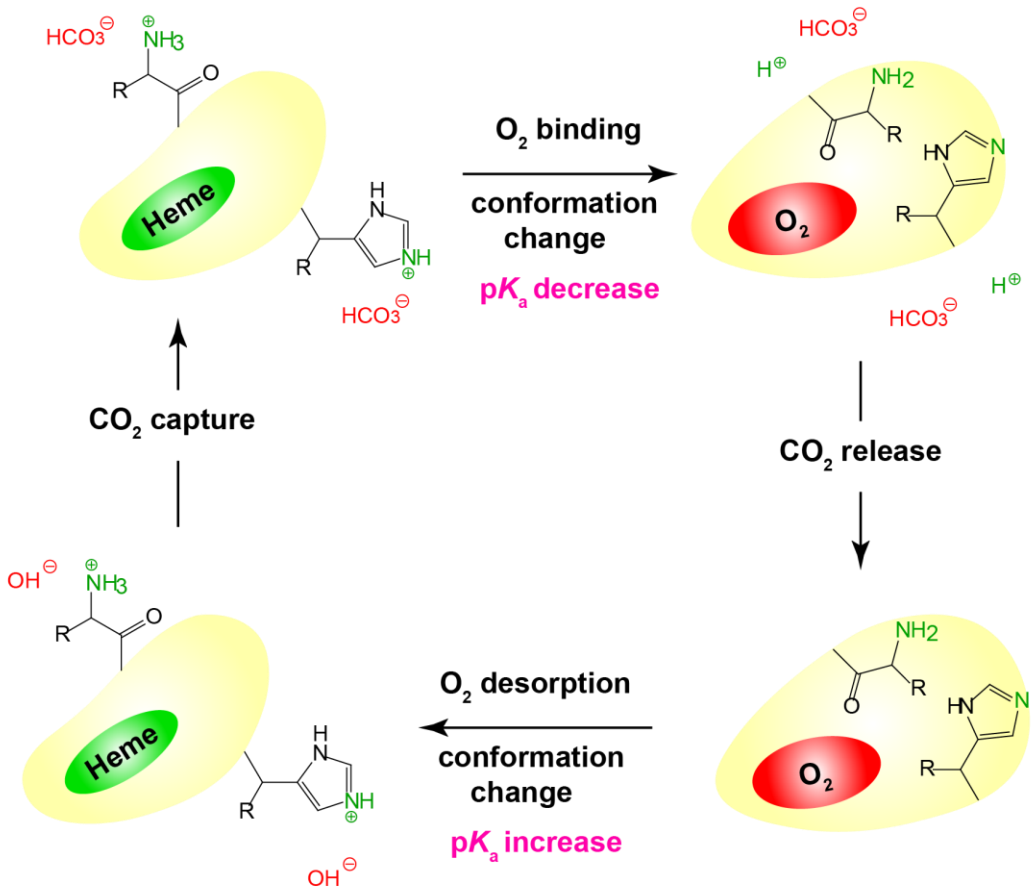

Figure 32. Schemetic illustration of Bohr effect of hemoglobin.

Inspired by the Bohr effect, it is expected that the conformation change of amine-incorporated thermal responsive GPs can also be used for the efficient CO_2 capture and release. The proposed mechanism was shown in figure 1-33. At low

temperature below the VPTT, the GPs are hydrophobic and swollen. The amine groups in the GPs are located in a microenvironment with small steric hindrance and high dielectric constant, therefore exhibiting high basicity and high pK_a value that is comparable to the amines in aqueous solution. As a result, the acidic gas CO_2 can be capture effectively by the strong base. However, when the temperature is increased above the VPTT, the GPs become hydrophobic and shrink, subsequently the steric hindrance around the amines increases, and the dielectric constant decreases. Therefore the pK_a value of the GPs decrease. As a result the captured CO_2 can be released and the GPs can be regenerated.

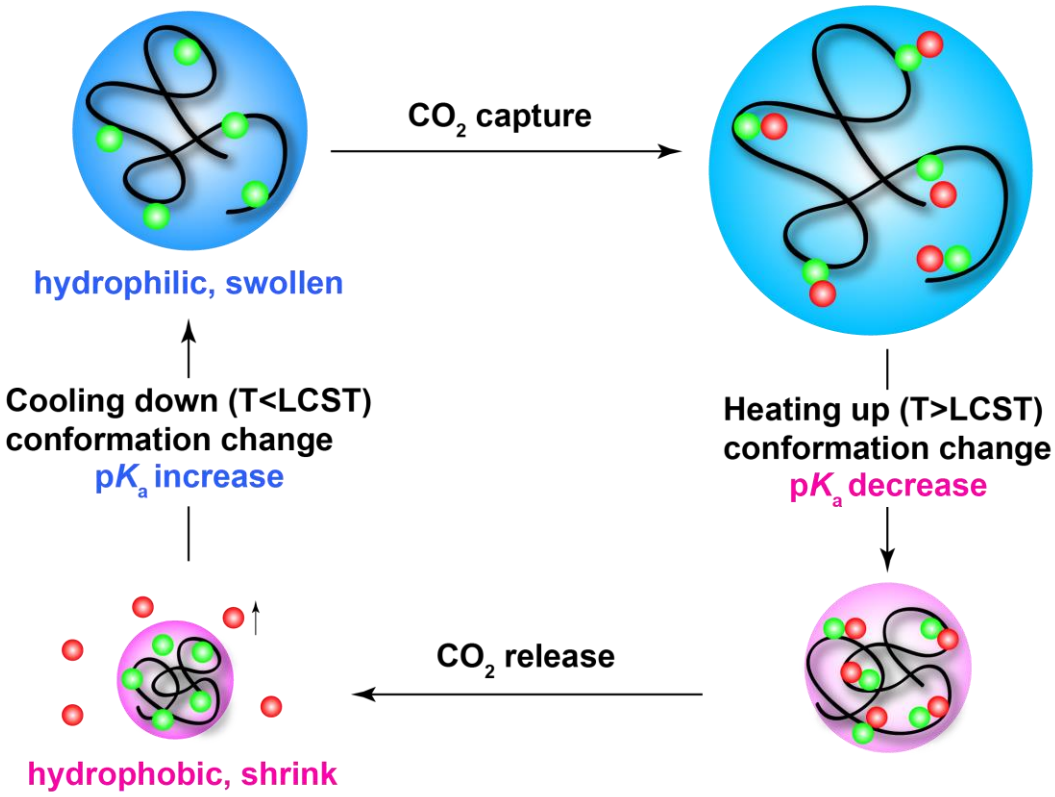

Figure 1-33. The proposed mechanism of reversible CO_2 capture and release by amine-functionalized thermal responsive GPs in temperature swing process.

According to the proposed mechanism, recently we have developed the aqueous solution of pNIPAm based thermal responsive mirogel particles (GPs) consisting of the tertiary amine *N*-[3-(dimethylamino)propyl]methacrylamide (DMAPM) as CO_2 absorbents to reversibly capture and release CO_2 from humid condition in a small temperature change (30-75 °C).[168] At 30 °C that below the VPTT of the GPs, most amines in the swollen GPs show stronger basicity and are capable of capture CO_2. While at 75 °C that above the VPTT, the collapse of the GPs caused the amines more hindered, lowering down the basicity, as a result the CO_2 was released. Figure 1-34b and c show that the GP solution exhibited excellent CO_2 capture stoichiometry (~1 mol CO_2/mol amine) and reversibility, in the small temperature change.

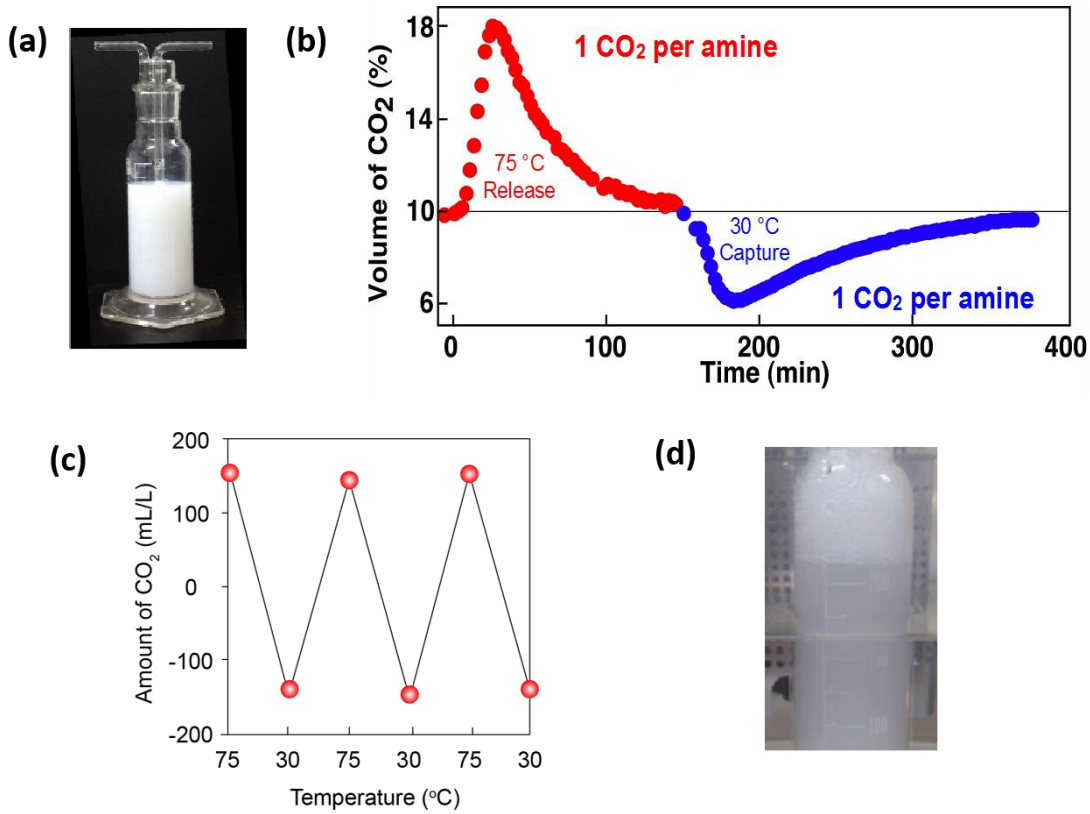

Figure 1-34. (a) Photograph of DMAPM-functionalized pNIPAm-based GP solution before CO_2 absorption. (b) CO_2 capture and release by the GP solution. (c)

Repeatability of CO_2 capture and release of the GP solution. (d) Photograph of foam formation in the GP solution during CO_2 bubbling.

The regeneration temperature (75 °C) was lower than the aqueous amine solution (> 140 °C), and the GP film are capable of working in highly humid environment. However it's difficult to increase the GP concentration in the solution due to the high viscosity and the drastic formation of foams during CO_2 flowing (see figure 1-34d). Thus the energy consumption of the GP solution in fact was not reduced due to the low concentration (1 mg/mL), despite of the lower regeneration temperature than the aqueous solution of small molecular amine.

In this study, in order to overcome the shortcomings of the GP aqueous solution (the low concentration, high viscosity and the foaming), a new type of CO_2 absorbent—the hydrogel film consisting of the thermal responsive GPs was developed (figure 1-35). The effect of some physical and chemical properties of the GPs, such as the pK_a value, the imprinted microenvironment, the size and the swelling ratio of the GPs on the reversible CO_2 capture stoichiometry was revealed. Thereby the CO_2 capture capacity was maximized. In order to further increase the CO_2 capture capacity per weight, the effect of hydrophobic modification of polyvinylamine (PVAm) that possesses the largest amine content per weight was also studied. Furthermore, the effect of inner structure of gels on the CO_2 capture and release kinetics was also studied.

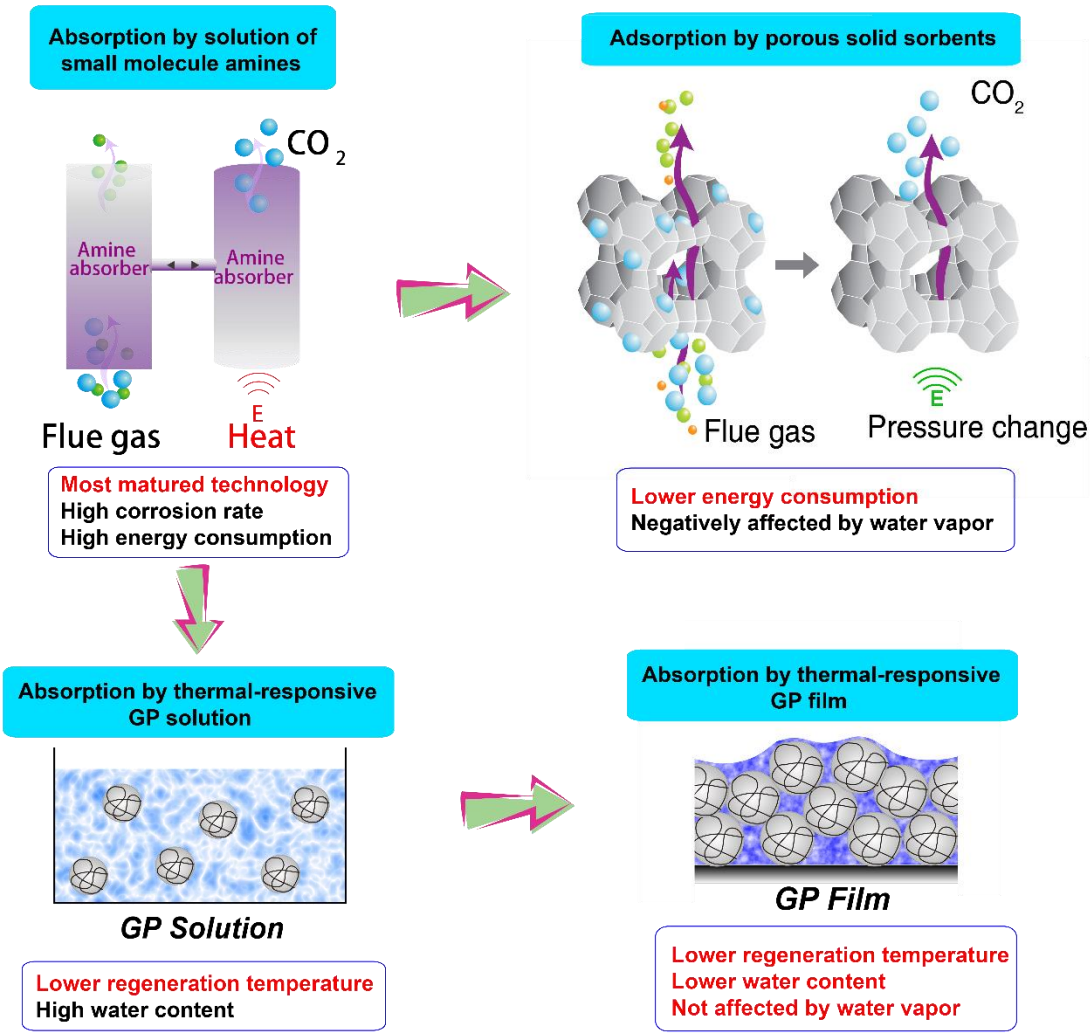

Figure 1-35. Development of thermal responsive GP film as CO_2 absorbent from wet environment.

1.4. References

[1] N. Stern, *Am. Econ. Rev.* 2008, *98*, 1-37.

[2] S. Solomon, D. Qin, M. Manning, Z. Chen, M. Marquis, K. B. Averyt, M. Tignor, H. L. Miller, Eds., *The Fourth Assessment Report of the Intergovernmental Panel on Climate Change* 2007, *Cambridge University Press:* New York, 2007.

[3] T. R. Karl, K. E. Trenberth, *science* 2003, *302*, 1719-1723.

[4] B. Metz, O. Davison, P. Bosch, R. Dave, L. Meyer, *Climate Change 2007: Mitigation of Climate Change, Cambridge University Press: Cambridge,* 2007.

[5] N. Stern, *Stern Review: The Economics of Climate Change, Cambridge University Press: Cambridge,* 2006.

[6] C. Stewart, M.-A. Hessami, *Energy Convers. Manage.* 2005, *46*, 403-420.

[7] B. Metz, O. Davison, H. Coninck, M. Loos, L. Meyer, *IPCC Special Report on Carbon Dioxide Capture and Storage. Prepared by Working Group III of the Intergovernmental Panel on Climate Change, Cambridge University Press: Cambridge,* 2005.

[8] A. A. Olajire, *Energy* 2010, *35*, 2610-2628.

[9] D. M. D'Alessandro, B. Smit, J. R. Long, *Angew. Chem. Int. Ed. Engl.* 2010, *49*, 6058-6082.

[10] R. S. Haszeldine, *Science* 2009, *325*, 1647-1652.

[11] J. D. Figueroa, T. Fout, S. Plasynski, H. McIlvried, R. D. Srivastava, *Int. J. Greenhouse Gas Control.* 2008, *2*, 9-20.

[12] L.I. Eide, D. W. Bailey, *Oil Gas Sci. Technol.* 2005, *60*, 475-484.

[13] V. s. P. o. CCS.

[14] Paul N. Dyera, R. E. Richards, S. L. Russek, D. M. Taylor, *Solid State Ionics* 2000, *134*, 21–33.

[15] A. Yamasaki, *J. Chem. Eng. Jpn.* 2003, *36*, 361-375

[16] H. Yang, Z. Xu, M. Fan, R. Gupta, R. B. Slimane, A. E. Bland, I. Wright, *J. Environ. Sci.* 2008, *20*, 14-27.

[17] C. H. Yu, C. H. Huang, C. S. Tan, *Aerosol Air Qual. Res.* 2012, *12*, 745–769.

[18] E. Sada, H. Kumazawa, M. A. Butt, *Can. J. Chem. Eng.* 1976, *54*, 421–424.

[19] H. Hikita, S. Asai, Y. Katsu, S. Ikuno, *AlChE J.* 1979, *25*, 793–800.

[20] S. Bishnoi, G. T. Rochelle, *AlChE J.* 2002, *48*, 2788–2799.

[21] P. D. Vaidya, E. Y. Kenig, *Chem.Eng.Technol.* 2007, *30*, 1467-1474.

[22] S. Bishnoi, G. T. Rochelle, *Chem. Eng. Sci.* 2000, *55*, 5531–5543.

[23] J. Xiao, C. W. Li, M.H. Li, *Chem. Eng. Sci.* 2000, *55*, 161–175.

[24] C. H. Liao, M. H. Li, *Chem. Eng. Sci.* 2002, *57*, 4569–4582.

[25] S. A. Freeman, R. Dugas, D. H. Van Wagener, T. Nguyen, G. T. Rochelle, *Int. J. Greenhouse Gas Control.* 2010, *4*, 119-124.

[26] S. A. Freeman, J. Davis, G. T. Rochelle, *Int. J. Greenhouse Gas Control.* 2010, *4*, 756-761.

[27] V. Ermatchkov , Á. P. S. Kamps. D. Speyer, G. Maurer, *J. Chem. Eng. Data* 2006, *51*, 1788–1796.

[28] R. Dugas, G. Rochelle, *Energy Procedia* 2009, *1*, 1163-1169.

[29] X. Han, D. W. Armstrong, *Acc. Chem. Res.* 2007, *40*, 1079–1086.

[30] A. Berthod, M. J. Ruiz-Angel, S. Carda-Broch, *J. chromatogr. A* 2008, *1184*, 6-18.

[31] R. D. Rogers, *Nature* 2007, *44*, 917-918

[32] J. F. Brennecke, E. J. Maginn, *AIchE J.* 2001, *47*, 2384–2389.

[33] D. Wappel, G. Gronald, R. Kalb, J. Draxler, *Int. J. Greenhouse Gas Control.* **2010**, *4*, 486-494.

[34] F. Karadas, M. Atilhan, S. Aparicio, *Energy Fuels* **2010**, *24*, 5817-5828.

[35] J. L. Anthony, J. L. Anderson, E. J. Maginn, J. F. Brennecke, *J. Phys. Chem. B* **2005**, *109*, 6366-6374.

[36] E. D. Bates, R. D. Mayton, I. Ntai, J. H. Davis, Jr, *J. Am. Chem. Soc.* **2002**, *124*, 926-927.

[37] Y. Zhang, S. Zhang, X. Lu, Q. Zhou, W. Fan, X. Zhang, *Chem.* **2009**, *15*, 3003-3011.

[38] F. Zhang, C. G. Fang, Y. T. Wu, Y. T. Wang, A. M. Li, Z. B. Zhang, *Chem. Eng. J.* **2010**, *160*, 691-697.

[39] S. Choi, J. H. Drese, C. W. Jones, *ChemSusChem* **2009**, *2*, 796-854.

[40] M. G. Plaza, S. García, F. Rubiera, J. J. Pis, C. Pevida, *Chem. Eng. J.* **2010**, *163*, 41-47.

[41] D. Saha, S. Deng, *J. colloid and interface sci.* **2010**, *345*, 402-409.

[42] A. Ghosh, K. S. Subrahmanyam, K. S. Krishna , S. Datta, A. Govindaraj, S. K. Pati, C. N. R. Rao, *J. Phys. Chem. C* **2008**, *112*, 15704–15707.

[43] S. C. Hsu, C. Lu, F. Su, W. Zeng, W. Chen, *Chem. Eng. Sci.* **2010**, *65*, 1354-1361.

[44] K. S. Walton, M. B. Abney, M. Douglas LeVan, *Microporous Mesoporous Mater.* **2006**, *91*, 78-84.

[45] Q. Wang, J. Luo, Z. Zhong, A. Borgna, *Energy Environ. Sci.* **2011**, *4*, 42-55.

[46] A. Sayari, Y. Belmabkhout, R. Serna-Guerrero, *Chem. Eng. J.* **2011**, *171*, 760-774.

[47] X. Liu, J. Li, L. Zhou, D. Huang, Y. Zhou, *Chem. Phys. Lett.* **2005**, *415*, 198-

201.

[48] Y. Sun, X. W. Liu, W. Su, Y. Zhou, L. Zhou, *Appl. Surf. Sci.* **2007**, *253*, 5650-5655.

[49] T. L. Chew, A. L. Ahmad, S. Bhatia, *Adv. colloid interface sci.* **2010**, *153*, 43-57.

[50] X. B. Russell, E. Morris, *Nat. Chem.* **2010**, *2*, 353-361.

[51] C. T. Kresge, W. J. Roth, *Chem. Soc. Rev.* **2013**, *42*, 3663-3670.

[52] L. Han, S. Che, *Chem. Soc. Rev.* **2013**, *42*, 3740-3752.

[53] R. Lyndon, K. Konstas, B. P. Ladewig, P. D. Southon, P. C. Kepert, M. R. Hill, *Angew. Chem. Int. Ed. Engl.* **2013**, *52*, 3695-3698.

[54] R. J. Kuppler, D. J. Timmons, Q.-R. Fang, J.-R. Li, T. A. Makal, M. D. Young, D. Yuan, D. Zhao, W. Zhuang, H. C. Zhou, *Coord. Chem. Rev.* **2009**, *253*, 3042-3066.

[55] J. R. Li, Y. Ma, M. C. McCarthy, J. Sculley, J. Yu, H. K. Jeong, P. B. Balbuena, H. C. Zhou, *Coord. Chem. Rev.* **2011**, *255*, 1791-1823.

[56] X. Xu, C. Song, B. G. Miller , A. W. Scaroni, *Ind. Eng. Chem. Res.* **2005**, *44*, 8113–8119.

[57] X. Ma, X. Wang, C. Song, *J. Am. Chem. Soc.* **2009**, *131*, 5777–5783.

[58] A. Sayari, Y. Belmabkhout, *J. Am. Chem. Soc.* **2010**, *132*, 6312–6314.

[59] W. J. Son, J. S. Choi, W. S. Ahn, *Microporous Mesoporous Mater.* **2008**, *113*, 31-40.

[60] C. Chen, W. J. Son, K. S. You, J. W. Ahn, W. S. Ahn, *Chem. Eng. Jo.* **2010**, *161*, 46-52.

[61] M. B. Yue, Y. Chun, Y. Cao, X. Dong, J. H. Zhu, *Adv. Funct. Mate.* **2006**, *16*, 1717-1722.

[62] M. B. Yue, L. B. Sun, Y. Cao, Y. Wang, Z. J. Wang, J. H. Zhu, *Chem. Eur. J.* **2008**, *14*, 3442-3451.

[63] M. G. Plaza, C. Pevida, A. Arenillas, F. Rubiera, J. J. Pis, *Fuel* **2007**, *86*, 2204-2212.

[64] M. G. Plaza, C. Pevida, B. Arias, J. Fermoso, A. Arenillas, F. Rubiera, J. J. Pis, *J. Therm. Anal. Calorim.* **2008**, *92*, 601-606.

[65] Y. Belmabkhout, G. De Weireld, A. Sayari, *Langmuir* **2009**, *25*, 13275-13278.

[66] Y. Belmabkhout, A. Sayari, *Energy Fuels* **2010**, *24*, 5273-5280.

[67] A. S. Peter J. E. Harlick, *Ind. Eng. Chem. Res.* **2006**, *45*, 3248-3255.

[68] P. J. E. Harlick, A. Sayari, *Ind. Eng. Chem. Res.* **2007**, *46*, 446–458.

[69] J. Wilcox, R. Haghpanah, E. C. Rupp, J. He, K. Lee, *Annu. Rev. Chem. Biomol. Eng.* **2014**, *5*, 479-505.

[70] T. J. Kim, B. Li, M. B. Hägg, *J. Polym. Sci. Part B: Polym. Phys.* **2004**, *42*, 4326-4336.

[71] W. J. Ward III, W. L. Robb, *Science* **1967**, *156*, 1481-1484.

[72] T. Yamaguchi, L. M. Boetje, C. A. Koval, R. D. Noble, C. N. Bowman, *Ind. Eng. Chem. Res.* **1995**, *34*, 4071–4077.

[73] H. Matsuyama, M. Teramoto, H. Sakakura, *J. Membr. Sci.* **1996**, *114*, 193–200.

[74] T. J. Kim, H. Vrålstad, M. Sandru, M. B. Hägg, *J. Membr. Sci.* **2013**, *428*, 218-224.

[75] M. Sandru, T. J. Kim, M. B. Hägg, *Desalination* **2009**, *240*, 298-300.

[76] L. Deng, T. J. Kim, M. B. Hägg, *J. Membr. Sci.* **2009**, *340*, 154-163.

[77] C. E. Powell, G. G. Qiao, *J. Membr. Sci.* **2006**, *279*, 1-49.

[78] S. Nayak, L. A. Lyon, *Angew. Chem. Int. Ed.* **2005**, *44*, 7686-7708.

[79] K. Dusek, D. Patterson, *J. Polym. Sci. Part A: Polym. Phys.* **1968**, *6*, 1209–1216.

[80] Y. Li, T. Tanaka, *J. Chem. Phys.* **1990**, *92*, 1365.

[81] C. D. Jones, L. A. Lyon, *Macromolecules* **2000**, *33*, 8301–8306.

[82] D. Duracher, F. Sauzedde, A. Elaissari, A. Perrin, C. Pichot, *Colloid Polym. Sci.* **1998**, *276*, 219-231.

[83] D. Duracher, F. Sauzedde, A. Elaïssari, C. Pichot, L. Nabzar, *Colloid Polym. Sci.* **1998**, *276*, 920-929.

[84] A. Suzuki, T. Tanaka, *Nature* **1990**, *346*, 345-347.

[85] T. Tanaka, I. Nishio, S. T. Sun, S. U. Nishio, *Science* **1982**, *29*, 467-469.

[86] T. Miyata, N. Asami, T. Uragami, *Nature* **1999**, *399*, 766-769.

[87] J. Kim, S. Nayak. L. A. Lyon, *J. Am. Chem. Soc.* **2005**, *127*, 9588–9592.

[88] H. G. Schild, *Prog. Polym. Sci.* **1992**, *17*, 163–249.

[89] M. Heskinsa, J. E. Guillet, *J. Macromol. Sci. Chem.* **1968**, *2*, 1441-1455.

[90] I. Berndt, W. Richtering, *Macromolecules* **2003**, *36*, 8780–8785.

[91] I. Berndt, J. S. Pedersen, W. Richtering, *J. Am. Chem. Soc.* **2005**, *127*, 9372–9373.

[92] A. Matsumoto, S. Ikeda, A. Harada, K. Kataoka, *Biomacromolecules* **2003**, *4*, 1410–1416.

[93] D. Duracher, A. Elaïssari, C. Pichot, *Colloid Polym. Sci.* **1999**, *277*.

[94] D. Roy, W. L. Brooks, B. S. Sumerlin, *Chem.Soci. Rev.* **2013**, *42*, 7214-7243.

[95] D. Ito, K. Kubota, *Macromolecules* **1997**, *30*, 7828–7834.

[96] Y. Maeda, T. Nakamura, I. Ikeda, *Macromolecules* **2001**, *34*, 1391–1399.

[97] I. Idziak, D. Avoce, D. Lessard, D. Gravel, X. X. Zhu, *Macromolecules* **1999**, *32*, 1260–1263.

[98] K. Suwa, K. Morishita, A. Kishida, M. Akashi, *J. Polym.Sci. Part A: Polym. Chem.* **1997**, *35*, 3087–3094.

[99] Kazuo Suwa, Y. Wada. Y. Kikunaga, K. Morishita, A. Kishida, M. Akashi, *J. Polym.Sci. Part A: Polym. Chem.* **1997**, *35*, 1763–1768.

[100] S. Kunugi, T. Tada, Y. Yamazaki, K. Yamamoto, M. Akashi, *Langmuir* **2000**, *16*, 2042–2044.

[101] A. C. W. Lau, C. Wu, *Macromolecules* **1999**, *32*, 581–584.

[102] N. Gonzalez, C. Elvira, J. S. Roman, *Macromolecules* **2005**, *38*, 9298–9303.

[103] M. Mertoglu, S. Garnier, A. Laschewsky, K. Skrabania, J. Storsberg, *Polymer* **2005**, *46*, 7726-7740.

[104] F. A. Plamper, M. Ruppel, A. Schmalz, O. Borisov, M. Ballauff, A. H. E. Muller, *Macromolecules* **2007**, *40*, 8361–8366.

[105] C. de Las H. Alarcon, S. Pennadam, C. Alexander, *Chem. Soc. Rev.* **2005**, *34*, 276-285.

[106] A. C. Colin, S. M. Cancho, R. G. Rubio, A. Compostizo, *Phys. Chem. Chem. Phys.* **1999**, *1*, 319–322.

[107] S. Zhou, B. Chu, *J. Phys. Chem. B* **1998**, *102*, 1364–1371.

[108] H. Suzuki, B. Wang, R. Yoshida, E. Kokufuta, *Langmuir* **1999**, *15*, 4283-4288.

[109] J. D. Debord, L. A. Lyon, *Langmuir* **2003**, *19*, 7662-7664.

[110] H. J. van der Linden, S. Herber, W. Olthuis, P. Bergveld, *The Analyst* **2003**, *128*, 325-331.

[111] D. Crespy, R. M. Rossi, *Polym. Int.* **2007**, *56*, 1461-1468.

[112] N. S. Save, M. Jassal, A. K. Agrawal, *Polymer* **2003**, *44*, 7979-7988.

[113] H. Kawaguchi, *J. Oleo Sci.* **2013**, *62*, 865-871.

[114] R. Freitag, F. G. Flaudy, *Langmuir* **2002**, *18*, 3434–3440.

[115] Y. Zhang , S. Furyk. D. E. Bergbreiter, P. S. Cremer, *J. Am. Chem. Soc.* **2005**, *127*, 14505–14510.

[116] F. Hoshino, T. Fujimoto, H. Kawaguchi, Y. Ohtsuka, *Polym. J.* **1987**, *19*, 241-247.

[117] A. S. Dubovik, E. E. Makhaeva, V. Y. Grinberg, A. R. Khokhlov, *Macromol. Chem. Phys.* **2005**, *206*, 915-928.

[118] K. Van Durme , H. Rahier, B. Van Mele, *Macromolecules* **2005**, *38*, 10155-10163.

[119] Y. H. Kim, I. C. Kwon, Y. H. Bae, S. W. Kim, *Macromolecules* **1995**, *28,* 939–944.

[120] E. E. Makhaeva, H. Tenhu. A. R. Khokhlov, *Macromolecules* **1998**, *31*, 6112–6118.

[121] F. M. Winnik, H. Ringsdorf, J. Venzmer, *Macromolecules* **1990**, *23*, 2415-2416.

[122] S. Kunugi, K. Takano, N. Tanaka, K. Suwa, M. Akashi, *Macromolecules* **1997**, *30*, 4499-4501.

[123] T. Tanaka, E. Sato, Y. Hirokawa, S. Hirotsu, J. Peetermans, *Phys. Rev. Lett.* **1985**, *55*, 2455-2458.

[124] T. Tanaka, D. J. Fillmore, *J. Chem. Phys.* **1979**, *70*, 1214.

[125] K. S. Oh, J. S. Oh, H. S. Choi, Y. C. Bae, *Macromolecules* **1998**, *31*, 7328–7335.

[126] M. J. Murray, M. J. Snowden, *Adv. Colloid Interface Sci.* **1995**, *54*, 73–91.

[127] I. Lynch, K. A. Dawson, *J. Phys. Chem. B* **2003**, *107*, 9629-9637.

[128] B. R. Saundersa, B. Vincent, A*dv. Colloid Interface Sci.* **1999**, *80*, 1-25.

[129] B. R. Saunders, N. Laajam, E. Daly, S. Teow, X. Hu, R. Stepto, A*dv. Colloid Interface Sci.* **2009**, *147-148*, 251-262.

[130] S. Neyret, B. Vincent, *Polymer* **1997**, *38*, 6129–6134.

[131] K. McAllister, P. Sazani, M. Adam, M. J. Cho, M. Rubinstein, R. J. Samulski, J. M. DeSimone, *J. Am. Chem. Soc.* **2002**, *124*, 15198–15207.

[132] S. Kazakov, M. Kaholek, D. Kudasheva, I. Teraoka, M. K. Cowman, K. Levon, *Langmuir* **2003**, *19*, 8086–8093.

[133] X. Wu, R. H. Pelton, A. E. Hamielec, D. R. Woods, W. McPhee, *Colloid Polym. Sci.* **1994**, *272*, 467-477.

[134] X. Hu, Z. Tong, L. A. Lyon, *Langmuir* **2011**, *27*, 4142-4148.

[135] M. H. Smith, E. S. Herman, L. A. Lyon, *J. Phys. Chem. B* **2011**, *115*, 3761-3764.

[136] B. R. Saunders, *Langmuir* **2004**, *20*, 3925-3932.

[137] I. Varga, T. Gilanyi, R. Meszaros, G. Filipcsei, M. Zrinyi, *J. Phys. Chem. B* **2001**, *105*, 9071-9076.

[138] J. Wang, D. Gan, L. A. Lyon, M. A. El-Sayed, *J. Am. Chem. Soc.* **2001**, *123*, 11284-11289.

[139] X. S. Wu, A. S. Hoffman, P. Yager, *J. Polym. Sci., Part A: Polym. Chem.* **1992**, *30*, 2121-2129.

[140] R. X. Zhuo, W. Li, *J. Polym. Sci., Part A: Polym. Chem.* **2003**, *41*, 152-159.

[141] J. T. Zhang, S. X. Cheng, S. W. Huang, R. X. Zhuo, *Macromol. Rapid Commun.* **2003**, *24*, 447-451.

[142] S. X. Cheng, J. T. Zhang, R. X. Zhuo, *J. Biomed. Mater. Res. Part A* **2003**, *67*, 96-103.

[143] O. Okay, *Prog. Polym. Sci.* **2000**, *25*, 711–779.

[144] A. Guyot, M. Bartholin, *Prog. Polym. Sci.* 1982, *8*, 277–331.

[145] O. Okay, *Polymer* 1999, *40*, 4117–4129.

[146] O. Okay, *J. Appl. Polym. Sci.* 1999, *74*, 2181–2195.

[147] Cigdem Sayil, O. Okay, *Polymer* 2001, *42*, 7639–7652.

[148] K. J. Shea, G. J. Stoddard, D. M. Shavelle, F. Wakui, *Macromolecules* 1990, *23*, 4497–4507.

[149] F. Svec, J. M. J. Frechet, *Macromolecules* 1995, *28*, 7580–7582.

[150] M. B. Huglin, D. C. F. Yip, *Macromolecules* 1992, *25*, 1333–1337.

[151] D. Horák, F. Lednický, M. Bleha, *Polymer* 1996, *37*, 4243–4249.

[152] R. Yoshida, K. Uchida, Y. Kaneko, K. Sakai, A. Kikuchi, Y. Sakurai, T. Okano, *Nature* 1994, *374*, 240-242.

[153] Y. Kaneko, K. Sakai, A. Kikuchi, R. Yoshida, Y. Sakurai, T. Okano, *Macromolecules* 1995, *28*, 7717–7723.

[154] Y. Kaneko, K. Sakai, A. Kikuchi, Y. Sakurai, T. Okano, *Macromol. Symp.* 1996, *109*, 41–53.

[155] S. Hirotsu, *Jpn. J. Appl. Phys.* 1998, *37*, 284.

[156] Y. Kaneko, S. Nakamura, K. Sakai, T. Aoyagi, A. Kikuchi, Y. Sakurai, T. Okano, *Macromolecules* 1998, *31*, 6099–6105.

[157] G. A. Olah, A. Goeppert, G. K. S. Prakash,, *Beyond Oil and Gas: The Methanol Economy, 2nd ed, Wiley-VCH: Weinheim, Germany* 2009.

[158] G. T. Rochelle, *Science* 2009, *325*, 1652-1654.

[159] T. Fout, J. T. Murphy, *DOE/NETL 2009/1356*, National Energy Technology Laboratory, Pittsburgh, PA, 2009.

[160] D. Aaron, C. Tsouris, *Sep. Sci. Technol.* 2005, *40*, 321–348.

[161] D. M. D'Alessandro, B. Smit, J. R. Long, *Angew. Chem., Int. Ed.* 2010, *49*,

6058-6082.

[162] Y. Park, D. Shin, Y. N. Jang, A.-H. A. Park, *J. Chem. Eng. Data* **2012**, *57*, 40-45.

[163] H. Y. Huang, R. T. Yang, *Ind. Eng. Chem. Res.* **2003**, *42*, 2427-2433.

[164] K. B. Lee, M. G. Beaver. H. S. Caram, S. Sircar, *Ind. Eng. Chem. Res.* **2008**, *47*, 8048–8062.

[165] A. Goeppert, M. Czaun, R. B. May, G. K. S. Prakash, G. A. Olah, S. R. Narayanan, *J. Am. Chem. Soc.* **2011**, *133*, 20164-20167.

[166] R. S. Guerrero, E. Da'na, A. Sayari, *Ind. Eng. Chem. Res.* **2008**, *47*, 9406–9412.

[167] D. Voet, J. G. Voet, *Biochemistry*, Wiley, New York, USA, **1995**.

[168] Y. Hoshino, K. Imamura, M. Yue, G. Inoue, Y. Miura, *J. Am. Chem. Soc.* **2012**, *134*, 18177-18180.

Chapter 2. Development of Temperature Responsive Microgel Particle Films as Reversible CO_2 Absorbents in Wet Environment

Abstract

Hydrogel films composed of temperature-responsive microgel particles (GPs) containing amine groups work as stimuli-responsive carbon dioxide absorbent with a high capacity of approximately 1.7 mmol/g. Although the dried films did not show significant absorption, the reversible absorption capacity dramatically increased by adding a small amount of water (1 mL/g). The absorption capacity was independent of the amount of added water beyond 1 mL/g, demonstrating that the GP films can readily be used under wet conditions. The amount of CO_2 absorbed by the GP films was proportional to their thickness up to 200-300 μm (maximum capacity of about 2 L/m^2). Furthermore, the films consisting of GPs showed faster and greater absorption and desorption of CO_2 than that of monolithic hydrogel films. These results indicated the importance of a fast stimulus response rate of the films that are composed of GPs in order to achieve long-range and fast diffusion of bicarbonate ions. Our study revealed the potential of stimuli-responsive GP films as energy-efficient absorbents to sequester CO_2 from high-humidity exhaust gases

2.1 Introduction

The worldwide use of fossil fuels has led to the accumulation of CO_2, a primary greenhouse gas, which has contributed to the global climate change.[1] At the same time, CO_2 can be a potential carbon source for the production of liquid fuels such as methanol and dimethyl ether by using regenerative energy.[2] Thus, the development of energy-efficient and scalable CO_2-capture processes from high-humidity exhaust gases of point sources such as fossil fuel power plants is essential for the future use of carbon-based energy.

The capture of CO_2 from high-humidity exhaust gases of power plants using aqueous solutions of amines such as ethanol amine and sterically hindered amines as absorbents has been considered to be the most implementable process.[3] The amine solutions absorbed CO_2 at a low temperature (about 40 °C) by an exothermic reaction and desorbed CO_2 upon heating (>140 °C).[4] Though these conventional methods exhibited a high capacity for CO_2 capture, they have drawbacks as well, such as reactor corrosion and high-energy consumption—equivalent to 20-40% of a typical power plant output because of the high regeneration temperature.[4, 5] Furthermore, amines and their reaction products in the solution that are easily volatilized during the regeneration process need to be recovered in order to avoid air pollution.[6] Thus, the development of nonvolatile sorbents that desorb CO_2 at low temperatures (<100 °C) has been required.[5]

The use of porous solid sorbents is one of the available remedies to circumvent the aforementioned problems. In recent years, a number of porous sorbents such as activated carbon,[7] metal-organic frameworks (MOF),[7, 8] zeolites,[7,8] and physically or chemically supported amine polymers[7–9] that can be regenerated under relatively mild conditions have been reported.[7–9] The porous solid sorbents showed an enormous binding capacity of up to 3 mmol CO_2 per gram[7–9] because of the large surface area of the pores. However, only a few studies have been conducted on solid CO_2 sorbents capable of capturing CO_2 under wet conditions, because the adsorption of water vapor competes with that of CO_2 on the pore surface and/or liquefied water blocks the capillaries and pores of the sorbents to prevent CO_2 from diffusing into or out of the pores.[7–9] Thus, nonvolatile sorbents capable of working reversibly under wet conditions by a low-temperature regeneration process are required.

We have reported that aqueous solutions of temperature responsive microgel particles (GPs) consisting of N-isopropyl acrylamide (NIPAm) and *N*-[3-(dimethylamino)propyl]methacrylamide (DMAPM) reversibly absorbed CO_2 by volume phase transition (VPT).[10] Poly(NIPAm) hydrogels underwent VPT from a swollen to a shrunken state at the volume phase transition temperature (VPTT).[10] The GPs were highly hydrated below the VPTT while above it, the water dissociated from the GPs, thereby allowing the shrinkage of the hydrogel structure.

It has been reported that poly(NIPAm) hydrogels comprising functional groups reversibly captured targets such as CO_2, [10, 11] dyes,[12] cancer drugs,[13] peptides,[14] proteins,[15] enzymes,[16] nucleotides,[17] and cells[18] through electrostatic, hydrophobic and/or hydrogen-bonding interactions at heating-cooling cycles across the VPTT. The interactions were switched off by either lowering the volume density of the functional groups in the hydrogel below the VPTT,[12, 13, 16] suppressing the flexibility of polymer chains above the VPTT,[19] or lowering the number of the charged functional groups[10, 17] by decreasing the dielectric constant around the functional groups above the VPTT. In the case of reversible CO_2 absorption by the amine-containing GPs, most amines in the swollen GPs were capable of forming ion pairs with the absorbed bicarbonate ions below the VPTT (30 °C). However, above the VPTT (75 °C), the shrinkage of the GPs lowered the pKa value of these amines, resulting in efficient desorption of CO_2.[10]

The capacity for CO_2 absorption per amine in the GPs in solution was either comparable or superior to the commercially available CO_2 absorbents consisting of ethanolamine.[10] However, the absorption capacity per weight of the solution was much smaller than that of the aqueous solution of ethanol amines because the concentration of GPs in solution (about 0.1 wt%) was much lower than that of the

amine solution (20– 30 wt%).[10] As a result, the energy consumed by the solution of GPs to sequester CO_2 was significantly larger than the amine solution in spite of using low temperature for the regeneration process. In order to improve the energy efficiency, the concentration of GPs had to be dramatically increased.[10]

In this study, a new class of solid sorbent films that consist of temperature-responsive GPs is developed. The films were expected to bring together the best of high stoichiometric absorption efficiency of GP solutions and large absorption capacity per weight of solid sorbents, even under wet conditions. Furthermore, it was expected that the temperature- responsive hydrogel films consisting of GPs would respond much faster to external stimuli compared to the monolithic hydrogel films.[20, 21]

Lyon and co-workers prepared microgel-based films using the layer-by-layer (LbL) method.[22] Dawson and Lynch made composite microgel films in the form of "plum-pudding" gels,wherein pNIPAm-based microgels were immobilized in a hydrogel matrix.[20] In spite of the large and monolithic appearance, these films retained the rapid response rate of the microgel building blocks.[20]

2.2. Materials and experiments

2.2.1. Materials

NIPAm (Wako Pure Chemical Industries, Ltd.) was purified by recrystallization from *n*-hexane and dried *in vacuo* at room temperature. *N*-[3-(Dimethylamino)propyl]methacrylamide (DMAPM, Tokyo Chemical Industry Co., Ltd.), 2,2′-azobis(isobutyronitrile) (AIBN, Wako Pure Chemical Industries, Ltd.), 2,2′-azobis(2-methylpropionamidine)dihydrochloride (AAPD, Wako Pure Chemical Industries, Ltd.), *N,N*′-methylenebis(acrylamide) (bis, Tokyo Chemical Industry

Co., Ltd.), cetyltrimethylammonium bromide (CTAB, Wako Pure Chemical Industries, Ltd.), 4- aminofluorescein (Aldrich Chemical Co., Ltd.), and acryloyl chloride (Sigma-Aldrich Chemical Co., Ltd.) were used as received. The dialysis membrane having a cut-off of 12–14,000 was purchased from Spectrum Laboratories, Inc. The anion-exchange resin (A2004-OH, Muromachi Technos Co., Ltd.) was first pretreated with 1 M NaOH, and then washed with deionized water. The water was purified using a Direct-Q Ultrapure Water System (Merck, Ltd.).

2.2.2. Synthesis of 4-Acrylamidofluorescein (AFA) Monomer (Fluorescein monomer)

4-aminofluorescein (1.25 g, 3.6 mmol) was suspended in 50 mL of anhydrous acetone in a 100 mL round-bottom flask containing a magnetic stir bar. The suspension was cooled down to 0 °C. Acryloyl chloride (0.32 mL, 3.9 mmol) was dissolved in 0.5 mL of anhydrous acetone and then added dropwise to the suspension at 0 °C over 10 min. After warming up to room temperature, the mixture was stirred for 3 h. Thereafter, the resulting yellow crystals were separated from the solution by filtration and then washed with acetone and diethyl ether. The final product was recrystallized twice from anhydrous THF and then dried *in vacuo* overnight.

2.2.3. Preparation of GPs

A series of pNIPAm GPs containing 0, 5, and 30 mol% DMAPM and 2 mol% cross-linker Bis (GP0, GP5, GP30, respectively) were prepared by precipitation polymerization[10] as described in scheme 2-1. Details about polymerization condition of GPs were summarized in table 2-1. According to the different polymerization condition of each GP described in table 2-1, NIPAm, DMAPM, and

Bis were first dissolved in water, resulting in the settled total monomer concentration. The AFA pre-dissolved in a small amount of methanol was then added into the monomer aqueous solution. Then surfactant CTAB was added to the monomer solution followed by heating to 70 °C. Then the solution was degased by nitrogen gas while stirring at 70 °C for 1 h. Later, aqueous solution of AAPD was added by syringe. The polymerization reaction was carried out at 70 °C for 3 h under nitrogen atmosphere, as illustrated in scheme 2-1. The resulting mixture was purified by dialysis against an excess volume of water over four days (water was changed more than three times a day). The anion-exchange of the GPs was conducted to remove the trace amount of counter anions and CO_2 absorbed by amines during dialysis.

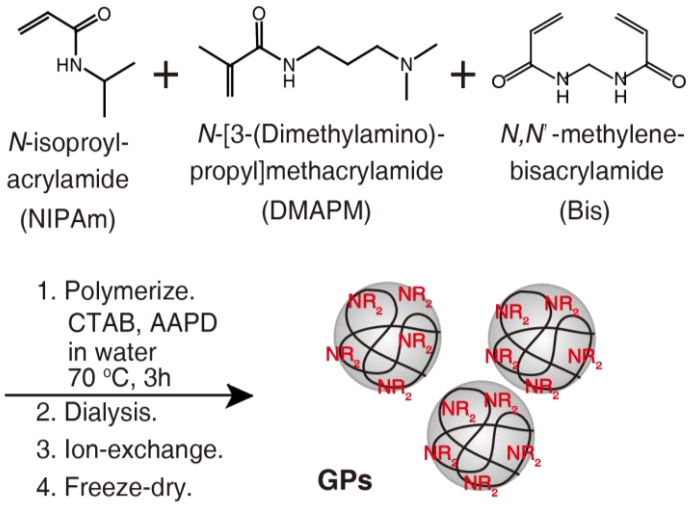

Scheme 2-1. Preparation of temperature-responsible GPs.

Table 2-1. Polymerization condition of GPs.

GPs	NIPAm (mol%)	DMAPM (mol%)	Bis (mol%)	AFA (mol%)	CTAB (mM)	AAPD (mM)
D0B2	98	0	2	0	2.0	2.5
D5B2	93	5	2	0	2.0	2.5
D30B2	68	30	2	0	2.0	2.5
D30B2-F	67.99	30	2	0.01%	2.0	2.5

2.2.4. Preparation of GP Films

The ion-exchanged GPs were dried using a lyophilizer, and then dissolved in methanol. The hydrogel films were prepared by casting the methanol solutions of GPs on the inner surface of a stainless steel container, followed by the addition of a specific volume of water after completely evaporating methanol. The film thickness was controlled by casting different volume of the methanol solution of GPs onto the surface of the stainless steel container (see scheme 2-2).

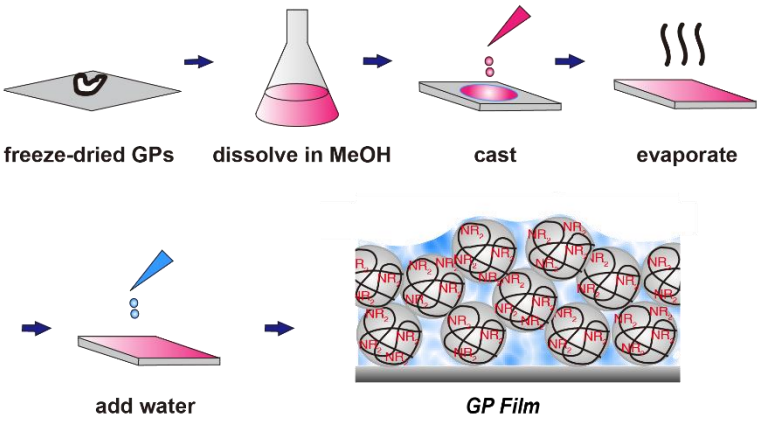

Scheme 2-2. Preparation of GP films.

The thickness of the hydrogel films was estimated by assuming the swollen GPs contain 1 wt.% polymer and 99 wt.% water. As a result, the polymer density of the

hydrogel film containing 4 mL water/g GPs (60% water inside GPs) will be 0.2 g/mL. The film thickness was calculated using the following equation:

$$t = m / (d * s)$$

where t, m, d, and s represent the thickness, weight, density, and surface area of the GP film, respectively.

2.2.5. Preparation of Fluorescent-labeled GP30 Film (GP30F film)

GP30 and GP30F solutions were mixed to bring the final weight ratio to 99:1. After lyophilization, the GPs were dissolved in methanol and then casted onto a glass bottom dish (Matsunami Glass Ind., Ltd.). Fluorescent-labeled GP30 film (GP30F film) was obtained after evaporation of methanol.

2.2.6. Preparation of Monolithic Film (M30)

Monolithic film containing 30 mol% DMAPM and 2 mol% bis was prepared as a control. NIPAm (68 mol%, 800.3mg), DMAPM (30 mol%, 559.17 μL), Bis (2 mol%, 32 mg) was dissolved in 4.432 mL deionized water. 6.5 μL TEMED was added as an accelerator. The monomer solution was degased with N_2 for 30 min, followed by the addition of APS (1.2 mg) which was pre-dissolved in 1 mL water. 360 mg monomers (corresponding to 1.8 mL pre-polymerization solution) was casted evenly on the surface of the stainless steel container, which was sealed with N_2 afterwards. The polymerization was carried out for 24 h at room temperature in the N_2 environment inside a vacuum glove box (see scheme 2-3). The resulted monolithic gel film was used directly as a CO_2 absorbent containing 4 mL water/g polymers without further processing.

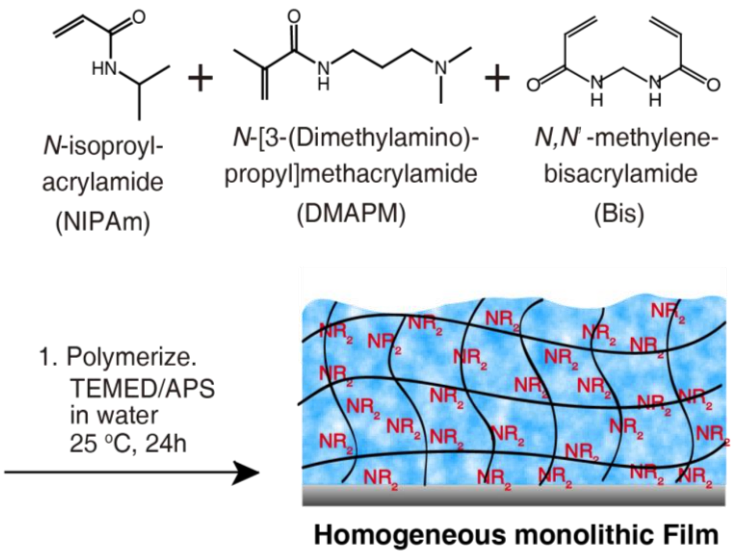

Scheme 2-3. Preparation of temperature-responsible homogeneous monolithic films.

2.2.7. Preparation of Fluorescent-labeled Monolithic Film (M30F)

NIPAm (68 mol%, 800.3 mg), DMAPM (30 mol%, 559.17 μL), bis (2 mol%, 32 mg), AFA (10^{-4} mol%, 13.6 μg) and TEMED (6.5 μL) was dissolved in 4.432 deionized water and degased with N_2 for 30 min, followed by the addition of APS (1.2 mg) which was pre-dissolved in 1 mL water One drop of the pre-polymerization solution was located on the surface of the glass bottom dish. Around the pre-polymerization solution drop, several water drop was placed to protect it from drying. The polymerization was carried out for 24 h at room temperature in the N_2 environment inside a vacuum glove box.

2.2.8. Quantification of hydrodynamic diameters

The hydrodynamic diameters of GPs were measured using a dynamic light scattering (DLS) instrument (Zetasizer Nano, Malvern Instruments Ltd.), which employed the ion-exchanged solutions sealed within the quartz cells filled with

nitrogen. The solutions were equilibrated at each temperature for 6 min prior to the measurement.

2.2.9. Quantification of amine content in GPs

A SevenMultiTM pH meter equipped with pH probes (InLab® Routine Pro, METTLER TOLEDO) was calibrated with three standard buffers (pH 7.00, 4.01 and 9.21) prior to use. Temperature of GP solution was controlled by water bath. pH titration with 0.01M HCl was performed at 30 °C and 75 °C under nitrogen. The solution was stirred at 1000 rmp during titration.

2.2.10. Observation of surface structure of GP film and monolithic gel film by SEM

GP30 film and M30 film deposited on surface of alumina foil were completely dried overnight in vacuum prior to use. Scanning Electronic Microscope (SEM) (SU8000, Hitachi Ltd.) was employed to observe the surface of the films.

2.2.11. Observation of inner structure of GP film and monolithic gel films by LSCSM

Fluorescent-labeled GP30/GP30F (99/1) film and M30F film were dried overnight in vacuum prior to use. Inner structure of the films were investigated using a confocal laser scanning microscope (LSM) (LSM 700, Carl Zeiss) equipped with the LSM Software ZEN 2011. The laser with excitation wavelength 488 nm was applied.

2.2.12. Measurement of reversible CO_2 absorption/desorption of GP films and

monolithic films

CO_2 absorption capacities of the films were quantified using a grease-free steel-Teflon tube system (see scheme 2-4). Here, 10 % CO_2 (90 % N_2, 10 mL/min) gas was bubbled into water (25 or 60 °C) to saturate the water vapor at the appointed temperature. The resulting water-saturated gas was guided into a stainless steel container with GP film or monolithic film on its surface, and then channeled to a gas chromatography instrument (GC, Shimadzu Corp.) equipped with a thermal conductivity detector (TCD) and Shincarbon ST 50/80 column (2 m, Shinwa Chemical Industries Ltd.; carrier gas: He, 40 mL/min; column temperature: 210 °C; detector temperature: 240 °C). All the films were equilibrated under the gas flow for ~2 h at 30 °C. Thereafter, CO_2 desorption capacity at 75 °C and absorption capacity at 30 °C of each film were quantified by monitoring concentration of CO_2 every 1.7 minutes by the GC-TCD for 25 min and 46 min respectively.

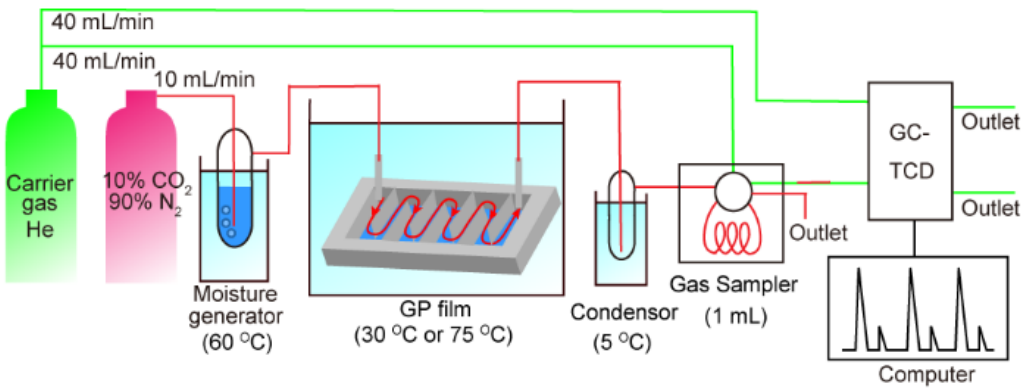

Scheme 2-4. Illustration of CO_2 absorption measurement system.

2.3. Results and Discussion

2.3.1. Structure of GP film and homogeneous monolith film

In this study, the GP films were prepared simply by casting a GP solution onto the surface of a solid substrate[23] without further immobilization of the GPs with

either polyelectrolyte (LbL gel film)[22] or cross-linked matrix polymers (plum-pudding gel film).[20] It is expected that the as cast GP films would be stable enough for gas-phase applications and respond fast enough to thermal stimuli. Monolithic film with the same composition was prepared as a control.

The two- and three-dimensional fluorescent images of the GP30F film and the M30F film taken by a confocal laser-scanning microscope (LSM 700, Carl Zeiss) are shown in figure 2-1. Figure 2-1a and 2-1c indicate that the submicron-sized granulous structure of GPs were not degraded and were homogeneously dispersed without forming aggregates in the GP30F film, although the GPs were lyophilized from water and then dissolved in methanol prior to casting. The average film thickness could also be obtained from the image. Figure 2-1b and 2-1d suggest that the M30F film has a very homogeneous structure.

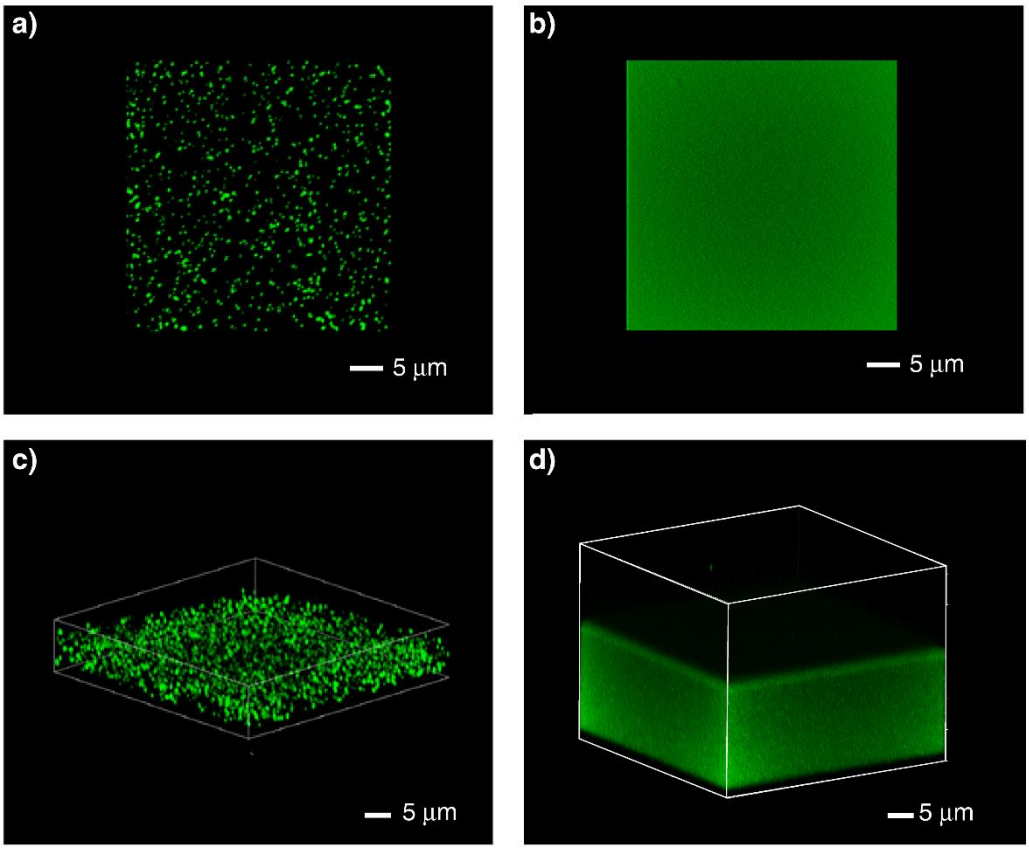

Figure 2-1. Confocal fluorescence images of a) a GP film comprising 99 wt% GP30

and 1 wt% GP30F and b) a monolithic gel film M30F, and 3D images of c) a GP film comprising 99 wt% GP30 and 1 wt% GP30F and d) a monolithic gel film M30F.

The surface image of dried GP film and homogeneous gel film measured by SEM are shown in figure 2-2. Both of the surfaces are relatively smooth.

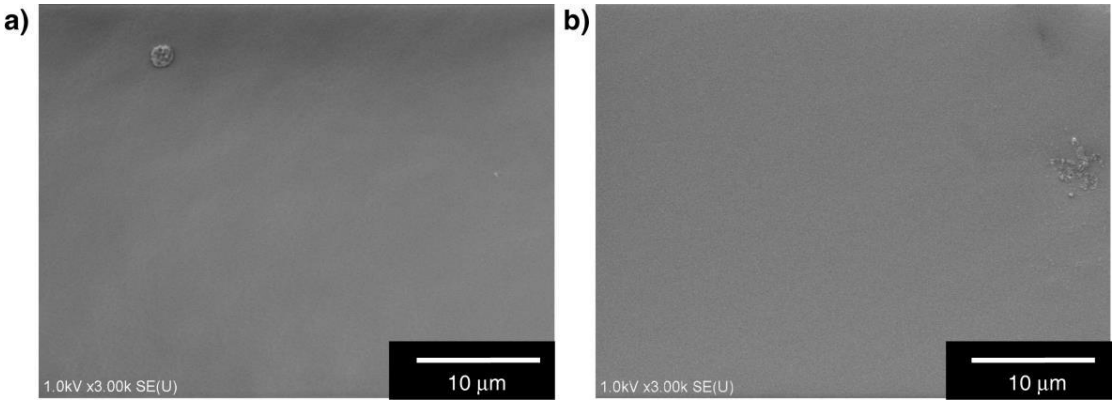

Figure 2-2. SEM image of dried a) G30 film and b) M30 film

2.3.2. Effect of added water amount on the CO_2 capture capacity of the GP films

Water-saturated gas containing CO_2 (10% CO_2, 90%N_2, 25 °C, 10 mL/min) was passed continuously on the surface of the GP films in the stainless steel container to quantify the capacity for reversible CO_2 absorption. After saturating the films with CO_2 at 30 °C for 2 h, the amount of CO_2 desorbed from the films at 75 °C was quantified by integrating the CO_2 level in the downstream gas every 1.7 minutes using a gas chromatograph (GC). As shown in figure 2-3a, the dried films, with or without amine (GP30 and GP0, respectively), did not show obvious CO_2 desorption. In addition, meager release of CO_2 was observed by the wet films consisting of GP0. However, a significant amount of CO_2 was desorbed from the hydrated films consisting of amine-containing gel particles (GP30). The volume of desorbed CO_2 increased dramatically on increasing the amount of added water up to 1 mL/g. Then the capacity for CO_2 desorption was not further affected by the volume of

water added when the film was hydrated with more than 1 mL/g (Figure 2-3b). This result clearly demonstrates that the amine-containing GP films can readily be used under wet conditions.

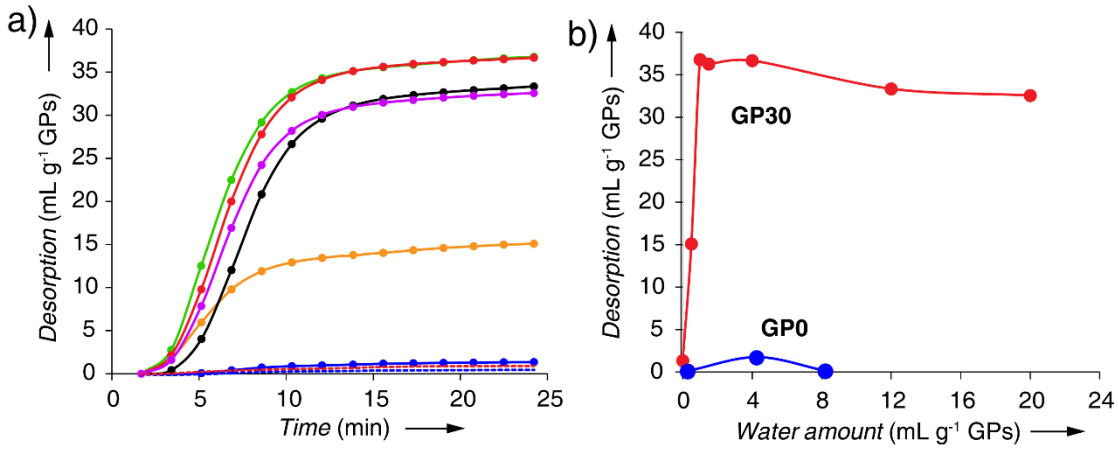

Figure 2-3. a) Time course of CO_2 absorption by a GP30 film hydrated with 0 (blue), 0.5 (orange), 1 (green), 4 (red), 12 (black), and 20 (purple) milliliters of water per gram of GPs and a GP0 film with 0 (blue dotted line) and 4 (red dotted line) milliliters of water per gram of GPs monitored by GC. b) Dependence of volume of water on CO_2 absorption capacity of GP30 (red) and GP0 (blue) films. A watersaturated gas containing CO_2 (10% CO_2, 90% N_2, 25 °C, 10 mL/min) was passed continuously on the surface of the GP films.

It has been reported that the reaction of CO_2 with tertiary amines occurred in one equivalent water to form bicarbonate anions and ammonium cations.[10] However, more than 55 mmol (about 1 mL) of water, which was 27 times greater than the number of tertiary amines in the film was required to achieve maximum desorption capacity (Figure 2-3b). This result suggests that the films have to be hydrated with water not only to react with CO_2 to form ammonium bicarbonate but also for the bicarbonate ions to diffuse into and out of the films.

2.3.3. Effect of film thickness on the CO_2 capture capacity

The effect of the film thickness on the amount of CO_2 desorbed was investigated using hydrated (4 mL/g) GP films (Figure 2-4). Surprisingly, the volume of the desorbed CO_2 increased linearly with increasing film thickness up to 200-300 μm (R^2 for GP5 and GP30 are 0.9973 and 0.9985, respectively), indicating that most of the amine groups inside the hydrogel films could be used to capture and release CO_2 by an efficiency analogous to that on the surface of the films. This result also suggests that diffusion of bicarbonate ions into and out of the GP films will not limit CO_2 capture/release when the films are thinner than 200-300 μm.

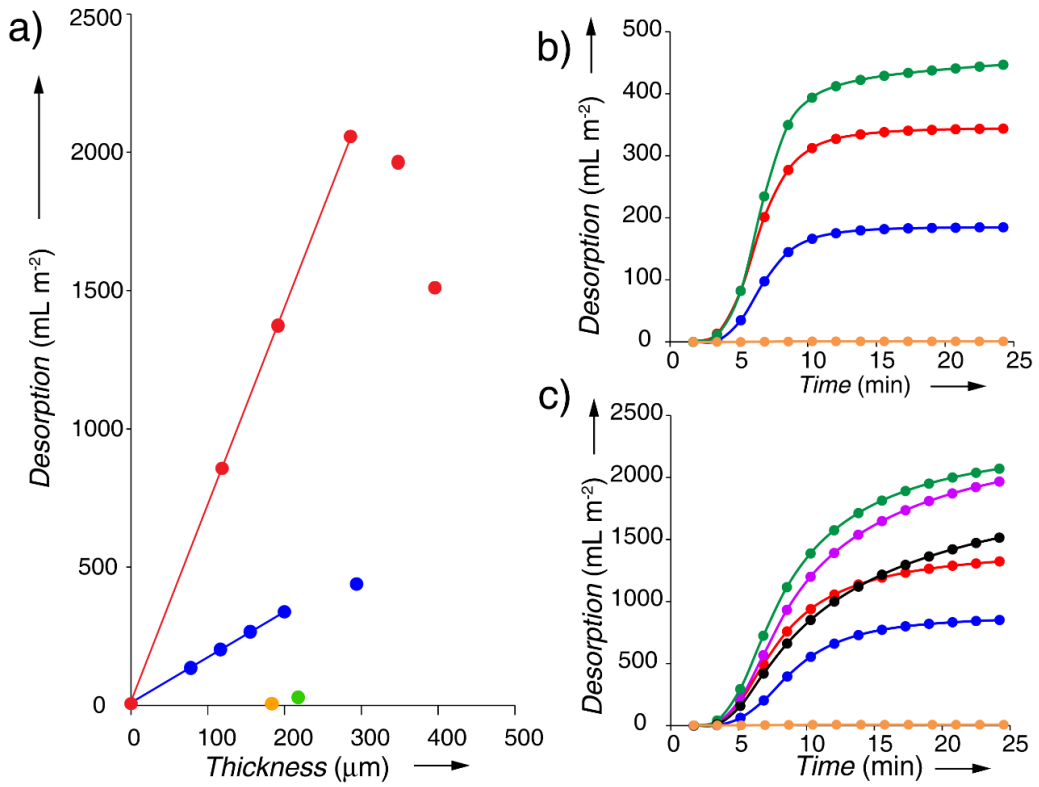

Figure 2-4. a) Amount of CO_2 released from a GP30 film (red), a GP5 film (blue), a GP0 film (green), and a dry GP5 film (orange) as a function of the film thickness. b) Time course of CO_2 desorption from the GP5 films with thickness of 0 (orange), 120 (blue), 200 (red), and 300 (green) micrometers. c) Time course of CO_2

desorption from GP30 films with thickness of 0 (orange), 120 (blue), 190 (red), 280 (green), 350 (purple), and 400 (black) micrometers. All the films contained 4 mL of water per gram of GPs except for the dry GP5 film. A water-saturated gas containing CO_2 (10% CO_2, 90% N_2, 25 °C, 10 mL/min) was passed continuously on the surface of the films.

2.3.4. The reversibility of CO_2 capture by GP film and homogeneous monolith film

To investigate the reversibility of CO_2 capture in an environment similar to that of the exhaust gases of power plants, high-temperature wet gas containing CO_2 (10% CO_2, 90% N_2, 60 °C, 10 mL/min) was passed continuously on the surface of the hydrated films. Then, the film was repeatedly heated (75 °C, 25 minutes) and cooled (30 °C, 46 minutes) to release and capture CO_2.

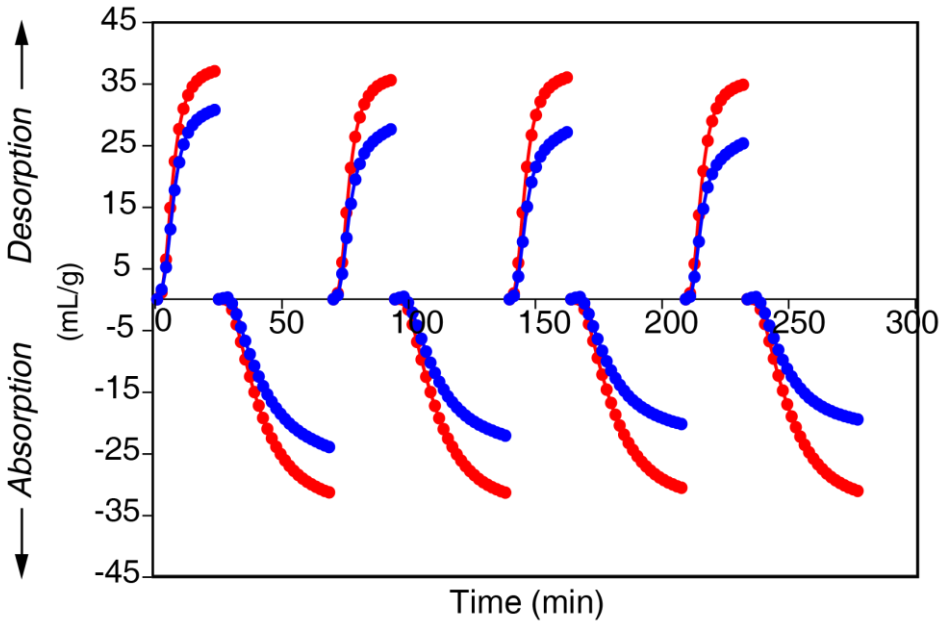

Figure 2-5. Temperature-responsive absorption (30 °C) and desorption (75 °C) of CO_2 by a GP30 film (red) and a M30 film (blue) over four cycles. A water-saturated gas containing CO_2 (10% CO_2, 90% N_2, 60 °C, 10 mL/min) was passed continuously on the surface of the films containing 4 mL of water per gram of polymer.

Figure 2-5 shows that the GP30 film reversibly absorbed and desorbed CO_2 without showing an obvious decrease in the performance. Although the temperature interval was only 45 °C and the surfaces of the films were flat (Figure 2-2), the capacity for reversible CO_2 absorption about 38 mL/g GPs, about 1.7 mmol/g GPs) was comparable to that of a highly porous solid adsorbent.[7–9] Furthermore, the GP30 film shows a faster absorption-desorption rate, a larger absorption-desorption capacity, and a better repeatability than the M30 film.

It has been reported that molecules and ions significantly smaller than the size of the polymer network in hydrogels are capable of diffusing into hydrogels as fast as in water.[24] Furthermore, the molecules diffuse faster into temperature responsive hydrogels consisting of GPs than into monolithic hydrogels,[20–25] because small GPs have a much larger surface area- to-volume ratio than the large monolithic gels, the transfer of water into and out of the hydrogel does not limit the shrinkage kinetics.[26] Furthermore, a dense surface layer will be formed on the large monolithic gel surface because the surface layer of the hydrogels shrunk faster than the internal gel.[20, 21] The dense layers prevent the release of internal water, limiting the shrinking kinetics of large gels. For the same reasons, stimuli-responsive capture and release of target molecules into and out of the monolithic hydrogels would be limited.[20, 21] Results in figure 2-4 and figure 2-5 indicate the importance of a fast stimulus response rate of the films that are composed of GPs in order to achieve the long-range and fast diffusion of bicarbonate ions as suggested by previous studies.[20–26]

The mechanism of CO_2 absorption and diffusion into the temperature-responsive GP film is different from surface adsorption by porous solid adsorbents assisted by rapid gas phase diffusion of CO_2 and chemical absorption by aqueous amine

solution assisted by rapid liquid-phase diffusion and convection, and provides a new strategy to prepare hydrogel based CO_2 absorbents.

2.4. Conclusion

In summary, hydrogel films comprising temperature responsive GPs were successfully prepared by simply casting the GP solution onto the surface of a solid substrate. The amount of CO_2 absorbed by the GP films was proportional to their thickness up to 200-300 μm (maximum capacity of about 2 L/m^2). The GP films reversibly absorbed CO_2 with a large absorption capacity in a wet environment (about 1.7 mmol/g) using cooling and heating cycles (30-75 °C). The GP films showed faster and greater absorption and desorption of CO_2 than that of monolithic gel films. Our results revealed the potential of the stimuli-responsive GP films as energy-efficient absorbents to sequester CO_2 from high-humidity exhaust gases. We anticipate that the molecular mechanism proposed in this work provides a novel strategy for the development of stimuli-responsive gas absorbent.

2.5. References

[1] S. Solomon, D. Qin, M. Manning, Z. Chen, M. Marquis, K. B. Averyt, M. Tignor, H. L. Miller, Eds., *The Fourth Assessment Report of the Intergovernmental Panel on Climate Change* 2007, *Cambridge University Press:* New York, 2007.

[2] A. Olah, A. Geoppert, G. K. S. Prakash, *Beyond Oil and Gas: The Methanol Economy*, Wiley-VCH: Weinheim, Germany, 2009.

[3] a) G. T. Rochelle, *science* 2009, *325*, 1652-1654; b) F. A. Chowdhury, H. Okabe, H. Yamada, M. Onoda, Y. Fujioka, *Energy Procedia* 2011, *4*, 201-208.

[4] a) T. Fout, J. T. Murphy, *DOE/NETL's Carbon Capture R&D Program for*

Existing Coal-Fired Power Plants, DOE/NETL 2009/1356, National Energy Technology Laboratory, Pittsburgh, PA, **2009**; b) D. Aaron, C. Tsouris, *Sep. Sci. Technol.* **2005**, *40*, 321–348.

[5] a) D. M. D'Alessandro, B. Smit, J. R. Long, *Angew. Chem. Intl. Ed.* **2010**, *49*, 6058-6082; b) Y. Park, D. Shin, Y. N. Jang, A. H. A. Park, *J. Chem. & Eng. Data* **2012**, *57*, 40-45; c) H. Y. Huang, R. T. Yang, *Ind. Eng. Chem. Res.* **2003**, *42*, 2427-2433.

[6] G. D. Pirngruber, S. Cassiano-Gaspar, S. Louret, A. Chaumonnot, B. Delfort, *Energy Procedia* **2009**, *1*, 1335-1342.

[7] S. Choi, J. H. Drese, C. W. Jones, *ChemSusChem* **2009**, *2*, 796–854.

[8] K.B. Lee, M. G. Beaver, H. S. Caram, S. Sircar, *Ind. Eng. Chem. Res.* **2008**, *47*, 8048–8062.

[9] a) A. Goeppert, M. Czaun, R. B. May, G. K. S. Prakash, G. A. Olah, S. R. Narayanan, *J. Am. Chem. Soc.* **2011**, *133*, 20164-20167; b) R. Serna-Guerrero, A. Sayari, *Ind. Eng. Chem. Res.* **2008**, *47*, 9406-9412; c) P. J. E. Harlick, A. Sayari, *Ind. Eng. Chem. Res.* **2007**, *46*, 446–458; d) A. Sayari, P. J. E. Harlick, *Ind. Eng. Chem. Res.* **2006**, *45*, 3248-3255; e) S. choi, M. L. Gray, C. W. Jones, *ChemSusChem* **2011**, *4*, 628-635.

[10] Y. Hoshino, K. Imamura, M. Yue, G. Inoue, Y. Miura, *J. Am. Chem. Soc.* **2012**, *134*, 18177-18180.

[11] a) D. Han, X. Tong, O. Boissière, Y. Zhao, *ACS Macro Letters* **2012**, *1*, 57-61; b) D. Han, O. Boissiere, S. Kumar, X. Tong, L. Tremblay, Y. Zhao, *Macromolecules* **2012**, *45*, 7440-7445.

[12] T. Oya, T. Enoki, A. Y. Grosberg, S. Masamune, T. Sakiyama, Y. Takeoka, K. Tanaka, G. Wang, Y. Yilmaz, M. S. Feld, R. Dasari, T. Tanaka, *science* **1999**,

286, 1543-1545.

[13] M. J. Serpe, K. A. Yarmey, C. M. Nolan, L. A. Lyon, *Biomacromolecules* **2005**, *6*, 408-413.

[14] Y. Hoshino,; W. W. Haberaecker III, T. Kodama, Z. Zeng, Y. Okahata, K. J. Shea, *J. Am. Chem. Soc.* **2010,** *132*, 13648-13650.

[15] a) S. H. Lee, Y. Hoshino, A. Randall, Z. Zeng, P. Baldi, R. A. Doong, K. J. Shea, *J. Am. Chem. Soc.* **2012**, *134*, 15765-15772; b) Y. Yonamine, Y. Hoshino, K. J. Shea, *Biomacromolecules* **2012**, *13*, 2952-2957.

[16] K. Yoshimatsu, B. K. Lesel, Y. Yonamine, J. M. Beierle, Y. Hoshino, K. J. Shea, *Angew. Chem. Int. Ed.* **2012**, *51*, 2405-2408.

[17] K Nagase, J. Kobayashi, A. Kikuchi, Y. Akiyama, H. Kanazawa, T. Okano, *Biomacromolecules* **2008**, *9*, 1340–1347.

[18] Y. Akiyama, A. Kikuchi, M. Yamato, T. okano, *Langmuir* **2004**, *2004*, 5506-5511.

[19] Y. Hoshino, M. Nakamoto, Y. Miura, *J. Am. Chem. Soc.* **2012**, *134*, 15209-15212.

[20] I. Lynch, K. A. Dawson, *J. Phys. Chem. B* **2003**, *107*, 9629-9637.

[21] S. Nayak, S. B. Debord, L. A. Lyon, *Langmuir* **2003**, *19*, 7374-7379.

[22] M. J. Serpe, C. D. Jones, L. A. Lyon, *Langmuir* **2003**, *19*, 6. 8759-8764.

[23] a) K. Tanaka, Y. Okahata, *J. Am. Chem. Soc.* **1996**, *118*, 10679–10683; b) Y. Hoshino, S. Tajima, H. Nakayama, Y. Okahata, *Macromol. Rapid Commun* **2002**, *23*, 253-255.

[24] S. Nayak, L. A. Lyon, *Angew. Chem. Int. Ed.* **2005**, *44*, 7686-7708.

[25] L. A. Lyon, Z. Meng, N. Singh, C. D. Sorrell, A. S. John, *Chem. Soc. Rev.* **2009**, *38*, 865–874.

[26] T. Tanaka, E. Sato, Y. Hirokawa, S. Hirotsu, J. Peetermans, J. *Phys. Rev. Lett.* **1985**, *55*, 2455-2458.

Chapter 3. Design Rationale of Thermally Responsive Microgel Particle Films That Reversibly Absorb Large Amounts of CO_2 and Maximization of CO_2 capture capacity

Abstract

Inspired by the efficient CO_2 transport mechanism of hemoglobin in blood known as Bohr effect, here we revealed the design rationale of amine-functionalized thermo-responsible gel particles (GPs) films that reversibly capture and release large amount of CO_2 efficiently from a model exhaust gas of fire power plants in a small temperature change (30 °C -75 °C). pK_a value of ammonium ions in the GPs at both CO_2 capture temperature (30 °C) and release temperature (75 °C) is found to be the primary factor responsible for the stoichiometry of reversible CO_2 capture by the amines in the GP films. The pK_a values can be tuned by the properties of GPs such as volume phase transition temperature (VPTT), the size, the swelling ratio and the imprinted microenvironment surrounding the amines. The optimal GP obtained according to the design rationale showed high capture capacity (68 mL CO_2/g GPs, 3.0 mmol CO_2/g GPs) that is comparable to most of solid sorbents though the regeneration temperature is as low as 75 °C. We anticipate that GPs films that can reversibly capture other acidic and basic gas can be achieved by the same strategy inspired by the Bohr effect of hemoglobin.

3.1. Introduction

The accumulation of CO_2 in the atmosphere due to burning of fossil fuels is considered the main cause of global climate change.[1] Meanwhile, CO_2 is expected to be a carbon source for the production of liquid fuels, such as methanol and dimethyl ether, through the use of regenerative energy. [2] Thus, the development of energy-efficient CO_2 separation and recovery processes for point sources, such as fossil fuel power plants, is essential not

only for minimizing climate change but also for the future use of carbon-based energy.

Conventional processes that recover CO_2 from the high humidity exhaust gases of power plants use aqueous solutions of ethanolamine as a CO_2 absorbent. CO_2 in the exhaust gases is selectively captured by the absorbent at a low temperature (~40 °C) and then recovered by heating the solution, typically above 140 °C. [3]- [5] Although the amine solution exhibits a high CO_2 absorption capacity, the high-energy consumption of the heating process limits its use in the environmentally friendly process. [4]-[8]

Porous solid adsorbents that can be regenerated under relatively mild conditions, such as metal-organic frameworks (MOFs), [9]-[10] zeolites, [9]-[10] and silica with physically or chemically supported amine polymers, [9]-[13] have recently been developed as alternatives to the aqueous amine solution. However, solid CO_2 sorbents are rarely capable of efficiently capturing CO_2 from highly humid gases because the adsorption of water molecules competes with that of CO_2 on the pore surfaces. Furthermore, the capillaries and pores of the sorbents are easily blocked by the liquefied water, preventing CO_2 from diffusing into the pores. [9]- [12] Thus, the development of sorbents that absorb/adsorb large amount of CO_2, even in humid environments, and desorb CO_2 at low temperatures (<100 °C) is of great importance.

It has been reported that poly-*N*-isopropylacrylamide (pNIPAm) undergoes a reversible volume phase transition from a hydrophilic swollen state to a hydrophobic collapsed state at temperatures below and above, respectively, the volume phase transition temperature (VPTT) of ~32 °C. [14]

The phase transition is induced by the entropy-driven dissociation of water from pNIPAm chains after heating above the VPTT. [14] The temperature responsive pNIPAm-based functional hydrogels have been widely used as materials to reversibly capture targets, such as dyes, [15] drugs, [16] peptides, [17] proteins, [18], [19] nucleotides, [20] cells, [21] and protons, [22] in aqueous media via the volume phase transition. The multipoint interactions are reversibly switched on/off by varying the volume density of hydrophobic functional groups, [16], [23], [24] the number of charged functional groups, [20], [25] and/or the rigidity of the polymer chains[26] at temperatures above and below the VPTT.

Recently, we reported that hydrogel films composed of temperature-responsive microgel particles (GPs) consisting of NIPAm and *N*-[3-(dimethylamino)propyl]methacrylamide (DMAPM) reversibly absorbed and released CO_2 via a volume phase transition during cooling (30 °C) and heating (75 °C) cycles, respectively. [27] Below the VPTT, amines in the swollen GPs were capable of forming ion pairs with absorbed bicarbonate ions. Above the VPTT, shrinkage of the GPs triggered CO_2 desorption. [25]

However, guidelines to design GP films that reversibly absorb CO_2 with high capacity and stoichiometry have not been revealed.

In the case of reversible CO_2 absorption by the blood of animals, the pK_a value of the Brønsted acid and base in the hemoglobin plays a crucial role for the control of CO_2 solution equilibrium: The pK_a value of the ammonium and imidazolium cations decreases due to the drastic conformational change of the hemoglobin caused by oxygen binding to the heme. The shift of the pK_a triggers the release of H^+ into the blood, leading to the release of CO_2 efficiently from lungs (Bohr effect). [28], [29]

Inspired by the Bohr effect of hemoglobin, we hypothesized that the pK_a value of the protonated amines (ammonium ions) within GPs (pK_a value of GPs) at the CO_2 capture temperature (30 °C) and release temperature (75 °C) would contribute to the reversible capture efficiency of CO_2.

In this study, in order to clarify the design rationale, a series of GPs with a variety of compositions using different polymerization conditions were prepared. The effects of the physical and chemical properties of GPs, such as VPTT, size, swelling ratio, on pK_a values and the reversible CO_2 capture stoichiometry against amines were systematically investigated. pK_a values of the ammonium ions in the GPs were also tuned by the "microenvironment-imprinting" strategy as we described in the recent report. [22] The reversible CO_2 capture capacity was maximized based on the design rational revealed in this study. Humidified gas (60 °C) consisting of 10% CO_2 and 90% N_2, which is comparable to the post-combustion gas of fire power plants, was used as feed gas. [6], [30] The CO_2 was captured at 30 °C and released at 75 °C.

3.2. Experiments

3.2.1 Materials

NIPAm (Wako Pure Chemical Industries, Ltd.) was purified by recrystallization from *n*-hexane and dried *in vacuo* at room temperature. *N*-[3-(Dimethylamino)propyl]methacrylamide (DMAPM, Tokyo Chemical Industry Co., Ltd.) was purified by Al_2O_3 column (Merck KGaA) prior to use. 2,2′-azobis(2-methylpropionamidine) dihydrochloride (AAPD, Wako Pure Chemical Industries, Ltd.), *N,N'*-methylenebis(acrylamide) (Bis, Tokyo Chemical Industry Co., Ltd.), cetyltrimethylammonium bromide (CTAB, Wako Pure Chemical Industries, Ltd.)

were used as received. The dialysis membrane (MWCO 12,000–14,000) was purchased from Spectrum Laboratories, Inc. The anion-exchange resin (A2004-OH, Muromachi Technos Co., Ltd.) was first activated by 1 M NaOH, and then washed carefully with deionized water. The water was purified using a Direct-Q Ultrapure Water System (Merck, Ltd.).

3.2.2 Preparation of GPs

A series of GPs containing NIPAm, crosslinker (Bis) and functional monomer of tertiary amine (DMPAM) were synthesized by precipitation polymerization as reported [27]. Bis amount was varied to prepare GPs with different crosslink degree and swelling ratio. GPs with same composition but different pK_a were synthesized in via "microenvironment imprinting" strategy by adding HCl or NaOH into monomer solution. [22] The GPs prepared in the presence of large amount of protons would show higher pK_a value because more hydrophilic microenvironment will be imprinted around the charged ammonium groups. GPs with larger size were obtained by decreasing concentration of surfactant while GPs with smaller size were prepared from solutions of lower total monomer concentration. To decrease VPTT of GPs more hydrophobic monomer TBAm was incorporated into GPs with large amount of functional monomer DMAPM. Details about polymerization condition of GPs were summarized in table 3-1.

Table 3-1. Polymerization conditions of the GPs

GPs	feed ratio				polymerization media	CTAB (mM)	AAPD (mM)	Concentration (mM)
	NIPAm (mol%)	DMAPM (mol%)	Bis (mol%)	TBAM (mol%)				
D5B2	93	5	2	0	water	2.0	2.5	312
D5B0	95	5	0	0	water	2.0	2.5	312
D5B5	90	5	5	0	water	2.0	2.5	312
D5B10	85	5	10	0	water	2.0	2.5	312
D5B2T40	53	5	2	40	water	2.0	2.5	312
D5B10-1/4HCl	85	5	10	0	1/4 eq. HCl	2.0	2.5	312
D5B2-1/2HCl	93	5	2	0	1/2 eq. HCl	2.0	2.5	312
D5B2-1/1HCl	93	5	2	0	1/1 eq. HCl	2.0	2.5	312
D5B2-1/2NaOH	93	5	2	0	1/2 eq. NaOH	2.0	2.5	312
D5B2-L	93	5	2	0	water	0.16	2.5	312
D5B2-S	93	5	2	0	water	2.0	0.625	78
D5B2-1/2NaOH-S	93	5	2	0	1/2 eq. NaOH	2.0	0.625	78
D30B2	68	30	2	0	water	2.0	2.5	312
D30B2T40	28	30	2	40	water	2.0	2.5	312
D55B2	43	55	2	0	water	2.0	2.5	312
D55B2T43	0	55	2	43	water	2.0	2.5	312

According to the different polymerization condition of each GP described in table 3-1, the monomers were first dissolved in water, resulting in the designed total concentration. For the one synthesized through microenvironment-imprinting method, specific amount of HCl or NaOH was added into the monomer solution. Then surfactant CTAB was added to the monomer solution followed by heating to 70 °C. TBAm was dissolved in small amount of methanol (0.64 g/mL) and injected into the hot monomer solution afterwards. Then the solution was degased by purging nitrogen gas while stirring at 70 °C for 1 h. Later, aqueous solution of AAPD was added by syringe. The polymerization reaction was carried out at 70 °C for 3 h under nitrogen atmosphere, as illustrated in scheme 3-1. The resulting mixture was purified by dialysis against an excess volume of water over four days (water was changed more than three times a day). The anion-exchange of the GPs was conducted to remove the trace amount of counter anions and CO_2 absorbed by amines during dialysis.

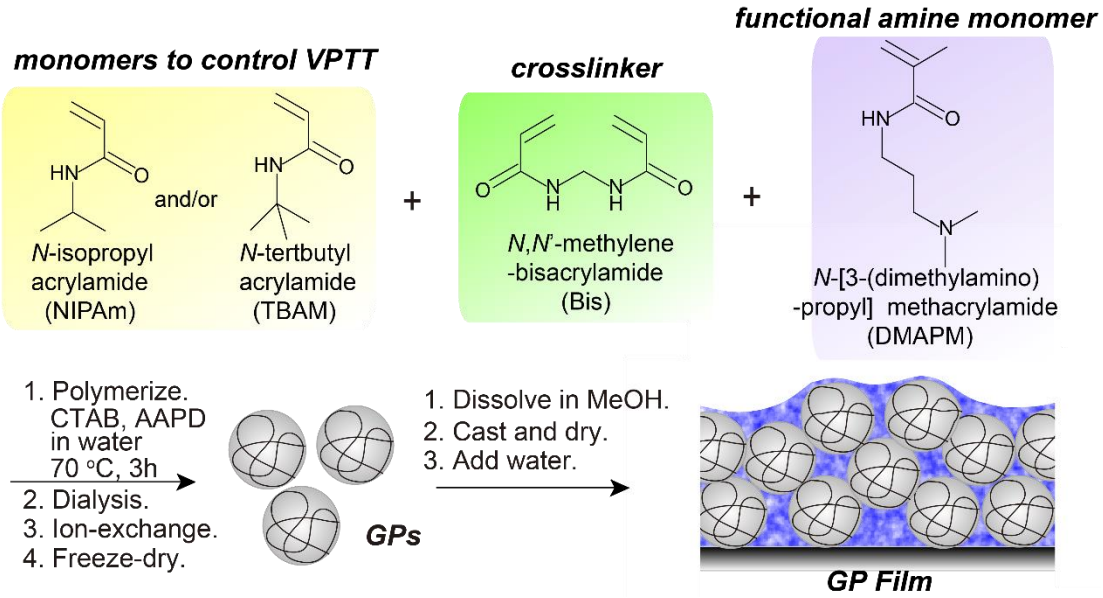

Scheme 3-1. Synthesis of GPs and preparation of GP films

3.2.3. Quantification of hydrodynamic diameter, VPTT and swelling ratio of GPs.

The hydrodynamic diameters and scattering intensity of GPs were measured by dynamic light scattering (DLS) instrument (Zetasizer Nano, Malvern Instruments Ltd.). The GP solutions were sealed within the quartz cells filled with nitrogen. The solutions were equilibrated at each temperature for 6 min prior to the measurement. Relative scattering intensity was defined here by equation (1). VPTT was determined as the temperature where the plateau of relative scattering intensity started. Swelling ratio was defined as the ratio of diameters at 30 °C (D_{30}) and 75 °C (D_{75}), as described by equation (2).

$$\text{Relative scttering intensity} = \frac{I - I_{min}}{I_{max} - I_{min}} \qquad (1)$$

$$\text{Swelling ratio} = \frac{D_{30}}{D_{75}} \qquad (2)$$

3.2.4. Quantification of amine content in GPs.

A SevenMulti pH meter equipped with pH probes (InLab® Routine Pro, METTLER TOLEDO) was calibrated with three standard buffers (pH 7.00, 4.01 and 9.21) prior to use. pH titration with 0.01 M HCl was performed at 30 °C and 75 °C under nitrogen purging with stirring at 1000 rpm. Temperature of GP solution was controlled by water bath.

3.2.5. Measurement of pK_a shift curve in heating process.

Since apparent pK_a is defined as pH value at the half neutralization point here, pK_a shift of GP solution was measured with the pH probe by the following method: half neutralized GP solution was first prepared by adding 0.5 equivalent of HCl to the GP solution after quantification of amine content of the GPs by pH titration.

Then under the nitrogen atmosphere with stirring 1000 rpm, pH value and temperature of the solution was recorded by the pH meter every three seconds during temperature swing process. Temperature was controlled by synthesis plant (EYELA PPW-2000, Tokyo Rikakikai Co., Ltd.).

3.2.6. Preparation of GP films

The lyophilized GPs were dissolved in methanol. The hydrogel films were then prepared by casting the methanol solutions of 120 mg of GPs on the inner bottom surface of a stainless steel container with surface area of 120 cm^2, followed by the addition of 4 mL of water per gram of GPs after completely evaporating methanol.

3.2.7. Measurement of CO_2 absorption capacity of GP films

CO2 absorption capacities of the GP films were quantified by a grease-free steel-Teflon tube system. As illustrated in scheme 3-2, 10 % CO2 (90 % N_2, 10 mL/min) gas was flowed into water of 60 °C to generate saturated water vapor at the temperature. The resulting 60 °C water-saturated gas mixture was guided into a stainless steel container with GP film on inner surface, and then channeled to a gas chromatography instrument (GC, Shimadzu Corp.) equipped with a thermal conductivity detector (TCD) and Shincarbon ST 50/80 column (2 m, Shinwa Chemical Industries Ltd.; carrier gas: He, 40 mL/min; column temperature: 210 °C; detector temperature: 240 °C). All the GP films were equilibrated under the gas flow for about 2 h at 30 °C. Thereafter, CO_2 desorption capacity at 75 °C and absorption capacity at 30 °C of each film were quantified by monitoring concentration of CO_2 every 1.7 minutes by the GC-TCD for 25 min and 46 min respectively.

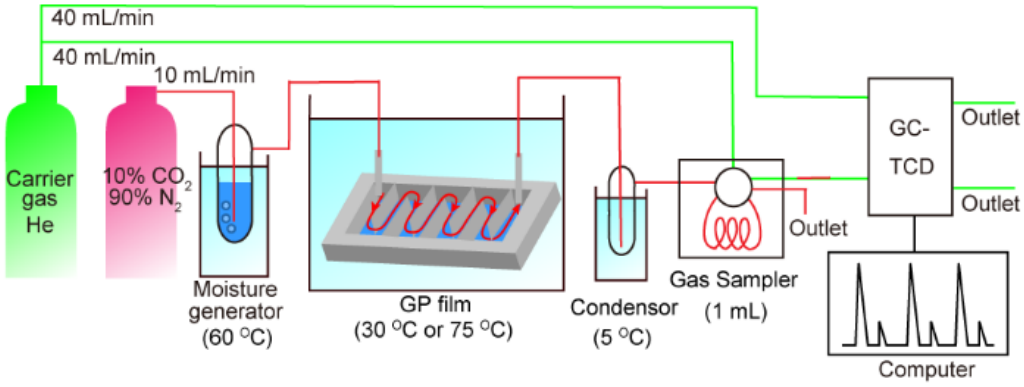

Scheme 3-2. Gas flow in the CO_2 absorption quantification system

3.3. Results and Discussion

3.3.1. Effect of pK_a values of GPs on the reversible CO_2 capture stoichiometry of GP films.

Dynamic and reversible transition of pK_a value of the Brønsted acid and base groups in proteins plays an important role in their functions such as molecule/ion transfer, enzymatic reaction, and molecular recognition. [29], [30] The pK_a value are significantly influenced by the microenvironment around the functional groups such as hydrophobicity, hydrogen bonding and distance to the neighboring charges.[29], [31]-[34] Thus, the pK_a value can be further dynamically shifted by the conformation change of polypeptide around the functional groups that induces a microenvironment change. For example, in the case of CO_2 transfer through the bloodstream of animals, pK_a value of the ammonium and imidazolium cations in/on the hemoglobin decreases due to the drastic conformational change of the polypeptides caused by oxygen binding to the heme. The shift of pK_a value triggers release of H^+ into the blood, lowers down the pH of blood and drives off the CO_2 efficiently from lungs (Bohr effect). [29], [35] Inspired by the function of hemoglobin, we expected that pK_a value of the protonated amines (ammonium ions) within GPs

(pK_a value of GPs) at the CO_2 capture temperature (30 °C) and release temperature (75 °C) would contribute to the reversible capture efficiency of the CO_2.

To clarify the effect of pK_a value of GPs on the reversible CO_2 capture stoichiometry of GP films in the temperature swing process from 30 °C to 75 °C, a series of GPs with the same composition but different pK_a value were prepared by the "microenvironment-imprinting" strategy. [36], [22] Imprinting is a method to create polymers with specific microstructures that show strong affinity to target molecules and ions by crosslinking the polymer networks in the presence of targets. [37], [38] It has been reported that pNIPAm based acrylic acids (AAc) containing GPs with different pK_a value can be prepared by the "proton-imprinted" strategy: the GPs polymerized in low pH below pK_a of AAc showed a much higher pK_a value than the ones prepared at high pH, because stronger proton-affinity sites were incorporated into the relatively hydrophobic microenvironment around the protonated AAc. [22]

We anticipated that amine-containing GPs with different pK_a value could also be prepared via the "microenvironment-imprinting" strategy. Thus, the GPs were polymerized in the presence of acid (1 or 1/2 equivalent of HCl against amine monomer DMAPM) or base (1/2 equivalent of NaOH). All GPs were polymerized in the aqueous monomer solution (312 mM) consisting of 5 mol% DMAPM, 2 mol% Bis and 93 mol% NIPAm at 70 °C using 2.5 mM AAPD as radical initiator and 2.0 mM CTAB as stabilizer.

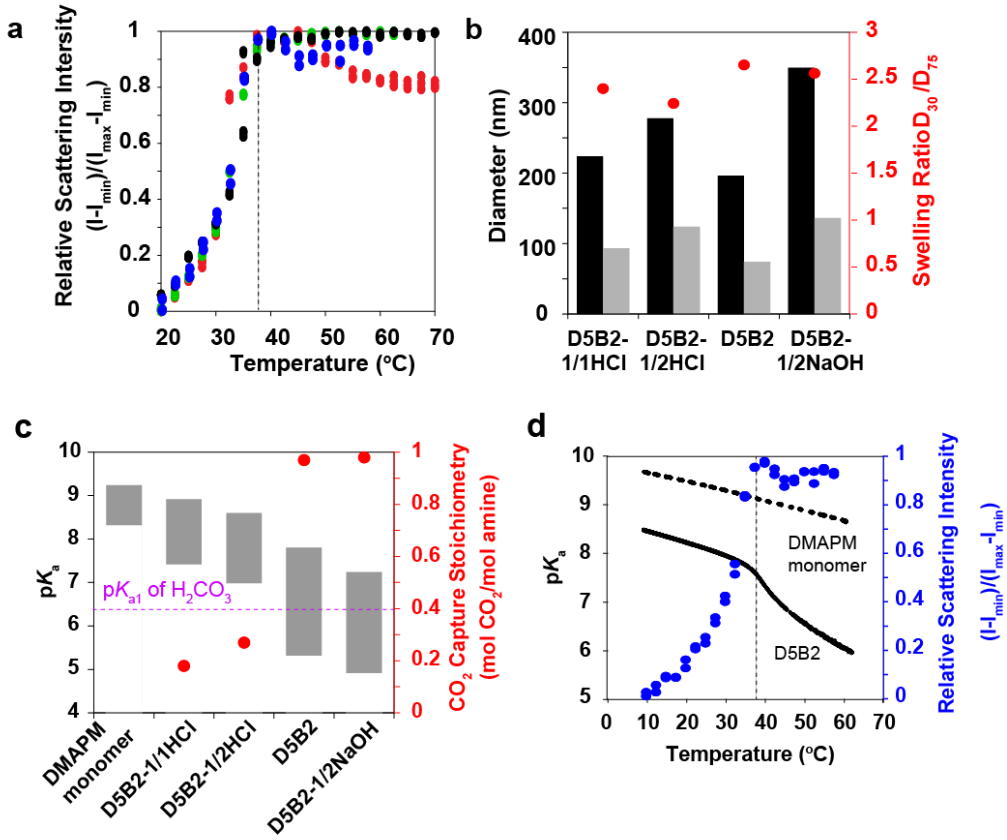

Figure 3-1. (a) Relative scattering intensity as a function of temperature for the GP D5B2 (blue), D5B2-1/1HCl (red), D5B2-1/2HCl (green) and D5B2-1/2NaOH (black). (b) Diameter (left Y axis) at 30 °C (black bar) and 75 °C (gray bar) and swelling ratio (right Y axis, red dot) between 30 °C and 75 °C of the GPs. (c) pK_a value (left Y axis) at 75 °C (bottom of bar) and 30 °C (top of bar) of the GPs, and the reversible CO_2 capture stoichiometry (right Y axis, red dot) of the GP films in the temperature range 30-75 °C. (d) pK_a shift (left Y axis) of GP D5B2 (black solid line) and the monomer DMAPM (black dashed line) in heating process, and the temperature dependent relative scattering intensity (right Y axis, blue dot) of GP D5B2.

VPTT of the GPs were determined by monitoring the scattering intensity of the GP solutions in heating process (Figure 3-1a). All the four GPs including the ones

polymerized with 1 and 1/2 equivalent of HCl (D5B2-1/1HCl, D5B2-1/2HCl), with 1 equivalent of NaOH (D5B2-1/2NaOH), and the one without HCl nor NaOH (D5B2) showed the similar VPTT at about 38 °C. Hydrodynamic diameter of GPs at 30 °C (D_{30}) and 75 °C (D_{75}) together with swelling ratio of GPs at 30 °C (D_{30}/D_{75}) were shown in figure 3-1b. The similar swelling ratio in the range of 2.3~2.7 was observed. From those results, it was concluded that, VPTT and swelling ration of GPs are independent from the polymerization condition.

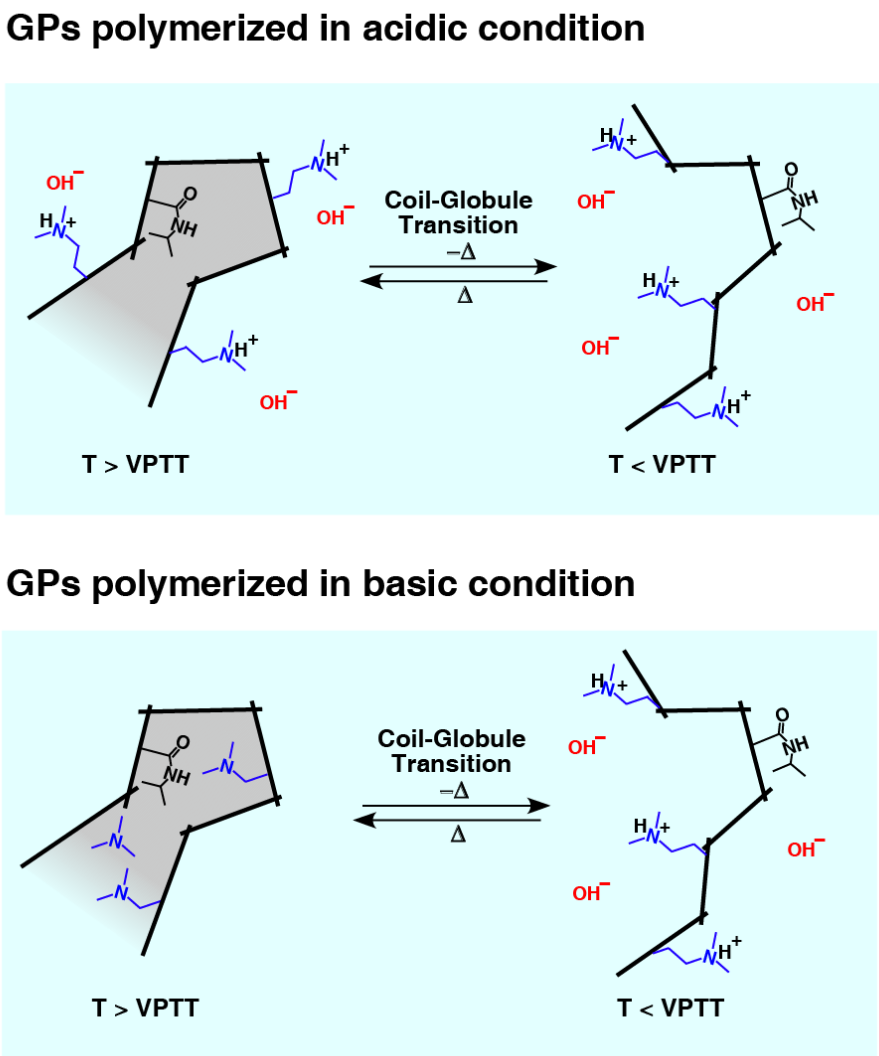

Scheme 3-3. Mechanism of effect of polymerization pH on pK_a of the resulted GPs.

Apparent pK_a value of the GPs at 30 °C and 75 °C was determined by acid/base titration of GP solutions and plotted as top and bottom of the black bars in Figure 3-1c.[25] All the GPs showed lower pK_a value than the amine monomer DMAPM at both temperatures, indicating the relatively low dielectric constant and high steric hindrance around the amine groups in GPs as well as the electrostatic repulsion between neighboring charges.[39], [40] Besides, in accordance with our expectation, pK_a value of D5B2-1/1HCl and D5B2-1/2HCl at 75 °C (7.4 and 7.0 respectively) was significantly higher than that of D5B2 and D5B2-1/2NaOH (5.3 and 4.9 respectively). The large difference in pK_a value can be explained by the microenvironment imprinting effect, as shown in scheme 3-3: When the GPs were polymerized in proton rich solution (in the presence of HCl), the protonated DMAPM was imprinted in the polar and hydrophilic microenvironment in the GPs (D5B2-1/1HCl and D5B2-1/2HCl), resulting in higher pK_a value than the ones polymerized in the proton poor solution (D5B2 and D5B2-1/2NaOH). Although diameter of the GPs was not exactly same, the large difference in pK_a value (>2) at 75 °C can't be caused by the difference in size, because the smallest GP D5B2 (74 nm) and the largest GP D5B2-1/2NaOH (136 nm) showed a pK_a difference of only 0.4 (5.3-4.9).

Figure 3-1c also showed that pK_a difference (ΔpK_a) of all the GPs (1.5~2.5) between 30 °C and 75°C was larger than that of monomer (0.9). In order to better understand the temperature dependent pK_a difference, the apparent pK_a value of GP D5B2 and the monomer DMAPM was recorded in a heating process. The result in figure 3-1d showed that a sharp pK_a transition of GP D5B2 occurred at the temperature around the VPTT of the GP, and a steep pK_a decrease continued in a wide temperature range above VPTT. However, this kind of sharp pK_a transition

was not observed in the case of monomer, indicating the sharp pK_a decrease was induced by volume phase transition, during which the increased hydrophobicity, steric hindrance and the decreased dielectric constant at high temperature make the amine groups more difficult to be protonated. [39]

In figure 3-1c, ΔpK_a of the GPs between 75 °C and 30 °C polymerized with HCl (D5B2-1/1HCl, D5B2-1/2HCl) (1.5, 1.6 respectively) were significantly smaller than the GP D5B2 and D5B2-1/2NaOH (2.5, 2.3), though swelling ratio were similar (2.3~2.7). We hypothesize that comparing with the GP D5B2 and D5B2-1/2NaOH that was polymerized with 0 and 0.5 equivalent of NaOH, the protonated DMAPM groups (ammonium) within the GP D5B2-1/1HCl and D5B2-1/2HCl are relatively far away from the hydrophobic pNIPAm moieties and backbones at collapsed state during polymerization, because the protonated amine groups are relatively polar and hydrophilic. In other words, the amine groups of the GPs prepared with HCl are located in the "pseudo-swollen" microenvironment that analogous to swollen state. After volume phase transition from collapsed state to swollen state, the effect of swelling on the amines within the "pseudo-swollen" GPs is smaller because the effect of swelling of pNIPAm moieties and backbones is partially neutralized by the already existed "pseudo-swollen" microenvironment around the amines. As a result, the ΔpK_a of the GPs prepared with HCl was smaller than others.

The reversible CO_2 capture stoichiometry of the GP films was also presented as red plots in figure 3-1c. The GP D5B2-1/1HCl and D5B2-1/2HCl showed a very low reversible CO_2 capture stoichiometry (0.18 and 0.27 mol CO_2/mol amine), while the value for GP D5B2 and D5B2-1/2NaOH were as high as 0.97 mol CO_2/mol amine. The difference in the stoichiometry can be interpreted by the acid-base theory: It

has been reported that the tertiary amines in GPs and the CO_2 forms ammonium ions (RN_3H^+) and bicarbonate ions (HCO_3^-) via base-catalyzed reactions. [41], [42] In a aqueous media containing RN_3H^+ and HCO_3^-, there is always an equilibrium between their corresponding conjugated base/acid, as described in scheme 3-4.

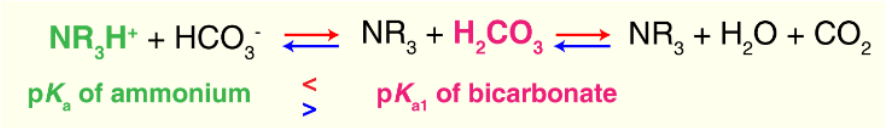

Scheme 3-4. Equilibrium of the tertiary amine-CO_2 reaction

In the cases that pK_a of NR_3H^+ is above pK_{a1} of H_2CO_3, which indicates the NR_3H^+ hold a proton more tightly than H_2CO_3 does, the proton will go from the stronger acid H_2CO_3 to the stronger base NR_3, as a result more NR_3 will be consumed and more CO_2 will be captured, as presented by the blue arrows in scheme 3-4. On the contrary when pK_a of NR_3H^+ is below pK_{a1} of H_2CO_3, more CO_2 will be released, as the red arrows in shceme 3-4. [43]

The pK_{a1} value of carbonic acid (H_2CO_3) was determined in the range of 6.35 ± 0.05 at both 30 °C and 75 °C by Harned and Davis, [44] however pK_a value of the amine-containing thermal responsive GPs dramatically depend on the temperature, as presented in the figure 3-1c and 3-1d. The high pK_a value of GP D5B2-1/1HCl and D5B2-1/2HCl at 75 °C (7.4 and 7.0 respectively) that was higher than pK_{a1} of H_2CO_3 (6.35) inhibited the release of CO_2. As a result the reversible CO_2 capture stoichiometry was low (0.18, 0.27 mol CO_2/mol amine), although the pK_a at 30 °C are high enough (8.9, 8.6) to capture CO_2 efficiently. For D5B2 and D5B2-1/2NaOH, the high reversible CO_2 capture stoichiometry (0.97 mol CO_2/mol amine) was achieved due to the low pK_a value at 75°C (5.3 and 4.9 respectively)

that are below pK_{a1} of H_2CO_3 and meanwhile the high pK_a value of the GPs at 30 °C (7.8 and 7.2) that are above pK_{a1} of H_2CO_3.

3.3.2 Effect of ΔpK_a of GPs on the reversible CO_2 capture stoichiometry of GP films.

In figure 3-1c, except for the low pK_a value of GP D5B2 and D5B2-1/2NaOH at 75 °C, their larger ΔpK_a between 30 °C and 75 °C (2.5 and 2.3 respectively) than that of GP D5B2-1/1HCl and D5B2-1/2HCl (1.5 and 1.6 respectively) may also be responsible for the high reversible CO_2 capture stoichiometry.

In order to distinguish the effect of pK_a value and ΔpK_a on the reversible CO_2 capture stoichiometry of the GP films, GP with smaller ΔpK_a than D5B2 was prepared by increasing cross-linker Bis to 10 mol% (D5B10), since it has been reported that crosslink degree influences ΔpK_a of the GPs. [22]

pK_a value of GP D5B2 and D5B10 at 30 °C and 75 °C was plotted as top and bottom of the bars in figure 3-2. ΔpK_a of GP D5B10 (1.4) was apparently smaller than D5B2 (2.5). The GP with small ΔpK_a (D5B10) showed lower reversible CO_2 capture stoichiometry (0.74 mol CO_2/mol amine) than the one with large ΔpK_a (D5B2) (0.97 mol CO_2/mol amine) (Figure 3-2b). However, other than the difference in ΔpK_a, another possible reason for the low stoichiometry of GP D5B10 is the low pK_a value at 30 °C (5.9) that is below pK_{a1} of H_2CO_3.

To identify the main factor that governs the reversible CO_2 capture stoichiometry, we designed another GP which has higher pK_a value than D5B10, and smaller ΔpK_a than D5B2 by the "microenvironment-imprinting" strategy as described in section **3.3.1**. The GPs was prepared by polymerizing D5B10 in the presence of appropriate amount of HCl (D5B10-1/4HCl).

Figure 3-2 showed pK_a value and ΔpK_a of D5B10-1/4HCl. pK_a values of D5B10-1/4HCl at 30 °C and 75 °C (6.8 and 5.3) was higher than that of D5B10 (5.9 and 4.5) but ΔpK_a of D5B10-1/4HCl (1.5) was comparable to that of D5B10 (1.4). GP D5B10-1/4HCl showed a much higher CO_2 capture stoichiometry (0.97 mol CO_2/mol amine) than GP D5B10 (0.74 mol CO_2/mol amine), despite of the similar ΔpK_a.

On the other aspect, as displayed in figure 3-2, pK_a value of D5B10-1/4HCl at 75°C (5.3) was similar with D5B2 (5.3) while ΔpK_a of D5B10-1/4HCl (1.5) was much smaller than D5B2 (2.5). However in figure 3-2b both of the two GPs exhibited high and comparable reversible CO_2 capture stoichiometry (0.97 mol CO_2/mol amine) though ΔpK_a was greatly different.

It is concluded from those results that ΔpK_a is a minor factor for the reversible CO_2 capture stoichiometry, and high reversible CO_2 capture stoichiometry is possible for GPs that exhibit smaller ΔpK_a as long as the pK_a value lies in the appropriate range: pK_a value of the GPs have to be tuned above pK_{a1} of H_2CO_3 (6.35) at CO_2 capture temperature (30 °C) and below pK_{a1} of H_2CO_3 (6.35) at release temperature (75 °C) in order to achieve the high reversible CO_2 capture stoichiometry.

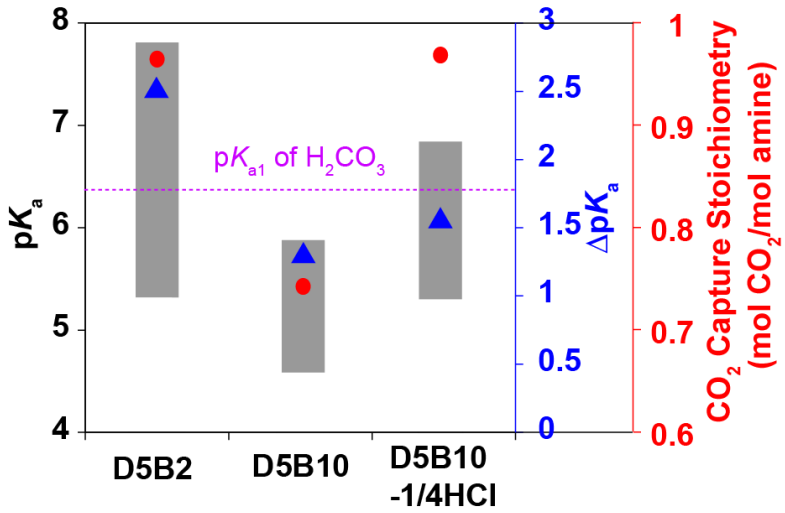

Figure 3-2. pK_a values (left Y-axis) at 75 °C (bottom of bar) and 30 °C (top of bar), and ΔpK_a values (blue right Y-axis, blue triangle) between 75 °C and 30 °C of D5B2, D5B10, and D5B10-1/4HCl, reversible CO_2 capture stoichiometries (red right Y-axis, red dot) of GP films in the temperature range 30-75 °C.

3.3.3. Effect of VPTT of GPs on the reversible CO_2 capture stoichiometry of GP films.

As shown in figure 3-1d, the thermal responsive volume phase transition of the GPs leads to a sharp pK_a transition. Meanwhile pK_a value of the GPs has been revealed to be essential for the reversible CO_2 capture stoichiometry. Therefore it is interesting to see the effect of VPTT of GPs on the reversible CO_2 capture stoichiometry of the GP films.

The GP with lower VPTT than D5B2 was synthesized by incorporating 40 mol% of TBAm that's more hydrophobic than NIPAm together with 5 mol% DMAPM and 2 mol% Bis (D5B2T40). The relative scattering intensity of the GPs solutions was shown in figure 3-3a. Compared with D5B2 (VPTT 38 °C), VPTT of GP D5BT40

decreased to 12 °C. The increased hydrophobic-hydrophobic interaction of the polymers by incorporating 40 mol% TBAm makes the entropy-driven collapse of GP D5B2T40 occurred at a lower temperature.[45], [46]

Figure 3-3b showed the temperature dependent pK_a value of GP D5B2 and D5B2T40. As observed for D5B2, the D5B2T40 also showed a sharp pK_a transition at the temperature around its VPTT (12 °C) and a steep pK_a decrease continued in a wide temperature range above the VPTT. As a result, pK_a value of GP D5B2T40 at both 30 °C and 75 °C (6.0 and 4.8) was low, and the ΔpK_a was small (1.2) as shown in Figure 3-3e. The reversible CO_2 capture stoichiometry of D5B2T40 (0.6 mol CO_2/mol amine) was lower than that of D5B2 (0.97 mol CO_2/mol amine). The low stoichiometric efficiency can be explained by the low pK_a value of D5B2T40 at 30 °C (6.0).

Another pair of GPs with different VPTT were also prepared by increasing the feed ratio of DMAPM to 30 mol% (D30B2).[45], [46] Figure 3-3c showed the VPTT of GP D30B2 was 65 °C. To lower down the VPTT of D30B2, 40 mol% of TBAm was incorporated into the 30 mol% DMAPM-containing GP (D30B2T40). Compared to GP D30B2, VPTT of GP D30B2T40 decreased to 40 °C (Figure 3-3c).

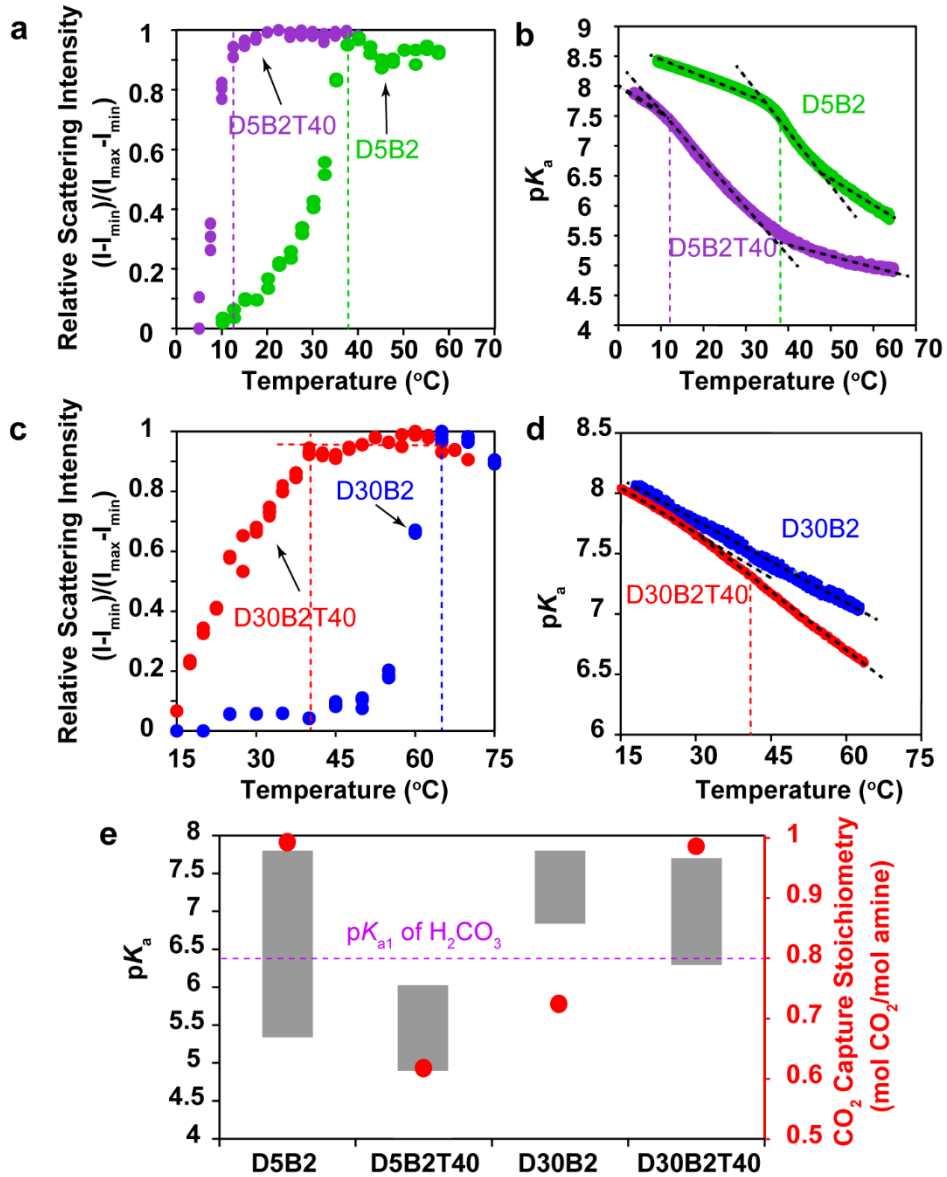

Figure 3-3. (a) Relative scattering intensity as a function of temperature for the GP D5B2 (green) and D5B2T40 (purple). (b) pK_a shift of the GP D5B2 (green) and D5B2T40 (purple) in heating process. (c) Relative scattering intensity as a function of temperature for the GP D30B2 (blue) and D30B2T40 (red). (d) pK_a shift of the GP D30B2 (blue) and D30B2T40 (red) in heating process. (e) pK_a value (left Y axis) at 75 °C (bottom of bar) and 30 °C (top of bar) of the GPs, and the reversible CO_2 capture stoichiometry (right Y axis, red dot) of the GP films in the temperature range 30-75 °C.

pK_a value of GP D30B2 linearly depend on temperature and no obvious sharp transition was observed in the temperature range due to the high VPTT (65 °C) (Figure 3-3d). However, pK_a value of D30B2T40 exhibited a transition from the temperature around its VPTT (40 °C), and a steeper pK_a decrease than D30B2 was observed in the temperature above VPTT. As a result, the GP D30B2T40 had a lower pK_a value at higher temperature range and a larger ΔpK_a than D30B2.

Degree of pK_a transition of the GPs containing 30 mol% DMAPM (figure 3-3d) induced by the phase transition was less significant than the ones containing 5 mol% DMAPM (figure 3-3b). It might be caused by the increased intra-charge repulsion within GPs caused by the smaller amine-amine distance.

pK_a value of GP D30B2 and D30B2T40 at 30 °C and 75 °C was (7.8, 6.8) and (7.7, 6.3) respectively (Figure 3-3e). Figure 3-3e also showed a low reversible CO_2 capture stoichiometry (0.72 mol CO_2/mol amine) of GP D30B2. However, the value of GP D30B2T40 increased to 0.97 mol CO_2/mol amine. The improvement in stoichiometric efficiency can be explained as a result of the relatively low pK_a value of GP D30B2T40 at 75 °C (6.3) that's below pK_{a1} of H_2CO_3. VPTT of GP D30B2T40, which is close to 30 °C, induced a sharp pK_a transition and a steep pK_a decrease in a wide temperature range above VPTT, lowered down the pK_a value at 75 °C, and consequently improved the reversible CO_2 capture stoichiometry.

In summary, results in figure 3-3 lead to the comparable conclusion to figure 3-1 and figure 3-2 that pK_a value of the GPs at 30 °C and 75 °C governs the reversible CO_2 capture stoichiometry. However, the VPTT of the GPs also plays a crucial part: The GPs with much lower VPTT than the CO_2 capture temperature (30 °C) will show low reversible CO_2 capture stoichiometry due to the low pK_a value.

Meanwhile, the presence of VPTT that gives rise to a large pK_a transition of GPs in a wide temperature range above the VPTT, should locate as close to 30 °C as possible be beneficial to the high reversible CO_2 capture stoichiometry.

However it should be noticed that the presence of VPTT above and close to 30 °C is not enough for high CO_2 capture stoichiometry if pK_a value at 30 °C and 75 °C lies in an improper level. For example, in figure 3-1, though VPTT of the GP D5B2-1/1HCl and D5B2-1/2HCl was 38 °C, the high pK_a value at 75 °C (7.4 and 7.0 respectively) seriously restricted the efficient CO_2 release (0.18 and 0.27 mol CO_2/mol amine respectively).

3.3.4. Effect of Size of GPs on the reversible CO_2 capture stoichiometry of GP films.

We have reported that the GP films exhibited larger CO_2 capture capacity than conventional bulk hydrogel film due to the small dimension of GPs that leads to fast responsibility and ion diffusion. [27] Herein effect of GPs size on the reversible CO_2 capture stoichiometry was discussed.

GPs with larger size can be prepared by increasing concentration of monomer or by decreasing concentration of surfactant. [47] In this study, the GP that shows larger hydrodynamic diameter (D5B2-L) than D5B2 was prepared by decreasing concentration of surfactant CTAB, while the GP that has smaller diameter (D5B2-S) was synthesized from monomer solution with lower total concentration.

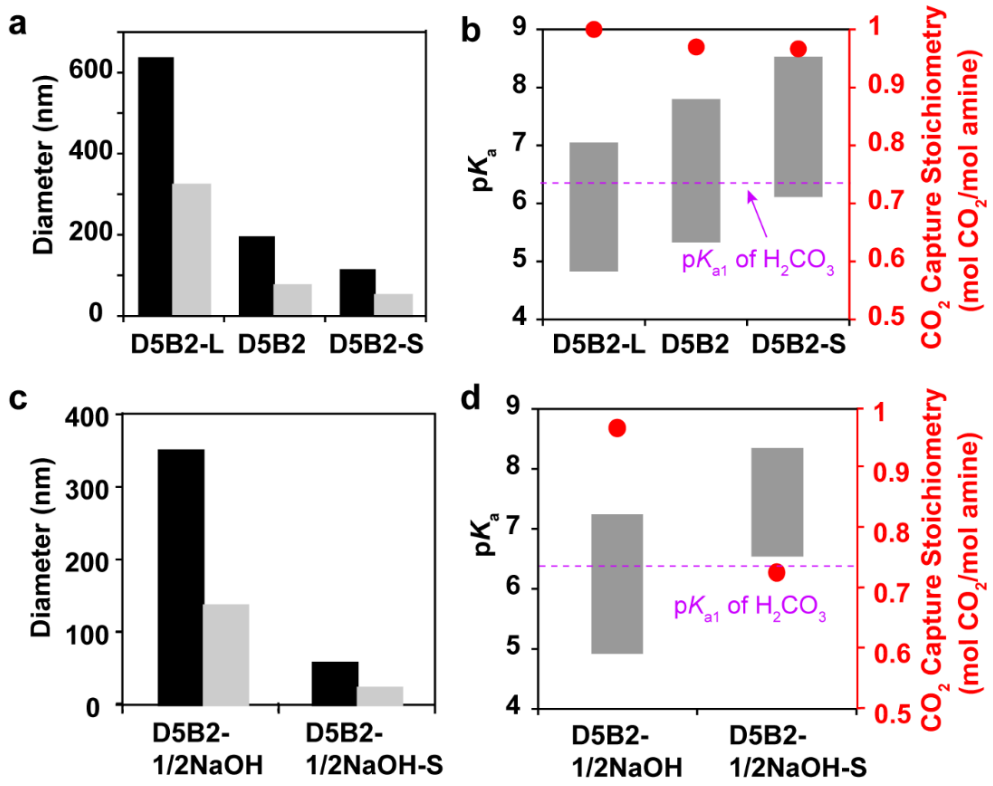

Figure 3-4. (a) Diameters at 30 °C (black bar) and 75 °C (gray bar) of D5B2-L, D5B2, and D5B2-S. (b) pK_a values (left Y-axis) at 75°C (bottom of bar) and 30°C (top of bar) of the GPs, and the reversible CO_2 capture stoichiometries (right Y-axis, red dot) of the GP films in the temperature range 30-75 °C. (c) Diameters at 30 °C (black bar) and 75 °C (gray bar) of D5B2-1/2NaOH and D5B2-1/2NaOH-S. (d) pK_a values (left Y-axis) at 75 °C (bottom of bar) and 30 °C (top of bar) of the GPs, and the reversible CO_2 capture stoichiometries (right Y-axis, red dot) of the GP films in the temperature range 30-75 °C.

Diameter of the GPs at 30 °C and 75 °C was shown in figure 3-4a. As expected, the GP D5B2-L (638 nm at 30 °C and 322 nm at 75 °C) has larger diameter than D5B2 (196 nm and 74 nm), and the D5B2 has the smallest size (115 nm and 49 nm). pK_a value of the GPs at 30 °C and 75 °C was presented as the top and bottom of the black bars in Figure 3-4b. It can be seen clearly that pK_a value of the GPs

at both temperature increased with decreasing diameter. The possible mechanism is shown in scheme 3-5. The amine groups located at the exterior of GPs are supposed to show higher pK_a value than the interior ones because of the higher dielectric constant as well as the less steric hindrance. In the meantime, the amine groups at the smaller GP exterior account for a much larger percentage than that of larger GPs. Thereby smaller GPs showed higher pK_a value than the larger ones. Figure 3-4b also showed all the three GPs exhibited similar high reversible CO_2 capture stoichiometry (0.96~1.0 mol CO_2/mol amine), despite of the difference in GP diameter and pK_a value.

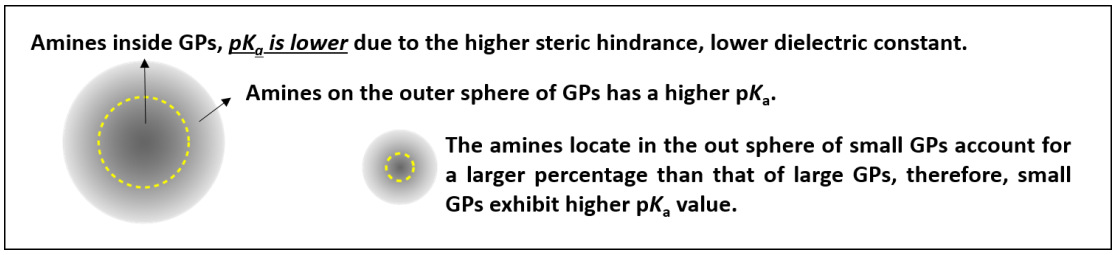

Scheme 3-5. Schematic illustration of the relationship between GP pK_a value and GP size.

Another couple of GPs that show different pK_a range from the GPs in Figure 3-4a and figure 3-4b were polymerized by the "microenvironment imprinting" strategy by adding 0.5 equivalent of NaOH to the monomer solution (D5B2-1/2NaOH and D5B2-1/2NaOH-S). The D5B2-1/2NaOH-S having smaller diameter than D5B2-1/2NaOH was prepared by lowering down the total monomer concentration.

Diameter and pK_a value of the GPs at 30 °C and 75 °C, was shown in figure 3-4c and 3-4d. In good agreement with the result in figure 3-4a, the diameter of GP D5B2-1/2NaOH-S (83 nm at 30 °C and 57 nm at 75 °C) is much smaller than D5B2-

1/2NaOH (715 nm and 349 nm). pK_a value of smaller GPs was also higher than that of larger one. However, the reversible CO_2 capture stoichiometry of GP D5B2-1/2NaOH-S (0.74 mol CO_2/mol amine) was lower than D5B2-1/2NaOH (0.98 mol CO_2/mol amine), as shown in figure 3-4d.

The different result in figure 3-4b and figure 3-4d could also be ascribed to the different pK_a value of GPs. The high pK_a value of D5B2-L, D5B2, D5B2-S and D5B2-1/2NaOH at 30 °C (7.0, 7.8, 8.5, 7.2 respectively) above pK_{a1} of H_2CO_3 (6.35), meanwhile the low pK_a value at 75 °C (4.8, 5.3, 6.1, 4.9 respectively) below pK_{a1} of H_2CO_3 resulted in the high reversible CO_2 capture stoichiometry. However pK_a value of GP D5B2-1/2NaOH-S at 30 °C and 75 °C in figure 3-4d was 8.4 and 6.6. Its high pK_a value at 75 °C (6.6) that's above pK_{a1} of H_2CO_3 restricted efficient release of CO_2, resulting in the low reversible CO_2 capture stoichiometry (0.74 mol CO_2/mol amine).

In general, the results in figure 3-4 lead to the conclusion that the reversible CO_2 capture stoichiometry of GPs can be improved by regulating pK_a value of GPs at both 30°C and 75°C through varying their diameter. The smaller the diameter, the higher the pK_a value.

3.3.5. Effect of swelling ratio of GPs on the reversible CO_2 capture stoichiometry of GP films.

Swelling ratio of the thermal responsive GPs plays an important role in the function of GPs such as the reversible target binding. [26], [48], [49] Swelling ratio of GPs is typically controlled by crosslink degree.[50] Herein, we prepared a series of GPs containing 5 mol% of DMAPM with 0 mol%, 2 mol%, 5 mol% and 10 mol%

crosslinker Bis (GP D5B0, D5B2, D5B5 and D5B10 respectively) to investigate the effect of swelling ratio on the reversible CO_2 capture stoichiometry of GPs.

Diameter at 30 °C and 75 °C, and swelling ratio of the GPs was plotted in figure 3-5a. It's noteworthy that diameter of GPs without Bis was also obtained, possibly due to the slight self-crosslinking. [51] As expected, swelling ratio of the GP D5B2 (2.7), D5B5 (2.0) and D5B10 (1.6) decreases with increasing crosslink degree. Diameter of the GPs at 75 °C increase slightly with increasing amount of crosslinker Bis, indicating that Bis influences the nucleation process during polymerization as observed by Pelton's group. [47]

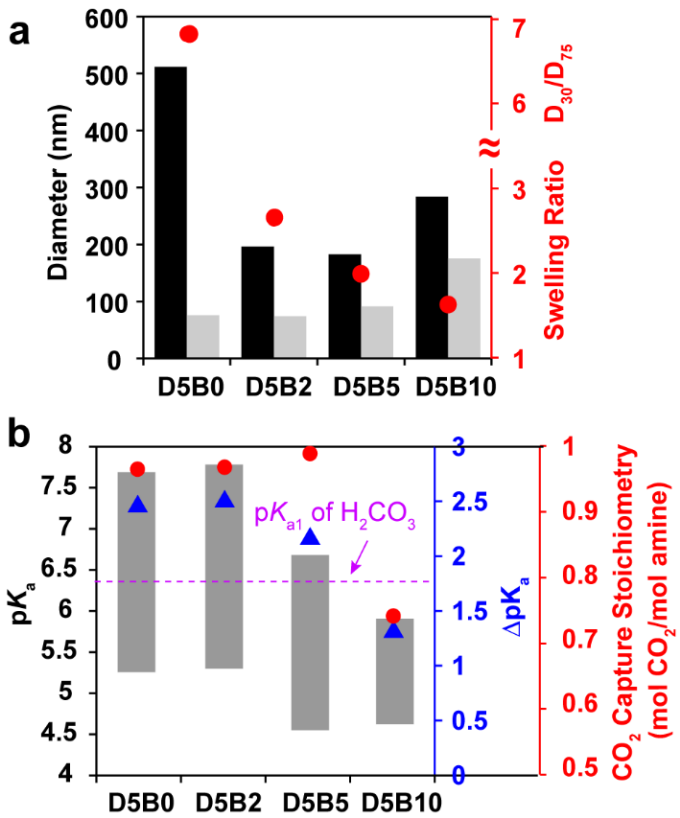

Figure 3-5. (a) Diameter (left Y axis) at 30 °C (black bar) and 75 °C (gray bar) and swelling ratio (right Y axis, red dot) between 30 °C and 75 °C of the GP D5B0, D5B2, D5B5 and D5B10. (b) pK_a value (left Y axis) at 75°C (bottom of bar) and 30°C (top of bar), and ΔpK_a (right Y axis, red dot) between 75 °C and 30°C of the

GPs. (c) Reversible CO_2 capture stoichiometry of the GP films in the temperature range 30-75 °C.

Figure 3-5b showed pK_a value of the GPs at 30 °C and 75 °C and ΔpK_a. ΔpK_a of D5B2 (2.5), D5B5 (2.1) and D5B10 (1.3) between 30 °C and 75 °C showed positive correlation with the swelling ratio of GPs (2.7, 2.0, 1.6 respectively), suggesting the change of microenvironment in GPs such as the dielectric constant and polymer density around the less crosslinked amines was greater than the highly crosslinked ones, as shown in scheme 3-6. pK_a value of the swollen GP D5B2 (7.8), D5B5 (6.7) and D5B10 (5.9) at 30 °C decreased by reducing swelling ratio, demonstrating the amines of the GP with smaller swelling ratio located in a more hydrophobic microenvironment in the swollen state at 30 °C, because the stretch of the GP was inhibited by the high crosslink degree. In other words, the GP with smaller swelling ratio collapsed to some extend at 30 °C comparing to the ones with higher swelling ratio. pK_a value of D5B2 at 30 °C (7.8) are similar with D5B0 (7.7) although D5B0 exhibited a much larger swelling ratio, indicating the D5B2 also underwent a fully swollen at 30 °C.

GP D5B0, D5B2 and D5B5 exhibited similar reversible CO_2 capture stoichiometry (0.97~1.0 mol CO_2/mol amine), while that of D5B10 (0.74 mol CO_2/mol amine) was much lower (Figure 3-5c). The difference in the reversible CO_2 capture stoichiometry can also be explained by their pK_a value. The higher pK_a value of GP D5B0, D5B2, D5B5 at 30 °C (7.7, 7.8, 6.7) above pK_{a1} of H_2CO_3, at the same time the lower pK_a value at 75 °C (5.2, 5.3, 4.4 respectively) below pK_{a1} of H_2CO_3 lead to the high reversible CO_2 capture stoichiometry. However pK_a value

of GP D5B10 at 30 °C (5.9) was too low and basicity is too weak to capture CO_2 efficiently.

Conclusively, swelling ratio is an effective method to tune the ΔpK_a and consequently pK_a value of GPs to improve the reversible CO_2 capture stoichiometry.

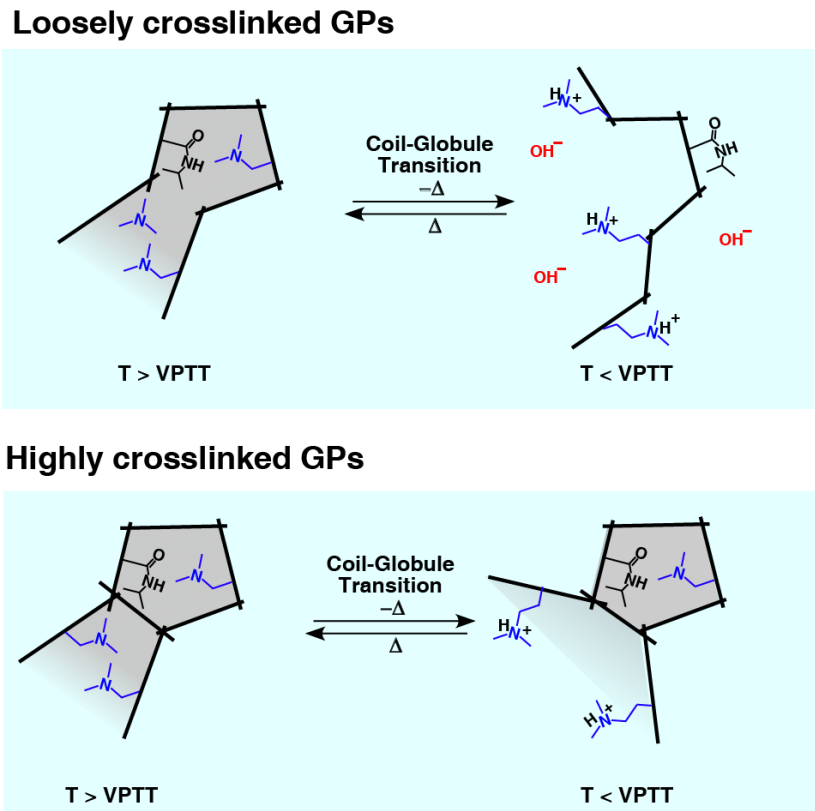

Scheme 3-6. Mechanism of the effect of crosslink degree on ΔpK_a of the GPs.

3.3.6. Rational design of GP film with large reversible CO_2 capture stoichiometry.

The above discussion has revealed the design rationale of GPs that show large reversible CO_2 capture stoichiometry from humid 10% CO_2 gas (90% N_2) in a small temperature range from 30 °C to 75 °C: pK_a value of the GPs at 30 °C and 75 °C is the principal factor that governs the reversible CO_2 capture stoichiometry. Higher pK_a value at 30 °C above pK_{a1} of H_2CO_3 (6.35) and lower pK_a value at 75 °C below

pK_{a1} of H_2CO_3 enables high reversible CO_2 capture stoichiometry of GP films. This is because the GPs are capable of capturing CO_2 efficiently at 30 °C due to the stronger basicity of amine than HCO_3^- and then releasing CO_2 sufficiently at 75 °C because of the weaker basicity. High reversible CO_2 capture stoichiometry can be achieved for GPs that exhibit smaller ΔpK_a as long as the pK_a value lies in the appropriate range.

pK_a value of the GPs can be readily adjusted to the desired level by varying VPTT of GPs above and close to the CO_2 capture temperature (30 °C in this study), because the volume phase transition of GPs always bring out a large pK_a transition in a wide temperature range above VPTT. pK_a value of the GPs can also be tuned by controlling size of the GPs since smaller GPs show higher pK_a value. Another method is to regulate GPs swelling ratio that influences ΔpK_a and consequently the pK_a value of GPs. Last but not least, imprinted microenvironment around amine groups in the GPs can also influence pK_a value of the GPs because the GPs synthesized in the presence of large amount of proton exhibit higher pK_a value. The inter-relationship between these factors is illustrated by scheme 3-7.

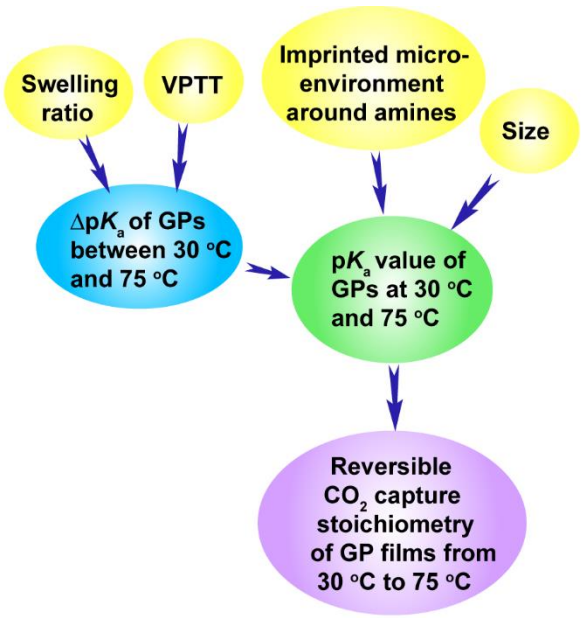

Scheme 3-7. Illustration of the design rationale for GPs that show large reversible CO_2 capture stoichiometry.

3.3.7. Maximization of reversible CO_2 capture capacity of GPs films.

In order to improve CO_2 capture capacity by GP films, incorporation ratio of the functional amine monomer DMAPM was maximized to 55 mol% (GPs with higher DMAPM concentration precipitated during polymerization process). However the GP D55B2 exhibited low CO_2 capture stoichiometry (0.73 mol CO_2/mol amine) due to its high pK_a value at 75 °C (6.8) as shown in figure 3-6a. According to the design rationale displayed above, high efficient CO_2 capture cycles could be received if pK_a value of the 55 mol% DMAPM-containing GP at 75 °C was lowered down below pK_{a1} of H_2CO_3 (6.35).

Since VPTT of GP D55B2 was not observed up to 75 °C, one way to reduce pK_a value of the 55 mol% DMAPM-containing GP at 75 °C is to lower down its VPTT. Thus 43 mol% TBAm was incorporated into the 55 mol% DMAPM-containing GPs (D55B2T43).

In accordance with the design rationale proposed above, pK_a value of GP D55B2T43 at 75 °C decreased to about 6.35 (figure 3-6a) due to the decreased VPTT via TBAm incorporation. Consequently high reversible CO_2 capture stoichiometry (0.93 mol CO_2/mol amine) was obtained. As a result of the high amine content and the high stoichiometric efficiency, as showed in figure 3-6b, the GP D55B2T43 showed the largest reversible CO_2 capture capacity (68 mL CO_2/g GPs, 3.0 mmol CO_2/g GPs) in this study that is comparable to most of the solid adsorbents. [9], [52]

Figure 3-6a also summarized the pK_a value and the reversible CO_2 capture stoichiometry of the GPs studied in this paper. From the whole picture, it can be

concluded clearly that the GPs with pK_a value at 30 °C above pK_{a1} of H_2CO_3 at the same time pK_a value at 75 °C below pK_{a1} of H_2CO_3 (the red ones) generally showed large reversible CO_2 capture stoichiometry than the others (the blue ones).

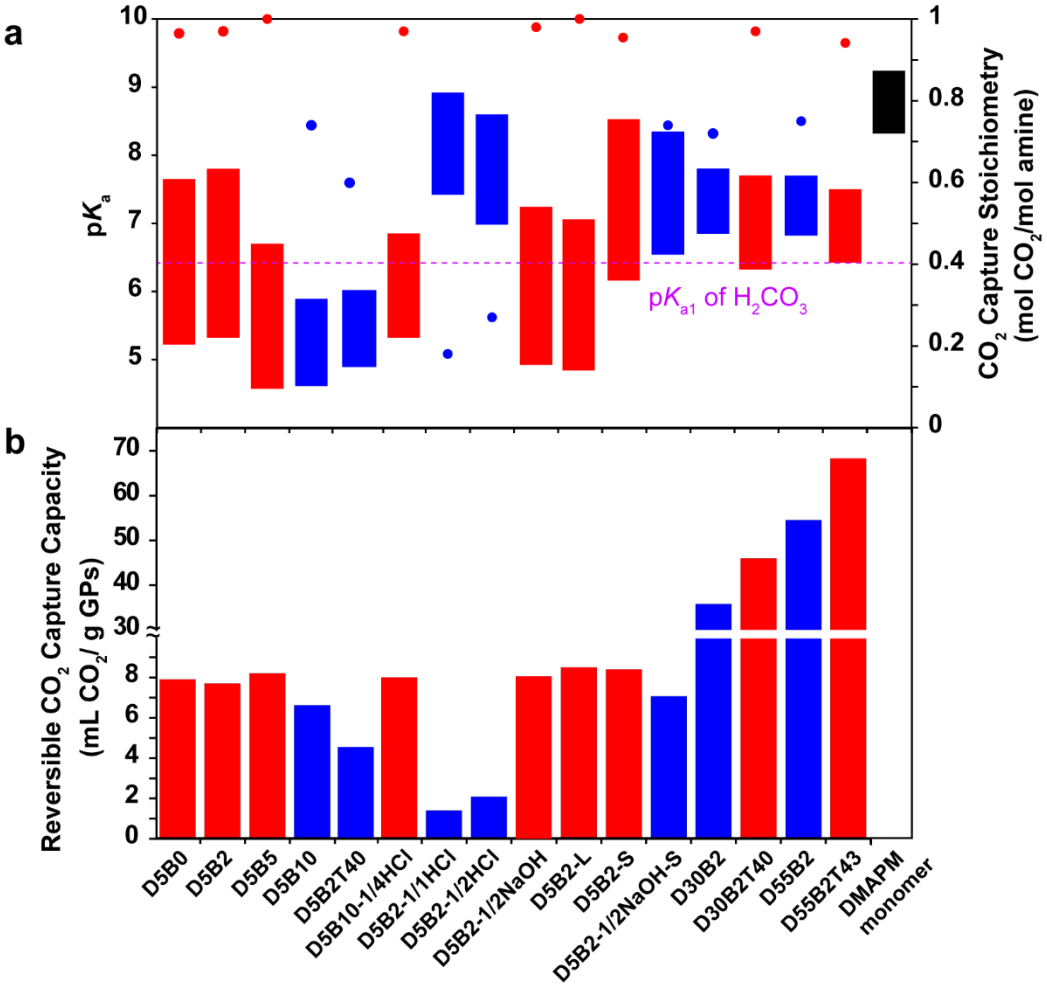

Figure 3-6. (a) pK_a value (left Y axis) at 75 °C (bottom of bar) and 30 °C (top of bar) of the GPs studied in this paper, and the reversible CO_2 capture stoichiometry (right Y axis, red dot) of the GP films in the temperature range 30-75 °C. (b) Reversible CO_2 capture capacity of the GP films in the temperature range 30-75 °C. Red represents GPs with high reversible CO_2 capture stoichiometry (>0.9 mol CO_2/mol amine) and blue is for the ones with low stoichiometry (<0.75 mol CO_2/mol amine).

3.3. Conclusion

Inspired by the efficient CO_2 transport mechanism of hemoglobin in blood known as Bohr effect, here we revealed the design rationale of amine-functionalized thermo-responsive gel particles (GPs) films that reversibly capture and release large amount of CO_2 efficiently from a model exhaust gas of fire power plants in a small temperature change (30 °C -75 °C). pK_a values of the GPs at CO_2 capture temperature (30 °C) and release temperature (75 °C) is essential for the reversible CO_2 capture stoichiometry of the GPs films: At 30°C, the high pK_a value of GPs above pK_{a1} of H_2CO_3 is required for the efficient CO_2 capture. Simultaneously, low pK_a value at 75°C of GPs below pK_{a1} of H_2CO_3 is required for the efficient release of CO_2.

pK_a value of the GPs can be readily adjusted to the desired level via 4 methods: (1) Controlling VPTT of the GPs above and close to 30 °C–phase transition induces a large pK_a transition in a wide temperature range above VPTT. (2) Controlling the size of the GPs–smaller GPs show higher pK_a value. (3) Controlling swelling ratio that influence ΔpK_a consequently pK_a value of GPs and (4) controlling imprinted microenvironment of the GPs–the GPs synthesized in the presence of large amount of proton exhibit higher pK_a value.

We successfully designed and acquired the GP D55B2T43 that exhibited large reversible CO_2 capture capacity (68 mL CO_2/g GPs, 3.0 mmol CO_2/g GPs) as well as high reversible CO_2 capture stoichiometry (0.93 mol CO_2/mol amine) by optimizing the pK_a value of GPs containing maximized amount of amine-monomer. We believe GPs with larger CO_2 capture capacity could further be designed by incorporating more hydrophobic co-monomers than TBAm into the tertiary amine-

containing GPs, and/or by using more hydrophobic tertiary amine monomers such as *N*-[3-(Diethylamino)propyl] methacrylamide. The advantages of the amine functionalized GP films such as the large capture capacity comparable to most of solid adsorbents,[9] the low regeneration temperature (75 °C) and the unique ability to work in wet environment would enables the use of GP films as an energy efficient CO_2 absorbent for the exhaust gas of the fire power plants. We anticipate that GPs films that can reversibly capture other acidic and basic gases with large capacity can also be achieved by the same strategy inspired by the Bohr effect of hemoglobin.

3.4. References

[1]Climate Change 2007: The Physical Science Basis; S. Solomon, D. Qin, M. Manning, Z. Chen, M. Marquis, K. B. Averyt, M. Tignor, H. L. Miller, Eds.; The Fourth Assessment Report of the Intergovernmental Panel on Climate Change; Cambridge University Press: New York, 2007.

[2] G. A. Olah, A. Goeppert, G. K. S. Prakash, Beyond Oil and Gas: The Methanol Economy, 2nd ed.; Wiley-VCH: Weinheim, Germany, 2009.

[3] G. T. Rochelle, *Science,* 2009, **325**, 1652.

[4] T. Fout, J. T. Murphy, DOE/NETL's Carbon Capture R&D Program for Existing Coal-Fired Power Plants; DOE/NETL 2009/1356; National Energy Technology Laboratory: Pittsburgh, PA, 2009.

[5] D. Aaron, C. Tsouris, *Sep. Sci. Technol.*, 2005, **40**, 321.

[6] D. M. D'Alessandro, B. Smit, J. R. Long, *Angew. Chem. Int. Ed.*, 2010, **49**, 6058.

[7] Y. Park, D. Shin, Y. N. Jang, A.-H. *A.* Park, *J. Chem. Eng. Data,* 2012, **57**, 40.

[8] H. Y. Huang, R. T. Yang, *Ind. Eng. Chem. Res.*, 2003, **42**, 2427.

[9] S. Choi, J. H. Drese, C. W. Jones, *ChemSusChem,* 2009, **2**, 796.

[10] K. B. Lee, M. G. Beaver, H. S. Caram, S. Sircar, *Ind. Eng. Chem. Res.,* 2008, **47**, 8048.

[11] A. Goeppert, M. Czaun, R. B. May, G. K. S. Prakash, G. A. Olah, S. R. Narayanan, *J. Am. Chem. Soc.,* 2011, **133**, 20164.

[12] R. Serna-Guerrero, E. Da'na, A. Sayari, *Ind. Eng. Chem. Res.,* 2008, **47**, 9406.

[13] P. J. E. Harlick, A. Sayari, *Ind. Eng. Chem. Res.,* 2007, **46**, 446.

[14] I. Nishio, S. Sun, G. Swislow, T. Tanaka, *Nature,* 1979, **281**, 208.

[15] T. Tanaka, C. Wang, V. Pande, A. Y. Grosberg, A. English, S. Masamune, H. Gold, R. Leavy, K. King, *Faraday Discuss.,* 1995, **101**, 201.

[16] M. J. Serpe, K. A. Yarmey, C. M. Nolan, L. A. Lyon, *Biomacromolecules,* 2005, **6**, 408.

[17] Y. Hoshino, W. W. Haberaecker III, T. Kodama, Z. Zeng, Y. Okahata, K. J. Shea, *J. Am. Chem. Soc.*, 2010, **132**, 13648.

[18] S. H. Lee, Y. Hoshino, A. Randall, Z. Zeng, P. Baldi, R. A. Doong, K. J. Shea, *J. Am. Chem. Soc.,* 2012, **134**, 15765.

[19] Y. Yonamine, Y. Hoshino, K. J. Shea, *Biomacromolecules,* 2012, **13**, 2952.

[20] K. Nagase, J, Kobayashi, A. Kikuchi, Y. Akiyama, H. Kanazawa, T. Okano, *Biomacromolecules,* 2008, **9**, 1340.

[21] Y. Akiyama, A. Kikuchi, M. Yamato, T. Okano, *Langmuir,* 2004, **20**, 5506.

[22] Y. Hoshino, R. C. Ohashi, Y. Miura, *Adv. Mater.,* 2014, **26**, 3718.

[23] T. Oya, *Science,* 1999, **286**, 1543.

[24] K. Yoshimatsu, B. K. Lesel, Y. Yonamine, J. M. Beierle, Y. Hoshino, K. J. Shea, *Angew. Chem. Int. Ed.,* 2012, **51**, 2405.

[25] Y. Hoshino, K. Imamura, M. Yue, G. Inoue, Y. Miura, *J. Am. Chem. Soc.,* 2012, **134**, 18177.

[26] Y. Hoshino, M. Nakamoto, Y. Miura, *J. Am. Chem. Soc.*, 2012, **134**, 15209.

[27] M. Yue, Y. Hoshino, Y. Ohshiro, K. Imamura, Y. Miura, *Angew. Chem. Int. Ed.,* 2014, **53**, 2654.

[28] J. V. Kilmartin, J. J. Breen, G. C. K. Roberts, C. Ho, *Proc. Natl. Acad. Sci.*, 1973, **70**, 1246.

[29] D. Voet, J. G. Voet, Biochemistry, 4th ed.; Wiley: New York, USA, 1995.

[30] J. Wilcox, R. Haghpanah, E. C. Rupp, J. He, K. Lee, *Annu. Rev. Chem. Biomol. Eng.,* 2014, **5**, 479.

[31] M. Eigen, *Angew. Chem. Int. Ed.,* 1964, **3**, 1.

[32] H. Li, A. D. Robertson, J. H. Jensen, *Proteins,* 2005, **61**, 704.

[33] D. W. Urry, D. C. Gowda, S. Q. Peng, T. M. Parker, R.D. Harris, *J. Am. Chem. Soc.,* 1992, **114**, 8717.

[34] W. Kühlbrandt, *Nature,* 2000, **406**, 569.

[35] V. K. Rastogi, M. E. Girvin, *Nature,* 1999, **402**, 263.

[36] Y. Hoshino, T. Kodama, Y. Okahata, K. J. Shea, *J. Am. Chem. Soc.,* 2008, **130**, 15242.

[37] K. Mosbach, O. Ramström, *Nat. Biotechnol.*, 1996, **14**, 163.

[38] G. Wulff, *Chem. Rev.,* 2002, **12**, 1.

[39] H. Feil, Y. H. Bae, J. Feijen, S. W. Kim, *Macromolecules,* 1992, **25**, 5528.

[40] M. H. Kwok, Z. Li, T. Ngai, *Langmuir,* 2013, **29**, 9581.

[41] P. D. Vaidya, E. Y. Kenig, *Chem. Eng. Technol.,* 2007, **30**, 1467.

[42] L. D. Terrence, Y. N. Nguyen, *Ind. Eng. Chem. Fundam.,* 1980, **19***,* 260.

[43] J. Mcmurry, Organic Chemistry, 7th ed.; Thomson Higher Education, Belmont, CA, 2008.

[44] H. S. Harned, R. D. Jr, *J. Am. Chem. Soc.*, 1943, **65**, 2030.

[45] J. D. Debord, L. A. Lyon, *Langmuir,* 2003, **19**, 7662.

[46] S. Nayak, L. A. Lyon, *Angew. Chem. Int. Ed.*, 2005, **44**, 7686.

[47] W. McPhee, K. C. Tam, R. Pelton, *J. Colloid Interface Sci.,* 1993, **156**, 24.

[48] M. Nakamoto, Y. Hoshino, Y. Miura, *Biomacromolecules,* 2014, **15**, 541.

[49] H. Tokuyama, Y. Kato, *Colloids Surf. B,* 2008, **67**, 92.

[50] I. Varga, T. Gilanyi, R. Meszaros, G. Filipcsei, M. Zrinyi, *J. Phys. Chem. B,* 2001, **105**, 9071.

[51] X. Hu, Z. Tong, L. A. Lyon, *Langmuir,* 2011, **27**, 4142.

[52] A. Samanta, A. Zhao, G. K. H. Shimizu, P. Sarkar, R. Gupta, *Ind. Eng. Chem. Res.,* 2012, **51**, 1438.

Chapter 4. Effect of Hydrophobic Modification of Polyvinylamine Films on the CO_2 Capture and Release Behavior: Comparison between Copolymers and Polymer Blends

Abstract

In this study, the Me, i-Pr and t-Bu modified PVAm with different modification ratio were used as CO_2 capture absorbents. The CO_2 capture stoichiometry of the copolymers can be improved by the "spacing effect" of the modification groups, the larger modification groups usually show stronger "spacing effect". Phase separation behaviour of the copolymers can also facilitate the CO_2 capture stoichiometry if the LCST is above and close to 30 °C. However excessively modified copolymer with LCST below 30 °C show significantly low CO_2 capture stoichiometry. LCST of the copolymers can be decreased by increasing the hydrophobic modification ratio or by using more hydrophobic modification groups. Besides, the copolymers showed larger CO_2 capture stoichiometry than the polymer blends at the same modification ratio, indicating the intra-polymer interaction between amine groups and hydrophobic modification groups are essential for the CO_2 capture.

4.1. Introduction

The accumulation of CO_2 in atmosphere caused by the burning of fossil fuels has caused serious climate change.[1] Meanwhile the CO_2 can be a carbon source to produce liquid fuels such as methanol and dimethyl ether. [2] Thus the sorption of CO_2 from the main emission sources such as fire power plants is essential to mitigate the greenhouse effect and to generate the carbon based energy.

Currently the most commercialized CO_2 recovery method from the humid exhaust gases of fire power plants is absorption by using aqueous solution of

small molecule amines. Though the aqueous amine solution showed large CO_2 capture capacity, the high energy consumption due to the high water content and high regeneration temperature (typically above 140 °C) make them less attractive.[3]-[8]

Recently we have developed the films consisting of the tertiary amine *N*-[3-(dimethylamino)propyl]methacrylamide (DMAPM) functionalized poly(*N*-isopropylacrylamide) (pNIPAm) based microgel particels (GPs) as CO_2 absorbents to reversibly capture and release CO_2 from humid condition in a small temperature change (30-75 °C).[9] The pNIPAm based gels undergo a reversible volume phase transition from swollen and hydrophilic state to the collapsed and hydrophobic state when the temperature increased above their lower critical solution temperature (LCST). At 30 °C that below the LCST of the GPs, most amines in the swollen GPs show stronger basicity comparable to that in water and are capable of capturing CO_2. While at 75 °C that above the LCST, the collapse of the GPs caused the amines more hindered, lowering down the basicity, as a result the CO_2 was released efficiently. Due to the contribution of the thermal induced phase separation behaviour, high CO_2 capture stoichiometry was achieved by the GPs, and the regeneration temperature (75 °C) was lower than the aqueous amine solution (> 140 °C). However the weight ratio of amine groups in the functional monomer DMAPM of the GP is quite low, higher CO_2 capture capacity is expected by replacing DMAPM by amine functional monomers with larger weight ratio of amines.

The polyvinylamine (PVAm) caught our attention because of its relatively high weight ratio of amine groups. In fact the PVAm composited facilitated

transport membranes for CO_2 separation have been extensively reported due to the potential of achieving both high permeability and high selectivity.[10]-[13] The amine groups electively react with CO_2 and transport the ions, while the gases such as N_2, H_2, CH_4 will permeate exclusively by the solution-diffusion mechanism. Furthermore, PVAm is an attractive platform to prepare the thermal responsive copolymers.[14] It is well known that the thermal responsive behaviour of any polymer is related to the balance of two or more opposite force between the polymer-polymer and polymer-solvent, such as the hydrogen bonding and the hydrophobic interaction, therefore the thermal responsibility can also be introduced into the hydrophilic PVAm by hydrophobic modification.[14]-[18] The pendant amine groups of PVAm are convenient for the modification as well as being the functional groups for CO_2 capture. Analogous to the DMAPM-functionalized thermal responsive GPs, the modified PVAm with phase separation behaviour are expected to show increased reversible CO_2 capture stoichiometries in a small temperature range (30-75 °C).

On the other hand, other than copolymers, blending of polymers is also capable of combining advantages of each component polymer into the new product. Moreover, blending can provide materials with extended useful properties beyond the range that can be obtained from single component polymer. The material with unique property can be generated readily by blending, which uses conventional technologies at low cost.[19]-[23] For example, the PVAm/poly(ethylene glycol) (PEG) (9/1) blend membranes showed significantly increased CO_2 permeance and selectivity against CH_4 than the PVAm membrane, because the addition of PEG inhibited the

formation of crystallization region in PVAm that acts as impermeable obstacles to the gas molecules transport.[24] The blending membrane of PVAm with more mechanically robust poly(vinyl alcohol) (PVA)[25], or with amine-richer ethylenediamine (EDA)[26] also exhibited improved mechanical strength, long term stability and higher CO_2 separation performance than the PVAm membranes.

In this study, the PVAm was covalently modified by various carboxylic acids. Resulting copolymers were used as CO_2 absorbents. The effect of the phase separation behaviour of the copolymers introduced by hydrophobic modification, and the hydrophobicity of the modification groups and the modification ratio on the reversible CO_2 capture stoichiometry was discussed. Blends of PVAm with corresponding 100% hydrophobically modified PVAm were also prepared, and the CO_2 capture stoichiometry of the polymer blends was compared with the copolymers.

4.2. Materials and experiments

4.2.1. Materials.

N-vinylformamide (NVF) was purified by vacuum distillation prior to use. 2,2'-azobis(2-amidinopropane) dihydrochloride (AAPD), isobutyric acid, butyric acid、pivalic acid, pentanoic acid, acetic acid, trimethylamine (TEA), condensation agent 4-(4,6-dimethoxy-1,3,5-triazin-2-yl)-4-methylmorpholinium Chloride n-Hydrate (DMT-MM), dialysis membrane (MWCO 12-14.000) were used as received. The anion-exchange resin (A2004-OH, Muromachi Technos Co., Ltd.) was first activated by 1 M NaOH, and then

washed carefully with deionized water. The water was purified using a Direct-Q Ultrapure Water System (Merck, Ltd.)

4.2.2. PVAm preparation

Scheme 4-1 describes the preparation of PVAm. 10 g of NVF was dissolved in MilliQ water, resulting to the total volume of 96mL. The monomer solution was heated to 60 °C and degas by N_2 for 30 min, following by the addition of initiator aqueous solution of AAPD (30.3 mg/4 mL). The reaction was conducted for 24 h at 60 °C under N_2 flowing. Excessive amount of aceton (200 mL) was added into the resulted solution to precipitate the polymers. The collected polymer was re-dissolved in co-solvent of MilliQ and MtOH (50 mL/100 mL). The precipitation-dissolve was carried out several times to remove unreacted monomers and oligomers. The transparent resin-like polyNVF can be after evaporating all the solvents.

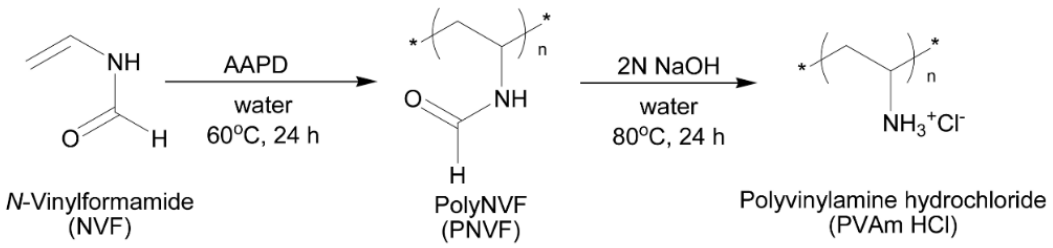

Scheme 4-1. Preparation of PVAm

The polyNVF was dissolved in the aqueous solution of NaOH (2N) with the final concentration of 5 wt%. The solution was stirred at 80 °C for 24 h, resulting to transparent and viscous liquid. Then the solution was dialyzed against large amount of MilliQ water for 3 days with changing water 3 times

every day. After dialysis, HCl was added into the solution until pH approached 3. After remove the excessive HCl by evaporating, the powder of polyvinylamine hydrochloride (PVAm·HCl) was achieved by freeze-drying.

4.2.3. Hydrophobic modification of PVAm

Five kinds of carbonic acid (isobutyric acid、butyric acid、pivalic acid、pentanoic acid and acetic acid) were used to modify the PVAm via condensation reaction (Scheme 4-2).

The reaction condition is listed in table 4-1. 400 mg of PVAm·HCl was dissolved in 30 mL MilliQ water under stirring, followed by the addition of TEA. The condensation agent DMT-MM was pre-dissolved in 20 mL MilliQ water together with the carbonic acid. Then the solution of DMT-MM and carbonic acid was added into the solution of PVAm·HCl. The reaction was carried out at room temperature for 6 h.

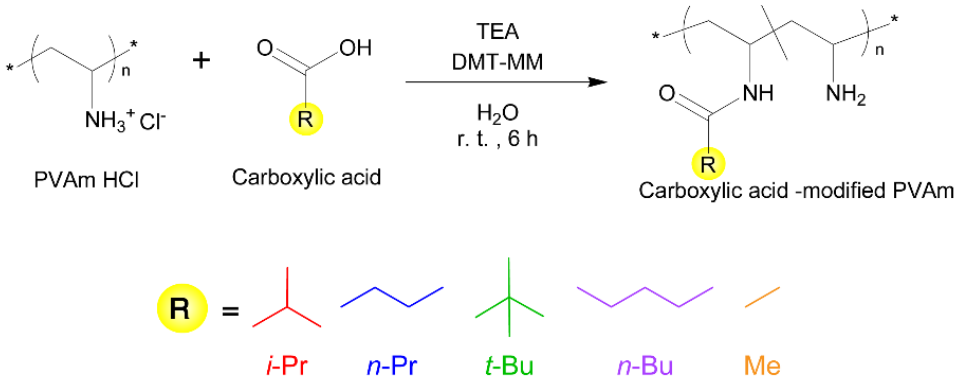

Scheme 4-2. Hydrophobic modification of PVAm

After reaction, the solution was dialyzed by the dialysis membrane. The water was changed frequently in the first two days to remove the unreacted carbonic acid. In the third day slight amount of HCl was added into the water

to remove the amine (4-methylmorpholine) produced by the decomposition of DMT-MM. The dialyzed polymer solution was further purified by anionic exchange beads. The powder of the polymers was achieved after freeze-drying.

Table 4-1. Reaction condition and result of the hydrophobic modification of PVAm

Entry	Carboxylic acid	Carboxylic acid, DMT-MM and TEA (eq.)	Reaction media	Modification ratio (%)	Amine amount (mmol/g)
i-Pr 0.5		0.5	water	23	13.0
i-Pr 0.75		0.75	water	43	7.8
i-Pr 1.0	Isobutyric acid	1.0	water	69	3.4
i-Pr 2.0		2.0	water	91	0.8
i-Pr 3.0		3.0	water	100	0.0
n-Pr 0.5		0.5	water	20	14.0
n-Pr 1.0	Butyric acid	1.0	water	65	3.9
n-Pr 2.0		2.0	water	93	0.6
t-Bu 0.5		0.5	water	28	10.8
t-Bu 0.75		0.75	water	55	5.0
t-Bu 1.0	Pivalic acid	1.0	water	69	3.1
t-Bu 1.25		1.25	water	79	1.9
t-Bu 2.0		2.0	water	89	0.9
n-Bu 0.5		0.5	water	18	14.1
n-Bu 0.75	Pentanoic acid	0.75	water	39	8.0

n-Bu 1.0		1.0	water	66	3.4
n-Bu 2.0		2.0	water	100	0.0
Me 1.0		1.0	water	45	8.9
Me 1.5	Acetic acid	1.5	water	73	3.7
Me 2.0		2.0	water	88	1.5
Me 2.5		2.5	water	93	0.9

4.2.4. ^{1}H NMR measurement

Lyophilized powder of ion exchanged polymers was dissolved in methanol-d_4 (10 mg/mL). The Dioctyl sodium sulfosuccinate (DSS) dissolved in D_2O (0.1 mg/mL) 37.5 μL was added as the internal standard. ^{1}H NMR experiments were conducted on a JEOL JNM-ECP400 instrument at 25 °C. Modification ratio and amine amount in the polymers was calculated from the ^{1}H NMR.

4.2.5. Quantification of LCST of the polymers

The scattering intensity of the polymers were measured by dynamic light scattering (DLS) instrument (Zetasizer Nano, Malvern Instruments Ltd.). The GP solutions were sealed within the quartz cells filled with nitrogen. The solutions were equilibrated at each temperature for 6 min prior to the measurement. Normalized scattering intensity was defined here by equation (1), where I_{max} and I_{min} is the maximum and minimum of the scattering intensity. LCST was determined as the temperature where the plateau of relative scattering intensity started.

$$\text{Normalized scttering intensity} = \frac{I - I_{min}}{I_{max} - I_{min}} \qquad (1)$$

In the case that the ratio between I_{max} and I_{min} is smaller than 2, the scattering intensity was regarded constant in the heating process.

4.2.6. Polymer film preparation

The lyophilized polymer was dissolved in methanol. The hydrogel films were then prepared by casting the methanol solutions of 120 mg of GPs on the inner bottom surface of a stainless steel container with surface area of 120 cm^2, followed by the addition of 4 mL of water per gram of GPs after completely evaporating methanol.

4.2.7. Quantification of reversible CO_2 absorption/desorption of polymer films

CO_2 absorption capacities of the polymer films were quantified by a grease-free steel-Teflon tube system (Scheme 4-3).

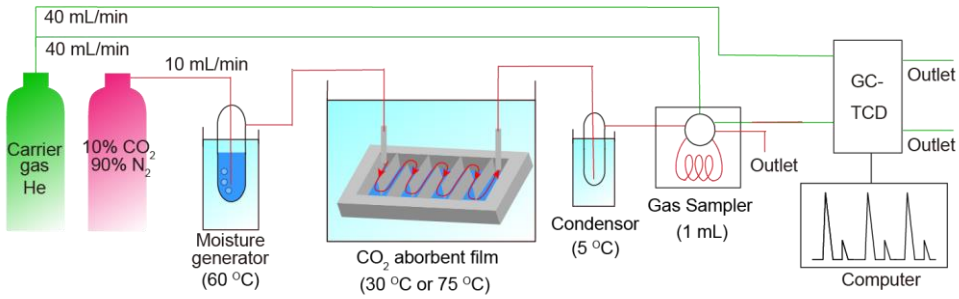

Scheme 4-3. Reversible CO_2 absorption amount quantification system

As illustrated in scheme 4-3, 10 % CO_2 (90 % N_2, 10 mL/min) gas was flowed into water of 60 °C to generate saturated water vapor at the temperature. The resulting 60 °C water-saturated gas mixture was guided into a stainless steel container with GP film on inner surface, and then channeled to a gas chromatography instrument (GC, Shimadzu Corp.) equipped with a thermal conductivity detector (TCD) and Shincarbon ST

50/80 column (2 m, Shinwa Chemical Industries Ltd.; carrier gas: He, 40 mL/min; column temperature: 210 °C; detector temperature: 240 °C). All the GP films were equilibrated under the gas flow for about 2 h at 30 °C. Thereafter, CO_2 desorption capacity at 75 °C and absorption capacity at 30 °C of each film were quantified by monitoring concentration of CO_2 every 1.7 minutes by the GC-TCD for 25 min and 46 min respectively.

4.3. Results and discussion

4.3.1. Preparation of the PVAm

PVAm is a useful water soluble polymer because of its nucleophilicity and convenience for chemical modifications. However, the simplest vinylamine monomer to PVAm is not available in the free state because it is readily tautomerized to acetaldehyde imine.[27] Therefore, PVAm has been synthesized only via indirect routes. The Hofmann reaction was suggested as a quick method to prepare PVAm from polyacrylamide.[28]-[30]

Another convenient method to produce PVAm is hydrolysis of poly(*N*-vinylamide)s,[31] such as poly(*N*-vinylacetamide)[32],[33]and poly(*N*-vinylacetamide)[34]. Since poly(*N*-vinylformamide) (PolyNVF) has no alkyl group on its side chain, it is reported hydrolysis of poly(NVF) is a most convenient method for producing PVAm.[27],[35]

In this study, PVAm was prepared via hydrolysis of polyNVF as reported.[27] Chemical structure of the resulting PVAm was characterized by ^{1}H NMR. As shown in figure 4-1, two signals were observed at 1.4 ppm and 3.0 ppm, corresponding to $-CH_2-$ and -CH- in the PVAm main chain, respectively.

4.3.2. Preparation and Modification of the PVAm

The PVAm was then modified by five kinds of carbonic acid via condensation reaction. Homogeneous solutions of the PVAm modified by Me, i-Pr, n-Pr (C≤4) at all modification ratio were obtained. However the t-Bu and i-Bu (C=5) modified PVAm with higher modification ratio precipitated due to the extremely high hydrophobicity.

Modification ratio and amine content of the polymers was quantified by ^{1}H NMR of the methanol-d4 solution of the polymers. A set of examples are shown in figure 4-1. After incorporating amide groups, the signal of -CH- in the modified PVAm main chain bonded to the amide groups shifted to 4.0ppm (peak b), caused by the stronger electron-withdrawing effect of the resulting amide groups than the amine groups. However, the signal of -CH- of the main chain connected with the unmodified amine groups does not change obviously (peak b), compared to the unmodified PVAm. Modification ratio and amine amount of polymers was calculated from the peak area of d and b.

The quantification result from ^{1}H NMR is summarized in table 4-1. Generally speaking, the modification ration increased on increasing the ratio of carboxyl acid during condensation reaction.

The quantification result from ^{1}H NMR is summarized in table 4-1. Generally speaking, the modification ration increased on increasing the ratio of carboxyl acid during modification.

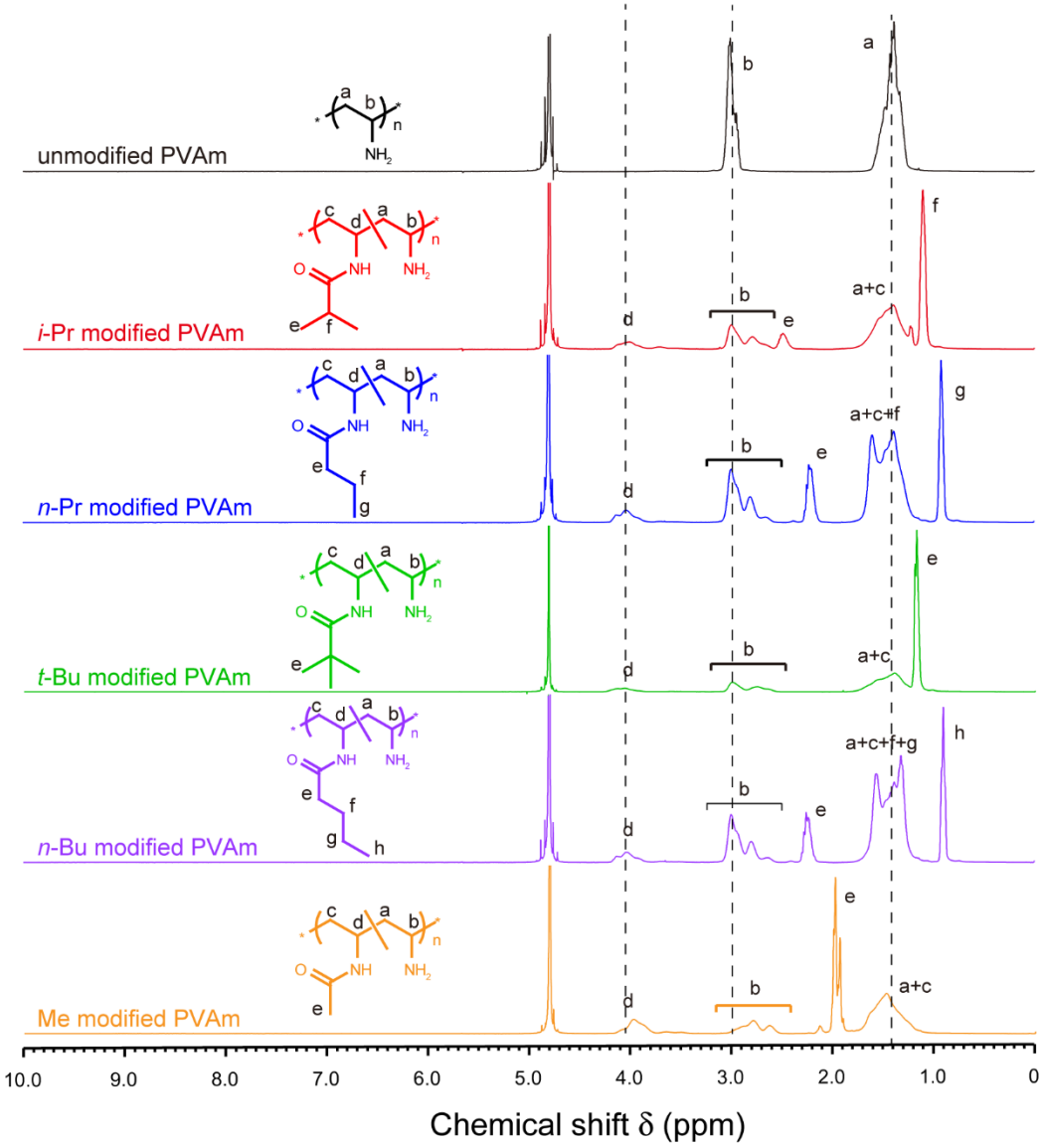

Figure 4-1. ^{1}H NMR (400 MHz, methanol-d_4) of the hydrophobically modified PVAm polymers.

4.3.3. LCST of the hydrophobically modified PVAm

The scattering intensity of the aqueous of the polymers were measured by DLS. The scattering intensity were then normalized, regarding I_{min} as 0 and I_{max} as 1, as shown in figure 4-2. LCST was determined as the temperature where the plateau of normalized scattering intensity started.

The LCST of i-Pr-91% and n-Pr-93%, t-Bu-73% and n-Bu-66%, and Me-93% was shown in figure 4-2. The n-Pr-93% showed slightly lower LCST (45 °C) than i-Pr-91% does (50 °C), though the hydrophobic modification ratio are resemble. Similarly, LCST of n-Bu-66% (20 °C) was obviously lower than t-Bu-73% (45 °C) despite the comparable modification ratio, indicating the normal alkyl groups was more hydrophobic than the isomeric ones. [17],[36]

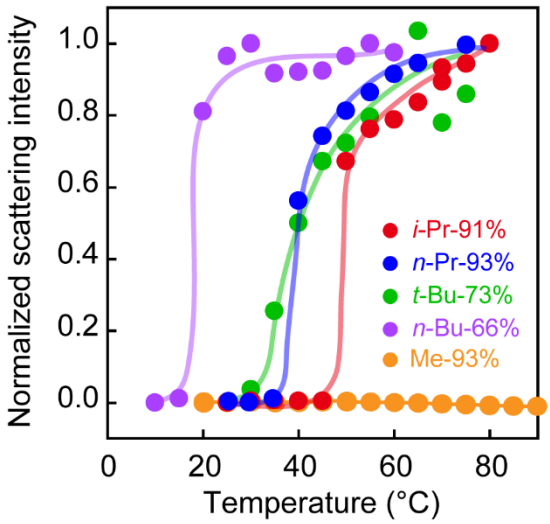

Figure 4-2. Normalized scattering intensity of the aqueous solution of PVAm modified by i-Pr, n-Pr, t-Bu, n-Bu and Me.

On the other hand, the n-Bu-66% (20 °C) shows lower LCST than n-Pr-93% (45 °C), even though the modification ratio of the propyl group is higher than the butyl group. Similarly, the t-Bu-73% (45 °C) shows lower LCST than i-Pr-91% (50 °C). These results indicates the butyl groups are more hydrophobic than propyl groups. LCST of Me-93% which was undetectable until 90 °C, is higher than i-Pr-91% (50 °C), suggesting the weaker hydrophobicity of Me groups than i-Pr groups.

Conclusively, the modification alky groups with more carbons show higher hydrophobicity,[17] and the groups with normal structure are more hydrophobic than the isometric ones (n-Bu>t-Bu>n-Pr>i-Pr>Me).[36] The PVAm modified by more hydrophobic groups with a larger modification ratio show lower LCST.[17],[36] The results are in good agreement with the previous reports. [17],[36]

4.3.4. Effect of modification ratio on the reversible CO_2 capture stoichiometry of the polymer films

The films consisting of the Me modified PVAm were used as the CO_2 absorbents to reversibly capture CO_2 from a wet condition. Figure 4-2 has shown that phase separation behavior was not observed until 90 °C for Me-93%, due to the weak hydrophobicity of Me groups. The Me-88%, Me-73%, Me-45% with lower modification ratio than Me-93% (>90 °C) have higher LCST than Me-93% because of the lower modification ratio and the higher amine content. Since LCSTs of all the Me modified PVAm are above 90 °C, the effect of phase separation behavior on the CO_2 capture stoichiometry of the polymers can be excluded.

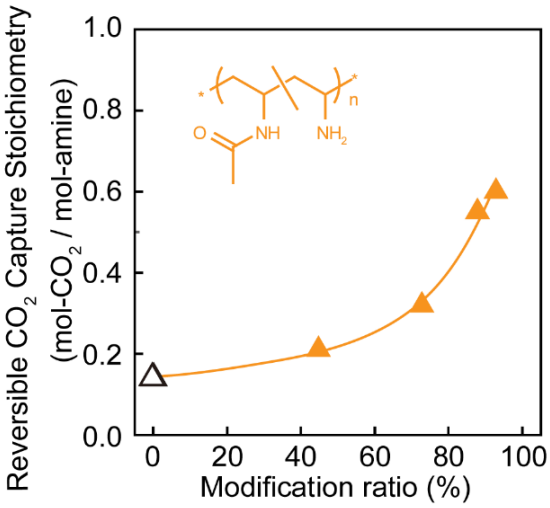

Figure 4-3. Reversible CO_2 capture stoichiometry of film of PVAm modified by Me with different modification ratio.

The CO_2 capture stoichiometry of polymers with different Me modification ratio is shown in figure 4-3. The PVAm without hydrophobic modification showed very low reversible CO_2 capture stoichiometry (0.16 mol CO_2/mol amine). On increasing the modification ratio, the reversible CO_2 capture stoichiometry increased dramatically. One possible reason is the stronger interaction between the closely localized amine groups in slightly modified PVAm. The ammonium ions resulting from CO_2 capture inhibits further ammonium formation, thereby decreasing the CO_2 capture stoichiometry. This effect, according to Coulomb's law, decreases as the distance between the amine groups increases.[37] Thus the effect of Coulomb repulsion is greatly diminished in the case of highly modified PVAm, because the amine groups are distant from each other due to the "spacing effect" of the hydrophobic modification, leading to a higher CO_2 capture stoichiometry

4.3.5. Effect of LCST on the reversible CO_2 capture stoichiometry of the polymer films

In order to clarify the effect of the volume phase transition behavior introduced by the hydrophobic modification, LCST of the polymer was lowered by modifying the PVAm with i-Pr groups and t-Bu groups which are more hydrophobic than Me groups. The reversible CO_2 capture stoichiometry of the modified polymers was plotted in figure 4-4 as a function of modification ratio.

As with Me modified PVAm, i-Pr modified PVAm also showed increased CO_2 capture stoichiometry with increasing modification ratio. Especially when the modification ratio was 91%, the stoichiometry was as high as 0.83 mol CO_2/mol amine that exceeded the theoretical value for primary amine (0.5).[38]

In figure 4-4b, the i-Pr-91% showed a LCST of 50 °C, and the i-Pr-69% showed a higher LCST above 90 °C because of the decreased content of hydrophobic i-Pr as well as the increased amount of the primary amine.

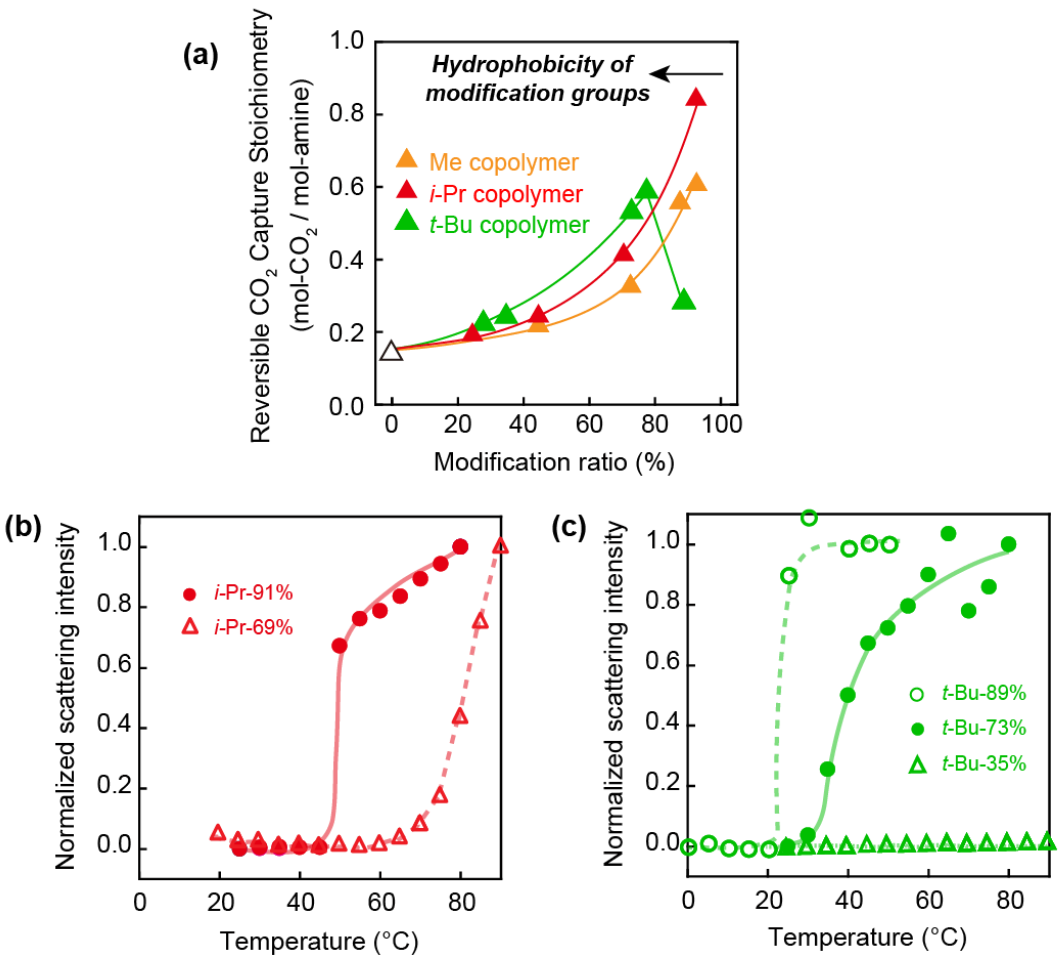

Figure 4-4. (a) Reversible CO_2 capture stoichiometry of film of PVAm modified by Me, i-Pr and t-Bu with different modification ratio. (b) Normalized scattering intensity of the aqueous solution of PVAm modified

by i-Pr-91% and i-Pr-69%. (c) Normalized scattering intensity of the aqueous solution of PVAm modified by t-Bu-89%, t-Bu-73% and t-Bu-35%.

The "spacing effect" also contributes to the dramatically increased reversible CO_2 capture stoichiometry of the i-Pr modified PVAm on increasing the modification ratio. The i-Pr-69% showed slightly higher stoichiometry than Me-73%, although the modification ratio of them was comparable and LCST of of them are both above 90 °C (figure 4-2 and figure 4-4b), indicating the i-Pr groups show stronger "spacing effect" that increases the distance of neighbouring amine groups due to their larger size.

Another contributor to the significantly higher stoichiometry of i-Pr-91% than i-Pr-69% might be the phase separation behavior of the i-Pr-91%. It has been reported by us that the LCST of GPs above and close to the CO_2 capture temperature is beneficial to a higher reversible CO_2 capture stoichiometry, because the volume phase transition of GPs on heating give rise to a large pK_a decrease of the GPs at a wide temperature range above LCST. Consequently CO_2 can be reversibly captured by the GPs with higher pK_a at 30 °C, and released by the GPs with lower pK_a at 75 °C efficienctly. The LCST of i-Pr-91% (50 °C) was just in the appropriate range according to the report, while the high LCST of i-Pr-69% (90 °C) was not. As a result the reversible CO_2 capture stoichiometry of i-Pr-91% is much higher than i-Pr-69%.

The positive effect of phase separation behavior can be seen by comparing the CO_2 capture stoichiometry of i-Pr modified polymers and Me modified polymers in figure 4-4a. The difference between i-Pr-91% and Me-93% is

obviously larger than that between i-Pr-69% and Me-73%, indicating the contribution of volume phase transition of i-Pr-91% to the high CO_2 capture stoichiometry.

The modification ratio dependent CO_2 capture stoichiometry of PVAm modified by more hydrophobic t-Bu groups was also displayed in figure 4-4a. At the low modification ratio (< 73%), the t-Bu modified PVAm showed increased reversible CO_2 capture stoichiometry by the increase of modification ratio. However, when the modification ratio increased to 89%, the CO_2 capture stoichiometry decreased dramatically.

Figure 4-4c shows the LCST of the t-Bu modified PVAm. Comparing with LCST of t-Bu-89% and t-Bu-73% decreased to 45 °C and 25 °C due to the stronger hydrophobicity of t-Bu groups. The LCST of t-Bu-35% is above 90 °C due to the low hydrophobic modification ratio.

The relatively higher stoichiometry of t-Bu-73% than t-Bu-35% is also a result of the coordination effect of phase separation and the "spacing effect": the LCST of t-Bu-73% (45 °C)was in the CO_2 capture and release temperature range (30-75 °C) and close to the capture temperature, while LCST of t-Bu-35 (>90 °C) is out of this range. As a result a large pK_a shift will be induced by the phase separation of the t-Bu-73% in a wide temperature range above its LCST. Meanwhile the "spacing effect" of t-Bu-73% is more significant than t-Bu-35%. Consequently the CO_2 capture stoichiometry of t-Bu-73% was increased comparing to t-Bu-35%. This result is consistent with the i-Pr modified PVAm.

Likewise, the drastically lower stoichiometry of t-Bu-89% than t-Bu-73% is also a result of the effect of phase separation. The excessively low LCST of

highly hydrophobic modified t-Bu-89% (25 °C) below the CO_2 capture temperature (30 °C) lead to the relatively hydrophobic polymer film in CO_2 capture process, resulting in the low reversible CO_2 capture stoichiometry, although the "spacing effect" is rather noticeable due to the large size and high modification ratio of butyl groups.

In conclusion, other than the "spacer effect", the phase separation occured between the CO_2 capture temperature and release temperature range also prompts the CO_2 capture stoichiometry the hydrophobically modified PVAm. The excessively modified PVAm with LCST below the CO_2 capture temperature will show low stoichiometry due to the high hydrophobicity of the polymer in CO_2 capture process (30 °C).

Additionally, effect of hydrophobicity of modification groups on the reversible CO_2 capture stoichiometry of the copolymers is also revealed in figure 4-4a. In the conditions where LCST of the hydrophobically modified copolymers is above 30 °C, the CO_2 capture stoichiometry of t-Bu modified copolymers is larger than the ones modified by i-Pr and Me at the same modification ratio. On the one hand, the "spacing effect" of larger alky groups is stronger. On the other hand, the contribution of phase separation behavior of the t-Bu modified copolymers is more significant than that of i-Pr and Me modified ones, because the LCST of t-Bu modified copolymer are lower than the i-Pr and Me modified ones at the same modification ratio. However, when the LCST of the modified polymers was lowered below 30 °C, the CO_2 capture stoichiometry will decrease dramatically.

4.3.6. CO_2 capture stoichiometry of blended polymer films

Blending of polymers is capable of providing materials with extended useful properties beyond the single component polymer can be generated at low cost.[19],[20],[21], [22],[23] The polymer blends in this study were prepared by mixing the methanol solution of PVAm with 100% modified PVAm. The CO_2 capture stoichiometry of the polymer blends and their corresponding hydrophobically modified copolymers are shown in figure 4-5.

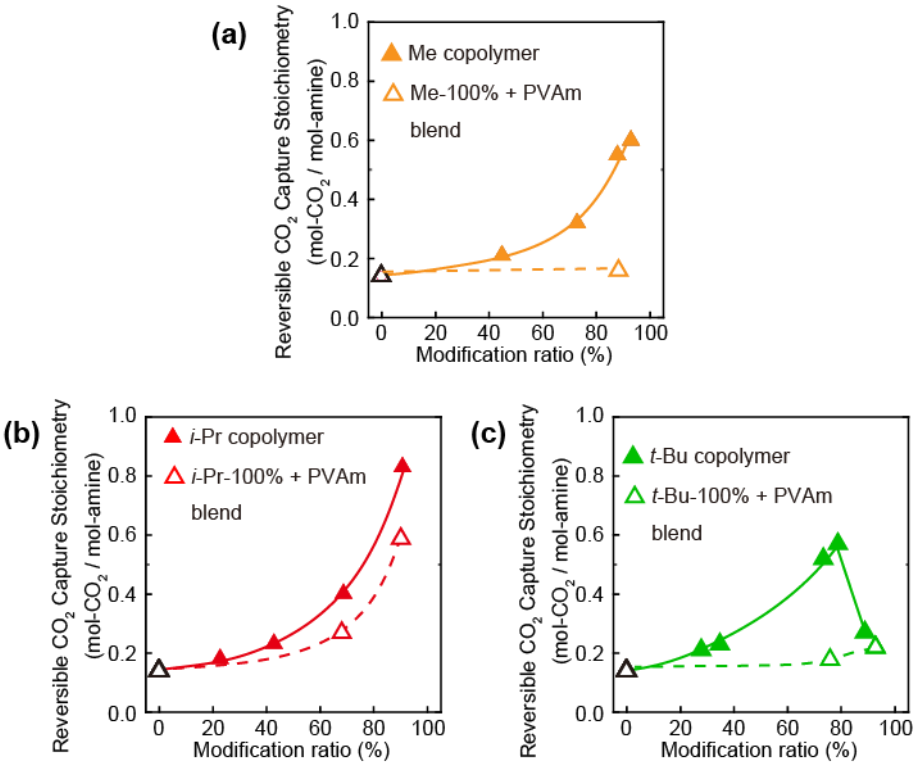

Figure 4-5. Reversible CO_2 capture stoichiometry of film of PVAm blended with (a) Me-100%, (b) i-Pr-100%, and (c) t-Bu-100%.

In figure 4-5a, the stoichiometry of the blend of PVAm/Me-100% is not improved even at high modification ratio, although the two polymers are miscible. It is supposed that the distance between the amine groups of PVAm

and Me groups of Me-100% are further than that in copolymers. Meanwhile the hydrophobicity of the Me groups is weak. Thus, the effect of the Me groups of Me-100% on the surrounding amine groups of PVAm in the blend is neglectable. As a result, the CO_2 capture stoichiometry of the polymer blend is not improved even at high modification ratio.

The reversible CO_2 capture stoichiometry of the blend PVAm/i-Pr-100% is shown in figure 4-5b. Similar to the i-Pr modified copolymers, the addition of the i-Pr-100% also increased the reversible CO_2 capture stoichiometry of the PVAm significantly, which is different from the polymer blend of Me-100% and PVAm in figure 4-5a. Though the the i-Pr groups of i-Pr-100% might be more distant from the primary amine groups of PVAm in the polymer blends than in copolymers, the i-Pr groups still influences the amines of PVAm, because of the stronger "spacing effect" of i-Pr groups than Me groups. Consequently, the reversible CO_2 capture stoichiometry of the blend was improved at high modification ratio. However, the stoichiometry of the polymer blends is still lower than the copolymers, indicating the inter-polymer interaction between the amines and modification groups in polymer blends is less effective than the intra-polymer interaction between amines and hydrophobic modification groups in copolymers.

Figure 4-5c showed the reversible CO_2 capture stoichiometry of the blend t-Bu-100%/PVAm. The blends exhibited similar reversible CO_2 capture stoichiometry to the unmodified PVAm (~0.2 mol CO_2/mol amine). Since the t-Bu-100% and PVAm are immiscible in aqueous media, it is supposed that in the films of the polymer blends, the t-Bu-100% cannot disperse homogeneously around PVAm, instead, the domain of t-Bu-100% and the

domain of PVAm co-exist in the films. As a result the hydrophobic t-Bu groups of t-Bu-100% domains hardly influence the amine groups of PVAm domains. Thus the CO_2 capture stoichiometry of the blend of t-Bu-100% and PVAm was not improved comparing to PVAm.

In conclusion, the CO_2 capture stoichiometry of PVAm can be improved by blending with miscible polymers with some hydrophobicity. The miscible polymers with relatively weak hydrophobicity cannot prompt the performance of PVAm, neither the immiscible polymers. Though polymer blending is more convenient and economical than copolymerizing, the inter-polymer interaction between the amines and modification groups in polymer blends is less effective than the intra-polymer interaction between amines and hydrophobic modification groups in copolymers.

4.4. Conclusions

The Me, i-Pr and t-Bu modified polymers with different modification ratio as CO_2 capture absorbents. The CO_2 capture stoichiometry of the copolymers can be improved by the "spacing effect" of the modification groups, the larger modification groups usually show stronger "spacing effect". Phase separation behavior of the copolymers can also facilitate the CO_2 capture stoichiometry if the LCST is above and close to 30 °C. However excessively modified copolymer with LCST below 30 °C show significantly low CO_2 capture stoichiometry. LCST of the copolymers can be decreased by increasing the hydrophobic modification ratio or by using more hydrophobic modification groups. Besides, the copolymers showed larger CO_2 capture stoichiometry than the polymer blends at the same modification ratio, indicating the intra-

polymer interaction between amine groups and hydrophobic modification groups are essential for the CO_2 capture.

We believe that the PVAm based materials with large amine content and high CO_2 capture stoichiometry can be acquired by carefully choosing the modification groups with high hydrophobicity and controlling the modification ratio and morphology of the polymers. We also believe the results in this study can improve the performance of hydrophobically modified copolymers as sorbents for other acidic or basic molecules.

4.5. References

[1] S. Solomon, D. Qin, M. Manning, Z. Chen, M. Marquis, K. B. Averyt, M. Tignor, H. L. Miller, Eds., *The Fourth Assessment Report of the Intergovernmental Panel on Climate Change* 2007, *Cambridge University Press:* New York, 2007.

[2] A. Olah, A. Geoppert, G. K. S. Prakash, *Beyond Oil and Gas: The Methanol Economy*, Wiley-VCH: Weinheim, Germany, 2009.

[3] a) G. T. Rochelle, *science* 2009, *325*, 1652-1654.

[4] F. A. Chowdhury, H. Okabe, H. Yamada, M. Onoda, Y. Fujioka, *Energy Procedia* 2011, *4*, 201-208.

[5] D. Aaron, C. Tsouris, *Sep. Sci. Technol.* 2005, *40*, 321–348.

[6] D. M. D'Alessandro, B. Smit, J. R. Long, *Angew. Chem. Intl. Ed.* 2010, *49*, 6058-6082.

[7] Y. Park, D. Shin, Y. N. Jang, A. H. A. Park, *J. Chem. & Eng. Data* 2012, *57*, 40-45;

[8] H. Y. Huang, R. T. Yang, *Ind. Eng. Chem. Res.* 2003, *42*, 2427-2433.

[9] Y. Hoshino, K. Imamura, M. Yue, G. Inoue, Y. Miura, *J. Am. Chem. Soc.* 2012,

134, 18177-18180.

[10] T.-J. Kim, B. Li, M.-B. Hagg, J. *Polym. Sci., Part B: Polym. Phys.* **2004**, *42*, 4326-4336.

[11] M. Sandru, T.-J. Kim, M.-B. Hägg, *Desalination* **2009**, *240*, 298-300.

[12] L. Deng, M.-B. Hägg, *J. Membr. Sci.* **2010**, *363*, 295-301.

[13] T.-J. Kim, H. Vrålstad, M. Sandru, M.-B. Hägg, *J. Membr. Sci.* **2013**, *428*, 218-224.

[14] X. Chen, R. Pelton, *Langmuir* **2005**, *21*, 11673-11677.

[15] S. Kunugi, Y. Yamazaki, *Langmuir* **2000**, *16*, 2042-2044.

[16] K. Suwa, Y. Kikunaga, K. Morishita, A. Kishida, M. Akashi, *J. Polym. Sci., Part A: Polym.Chem.* **1996**, *35*, 1763–1768.

[17] K. Suwa, A. Kishida, M. Akashi, *J. Polym. Sci., Part A: Polym.Chem.* **1997**, *35*, 3087–3094.

[18] S. Kunugi, N. Tanaka, K. Suwa, M. Akashi, *Macromolecules* **1997**, *30*, 4499-4501.

[19] B. D. Favis, J. P. Chalifoux, *Polymer* **1988**, *29*, 1761-1767.

[20] B. D. Favis, D. Therrien, *Polymer* **1991**, *32*, 1474-1481.

[21] S. Y. Heriot, R. A. Jones, *Nature materials* **2005**, *4*, 782-786.

[22] L. Yu, K. Dean, L. Li, *Prog. Polym.Sci.* **2006**, *31*, 576-602.

[23] B. Barham, G. Voge, D. Waldow, *Macromolecules* **2001**, *34*, 514-521.

[24] C. Yi, Z. Wang, M. Li, J. Wang, S. Wang, *Desalination* **2006**, *193*, 90-96.

[25] L. Deng, T.-J. Kim, M.-B. Hägg, *J. Membr. Sci.* **2009**, *340*, 154-163.

[26] S. Yuan, Z. Wang, Z. Qiao, M. Wang, J. Wang, S. Wang, *J. Membr. Sci.* **2011**, *378*, 425-437.

[27] K. Yamamoto, E. Nagatomo, T. Serizawa, Y. Muraoka, M. Akashi, *J. Appli. Polym. Sci.* **2003**, *89*.

[28] H. Tanaka, R. Senju, *R. Bull Chem Soc Japan* **1976**, *49*, 2821.

[29] H. Tanaka, *J. Polym. Sci. Polym. Lett. Ed.* **1978**, *15*, 87.

[30] H. Tanaka, *J. Polym. Sci. Polym. Chem. Ed.* **1979**, *17*, 1239.

[31] D. D. Reynolds, W. O. Kenyon, *J. Am. Chem. Soc.* **1947**, *69*, 911–915.

[32] D. J. Dawson, D. G. Richard, E. W. J. Robert, *J. Am. Chem. Soc.* **1979**, *98*, 5996–6000.

[33] W. S. Robert, H. S. Richard, *Ind. Eng. Chem. Prod. Res. Dev.* **1985**, *24*, 242–246.

[34] M. Akashi, E. Yashima, T. Yamashita, N. Miyauchi, S. Sugita, K. Marumo, *J Polym Sci, Part A: Polym. Chem.* **1990**, *28*, 3487–3497.

[35] K. Yamamoto, T. Serizawa, Y. Muraoka, M. Akashi, *J Polym Sci, Part A: Polym. Chem.* **2000**, *38*, 3674–3681.

[36] D. Roy, W. L. Brooks, B. S. Sumerlin, *Chem.Soc. rev.* **2013**, *42*, 7214-7243.

[37] D. Voet, J. G. Voet, *Biochemistry*, 4th ed., Wiley: New York, USA, **1995**.

[38] P. D. Vaidya, E. Y. Kenig, *Chem. Eng. Technol.* **2007**, *30*, 1467-1474.

Chapter 5. Effect of Film Inner Structure on the CO_2 Release and Capture Kinetics

Abstract

In this chapter, the effect of inner gel structure on the CO_2 capture and release kinetics of the films were revealed by comparing gel films with different inner structure: the film consisting of larger GPs (GP-big film) and smaller GPs (GP-small film), the gel film with uniform structure (Homogeneous gel film), the gel film with GPs embedded (pudding gel film), and the gel film with macropores (Macroporous gel film). It is found that the large inter-GP pores formed between the rigid collapsed GPs facilitated the molecule diffusion in the CO_2 release process at 75 °C (above VPTT 38 °C). The fast thermal responsibility of IPN gel film also improved the molecule diffusion in the film by preventing the formation of dense skin layer. The inner pores of the gel film also improve the capture kinetics in the CO_2 capture process at 30 °C (below the VPTT 38 °C). However the inner pores of slightly crosslinked gels will significantly diminish at their swollen state. This study provided a guidance to design a gel film with fast CO_2 capture and release kinetics.

5.1. Introduction

The accumulation of CO_2 mainly generated from burning of fossil fuels has caused serious global climate change. Meanwhile, CO_2 can be a potential carbon source to produce liquid fuels such as methanol and dimethyl ether by using regenerative energy.[1] Thus, the development of energy-efficient CO_2-capture-release methods for point sources such as fossil fuel power plants is essential for not only minimizing the greenhouse effect but also the future use of carbon-based energy. A new method to capture and release CO_2 reversibly in wet conditions via

a small temperature swing process from 30 °C to 75 °C by hydrogel films consisting of *N*-isopropylacrylamide (NIPAm) based amine containing gel particles (GPs) has been reported by our group.[2] Stoichiometric amine efficiency during the reversible CO_2 capture process has been optimized from the aspects such as volume phase transition, size, swelling ratio, microenvironment and pK_a of the GPs.[3]

However, the CO_2 capture/release rate is still unknown and has to be optimized. It's supposed that the large inter-GP pores would facilitate the transport of ions/molecules, so does the mobility of the GPs in the GP films during moisture absorption and the phase separation behavior. The rapid responsibility of GPs in the film may also contribute to a fast CO_2 capture/release rate of GP films.

In this study, the existence of the mobility of GPs in GP films during moisture absorption was observed by laser scanning confocal microscope. The importance of the inter-GP pores and the rapid thermal responsibility of the GPs during the reversible CO_2 capture release process was investigated by comparing the reversible CO_2 capture rate of GP films with other hydrogel films with different structures, such as homogeneous monolithic gel film, pudding gel film and macro-porous gel film. The structure of the above mentioned gels are schematically illustrated in scheme 5-1. Understanding the effect of these factors on the CO_2 capture/release rate will guide us the right direction to design a structure with faster CO_2 capture/release kinetics.

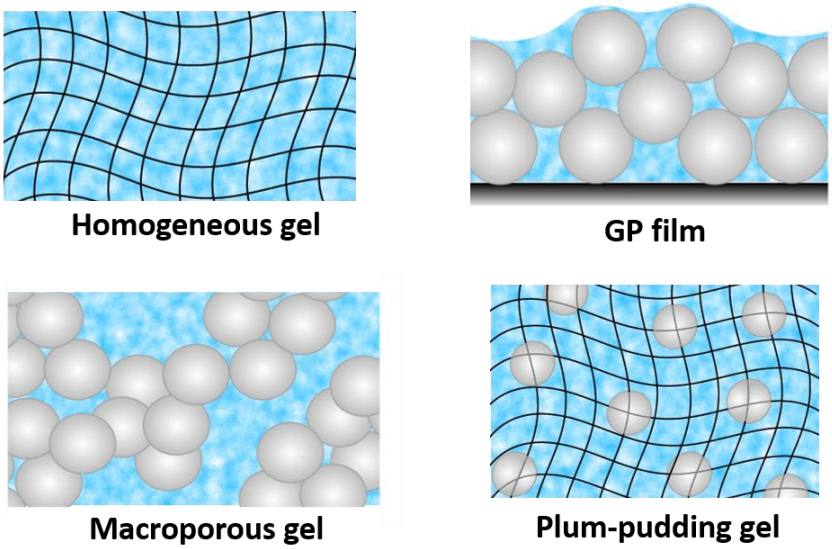

Scheme 5-1. Structure of different gel networks

The conventional homogeneous monolithic gel is usually prepared without phase separation, resulting in an even inner structure. The pore size of a conventional pNIPAm hydrogel is relatively small and its response to thermal cycling is relatively slow.

Plum-pudding gel is a new structure to improve both thermal response rate and mechanical strength of hydrogel. The structure of plum-pudding gel, with the chains of the network passing through the pores of the GPs, combined with the sponginess and rapid shrinking properties of the pNIPAm GPs seemed like a possible mechanism for speeding up the shrinking process of bulk gels, which are often hampered by the formation of a dense layer of collapsed polymer on the gel surface which slows down the subsequent shrinking dramatically. The reason was 2-fold: first that the presence of the collapsing PNIPAM GPs would provide hydrophobic patches throughout the gel which would act to nucleate the collapse process, and second that the collapse of the PNIPAM GPs would pull the network chains that pass through them together and thus the entire gel should have faster

response times to changes in the surrounding temperature.[4]

Hydrogels with pore sizes significantly larger than those of conventional hydrogels are referred to here as "macro-porous" hydrogels. They are characterized by large pore sizes, high pore volumes, and high specific surface area.[5] To prepare macro-porous pNIPAm networks, the normal method is to polymerize the gel above LCST. The macroporous gels were also synthesized above their LCST in the presence of porogens such as hydroxypropyl cellulose (HPC)[5], poly(ethylene glycol) (PEG)[6], sucrose[7] to control the pore size and size distribution. Macro-porous pNIPAm gel can also be prepared in NaCl solution at room temperature because LCST of pNIPAm will be decreased in the presence of NaCl.[8] In order to obtain macro-porous structures, a phase separation must occur during the course of the crosslinking process so that the two-phase structure is fixed by the formation of additional crosslinks. In the gel formation process the gel deswells at the critical point for phase separation and becomes a microsphere, whereas the separated liquid phase remains as a continuous phase in the reaction system. As the reaction proceeds, new microspheres are continuously generated due to the successive separation of the growing polymers. Agglomeration of microspheres leads to the formation of a macro-porous network consisting of two continuous phases.[9]

5.2. Materials and experiments

5.2.1. Materials

NIPAm (Wako Pure Chemical Industries, Ltd.) was purified by recrystallization from *n*-hexane and dried *in vacuo* at room temperature. *N*-[3-(Dimethylamino)propyl]methacrylamide (DMAPM, Tokyo Chemical Industry Co., Ltd.), 2,2′-azobis(isobutyronitrile) (AIBN, Wako Pure Chemical Industries, Ltd.),

2,2′-azobis(2-methylpropionamidine)dihydrochloride (AAPD, Wako Pure Chemical Industries, Ltd.), *N,N'*-methylenebis(acrylamide) (bis, Tokyo Chemical Industry Co., Ltd.), cetyltrimethylammonium bromide (CTAB, Wako Pure Chemical Industries, Ltd.), 4- aminofluorescein (Aldrich Chemical Co., Ltd.), and acryloyl chloride (Sigma-Aldrich Chemical Co., Ltd.) were used as received. The dialysis membrane having a cut-off of 12–14,000 was purchased from Spectrum Laboratories, Inc. The anion-exchange resin (A2004-OH, Muromachi Technos Co., Ltd.) was first pretreated with 1 M NaOH, and then washed with deionized water. The water was purified using a Direct-Q Ultrapure Water System (Merck, Ltd.).

5.2.2. Preparation of GPs with different size

In order to clearly observe mobility of the GPs in GP film by laser scanning confocal microscope (LSCM), GP-D5 with larger size were synthesized by reducing amount of surfactant CTAB during polymerization. The ordinary GP-D5 previous used was polymerized in the presence of 2.0mM CTAB. To prepare larger GP-D5, 0.8, 0.4, 0.2 mM CTAB was used, as shown in table 5-1.

Table 5-1. Polymerization recipe of the GPs with different size

		D5	D5-L1	D5-L2	D5-L3
DMAPM (uL)	5%	141.25	141.25	141.25	141.25
NIPAm (mg)	93%	1642	1642	1642	1642
Bis (mg)	2%	48	48	48	48
CTAB	mM	2.0	0.8	0.4	0.2
AAPD (mg)	2.5mM	35	35	35	35

NIPAm, DMAPM, and Bis were first dissolved in water, resulting in the settled

total monomer concentration. Then surfactant CTAB was added to the monomer solution followed by heating to 70 °C. Then the solution was degased by nitrogen gas while stirring at 70 °C for 1 h. Later, aqueous solution of AAPD (2.5 mM) was added by syringe. The polymerization reaction was carried out at 70 °C for 3 h under nitrogen atmosphere. The resulting mixture was purified by dialysis against an excess volume of water over four days (water was changed more than three times a day). The anion-exchange of the GPs was conducted to remove the trace amount of counter anions and CO_2 absorbed by amines during dialysis. The GP with largest diameter and good dispersibility is used as GP-D5-L in the following study.

5.2.3. Preparation of fluorescent GPs

0.01 mol% AFA and 0.01 mol% MTRh were incorporated into the GP-D5-L respectively to observe movement of GPs by LSCM. Fluorescent monomers were pre-dissolved in MeOH and then added 0.5mL of the MeOH solution into monomer solution. Other process was same as described in **5.2.2**.

5.2.4. Preparation of GP films

The ion-exchanged GPs were dried using a lyophilizer, and then dissolved in methanol. The hydrogel films were prepared by casting the methanol solutions of GPs on the inner surface of a stainless steel container, followed by the addition of a 9 mL water/g GPs (total polymer concentration: 10 wt%) after completely evaporating methanol. The film thickness was controlled by casting different volume of the methanol solution of GPs onto the surface of the stainless steel container.

The thickness of the hydrogel films was estimated by assuming the swollen GPs

contain 1 wt.% polymer and 99 wt.% water. As a result, the polymer density of the hydrogel film containing 9 mL water/g GPs (90% water inside GPs) will be 0.1 g/mL (10 wt%). The film thickness was calculated using the following equation:

$$t = m / (d * s)$$

where t, m, d, and s represent the thickness, weight, density, and surface area of the GP film, respectively.

5.2.5. Preparation of 2-layer GP films consisting D5-L-AFA0.01 and D5-L-MTRh0.01

As illustrated in scheme 5-2, D5-L and D5-L- MTRh 0.01 aqueous solutions were mixed to bring the final weight ratio to 99:1. After lyophilization, the GP D5-L/D5-L-MTRh0.01 (99:1) were dissolved in methanol. So did the D5B2-L and D5B2-L-AFA0.01. Then the methanol solution of D5-L/D5-L- MTRh0.01 (99:1) was casted onto a glass bottom dish (Matsunami Glass Ind., Ltd.). MTRh-labeled D5-L film was obtained after evaporation of methanol.

Subsequently, the methanol solution of D5-L/D5-L-AFA0.01 (99:1) was cast on the surface of of MTRh-labeled D5-L film, followed by the rapid evaporation of methanol solvent to prevent the GPs from diffusing.

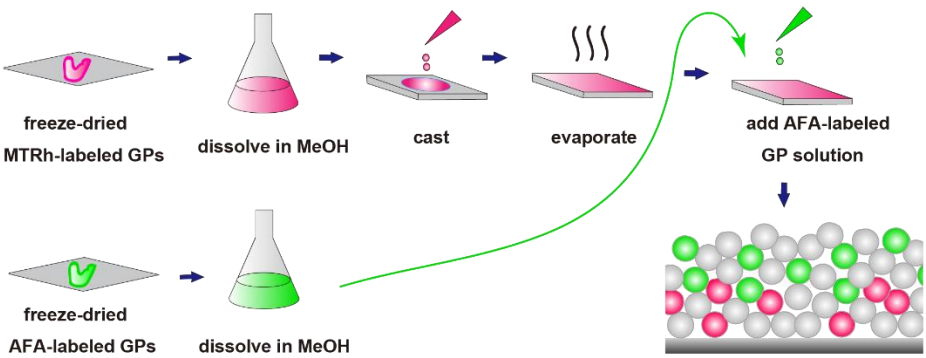

Scheme 5-2. Preparation of 2-layer GP films consisting D5-L-AFA0.01 and D5-L-

5.2.6. Preparation of homogeneous monolith gel films

Usually the conventional homogeneous monolith gel were prepared by initiating the aqueous solution of monomers at room temperature by water soluble redox pair APS-TEMED where TEMED work as accelerator. However the high surface tension (72.75 m*N/m) of water make casting thin monomer solution film (~100 μm) difficult. As a solution, homogeneous monolith gel film in this study were synthesized from ethanol solution (22.75 m*N/m) with oil soluble redox pair of benoyl peroxide (BPO) and *N, N*-dimethylaniline (DMA). The total monomer concentration is same to the polymer concentration of GP films (10 wt%).

Table 5-2. Recipe for homogeneous monolith gel preparation: (a) Concentration of monomer and initiator. (b) The amount of monomer solution and initiator solution needed to prepare films with different thickness.

(a)	Monomer	DMAPM	5 mol%	46.6 μL	Dissolve in 5 mL ethanol
		NIPAm	93 mol%	547.27 mg	
		Bis	2 mol%	16 mg	
	Initiator	DMA	200 mol% of BPO	13.2 μL	
		BPO	2 wt%	12 mg	In 0.5mL aceton

		Film weight (thickness)			
(b)		120 mg (100 μm)	240 mg (200 μm)	360 mg (300 μm)	480 mg (400 μm)
	Monomer solution	1.12 mL	2.24 mL	3.31 mL	4.48 mL
	BPO solution	0.1 mL	0.2 mL	0.3 mL	0.8 mL

The monomer solution and BPO solution was prepared according to the

ingredient shown in table 5-2a. The monomer solution and BPO solution were then degased by N_2 separately and delivered into glove box. Specific amount of the monomer solution and BPO solution was mixed in a vial (table 5-2b) followed by casting the mixture in the container surface at room temperature (23 °C). The container was then covered by an acrylic plate. The gelation occurred within 15min and was carried on for another 3h. After polymerization the gel was washed by MilliQ water for 30min (changing water every 5 min) to remove unreacted monomers and then dried in draft. 9 g-water/g-gel was added into the film for CO_2 absorption

5.2.7. Preparation of plum-pudding gel films

Pudding gel film was synthesized in the same way as the homogeneous monolith gel with adding extra GP-D5-L accounting for 30 wt% of total weight. The amount of monomers, GPs and initiator was shown in table 5-3.

Table 5-3. Recipe for plum-pudding gel preparation: (a) Concentration of monomer, GPs and initiator. (b) The amount of monomer+GP solution and initiator solution needed to prepare films with different thickness.

(a)	monomer	DMAPM	5 mol%	46.6 μL	Dissolve in 5.6 mL EtOH
		NIPAm	93 mol%	547.27 mg	
		Bis	2 mol%	16 mg	
	GPs	GP-D5-L	30 wt%	0.2428 g	
	initiator	DMA	200mol% * BPO	13.2 μL	
		BPO	2wt%	12 mg	In 0.5 mL aceton

	Film weight (thickness)			
(b)	120 mg (100 μm)	240 mg (200 μm)	360 mg (300 μm)	480 mg (400 μm)

	Monomer +GP solution	1.12 mL	2.24 mL	3.31 mL	4.48 mL
	BPO solution	0.1 mL	0.2 mL	0.3 mL	0.8 mL

5.2.8. Preparation of macroporous gel films

In order to prepare macroporous gel, phase separation behavior during polymerization is necessary. Therefore the polymerization should be carried out in aqueous system. However, as mentioned above, it is difficult to prepare thin flat gel film from aqueous system by casting method due to the high surface tension of water. Thus the macroporous gel film was polymerized by sandwiching the polymer solution in this study. The monomer and the initiator (Table 5-4) was mixed at room temperature, without adding any surfactant. The solution was degassed by N2 for 15 min, followed by the injection of the solution in to a well spaced by a ring-shaped silicon rubber with thickness of 500 μm. Then the well was fixed by clips. The polymerization was carried out at 70 °C for 3 h.

Table 5-4. Recipe for macroporous gel.

monomer	DMAPM	5 mol%	46.6 μL	Dissolve in 6.0 mL water (10 wt%)
	NIPAm	75 mol%	441.35 mg	
	Bis	20 mol%	160 mg	
initiator	AAPD	2 wt%	12.8 mg	

Thickness of the resulting film will be thinner than the soft silicon rubber spacer, because the spacer was stressed by clips. Therefore the thickness of the macroporous film was determined after measuring the weight of the freeze-dried polymers by the following equation after CO_2 capture experiment.

$$t = m / (d * s)$$

where t, m, d, and s represent the thickness, weight, density, and surface area of

the GP film, respectively

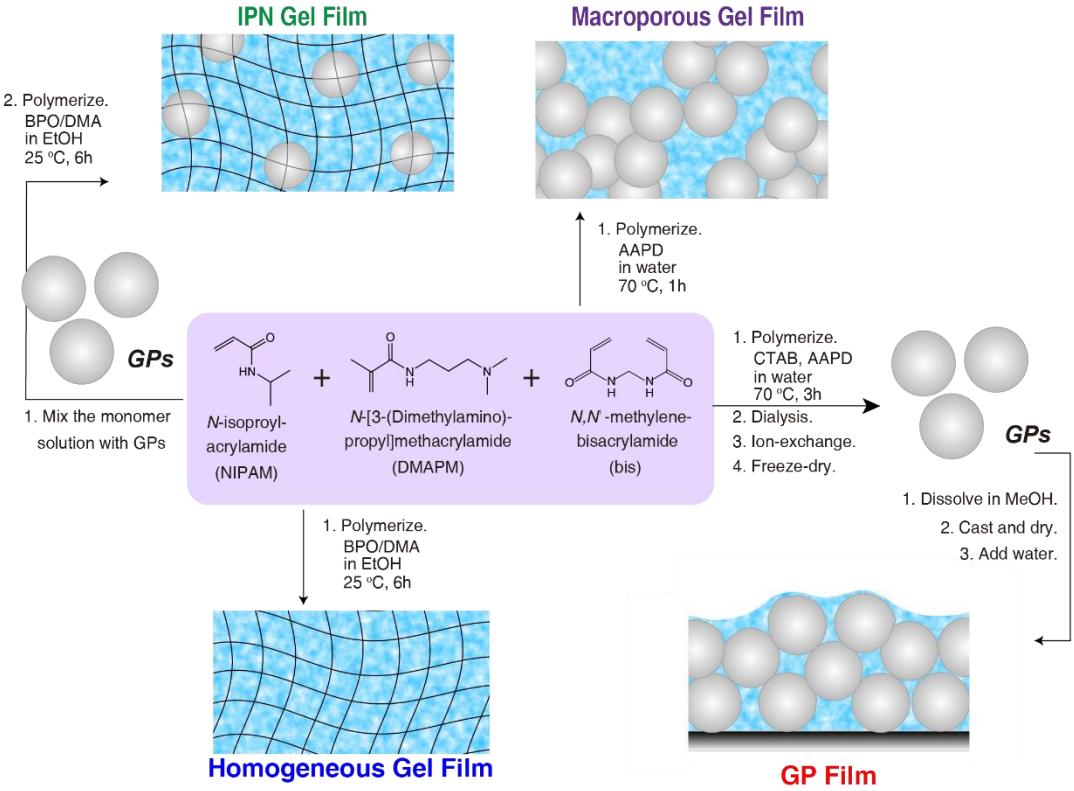

Scheme 5-3. Preparation of gel films with different structure.

5.2.9. GP mobility in GP films observation by LSCM

Inner structure of the dried fluorescent-labeled 2-layer GP film was investigated using a confocal laser scanning confocal microscope (LSCM) (LSM 700, Carl Zeiss) equipped with the LSM Software ZEN 2011. The laser with excitation wavelength 488 nm was applied for AFA-labeled GPs and 548 nm was used for MTRh-labeled GPs. After LSCM measurement, the film was kept absorbing 75 °C moisture for 40 min. The inner structure of the 2-layer GP film was then observed after drying the film.

5.2.10. CO_2 release/capture rate measurement

10 % CO_2 (90 % N_2, 10 mL/min) gas was bubbled into water (60 °C) to saturate the water vapor at the appointed temperature. The resulting water-saturated gas was guided into a stainless steel container with CO_2 absorbent film on its surface, and then channeled to a CO_2 analyzer (GC, Shimadzu Corp.). All the films were equilibrated by the 10% CO_2 gas at 30 °C. Thereafter, CO_2 desorption rate at 75 °C and absorption rate at 30 °C of each film were quantified by monitoring concentration of CO_2 every 1 s.

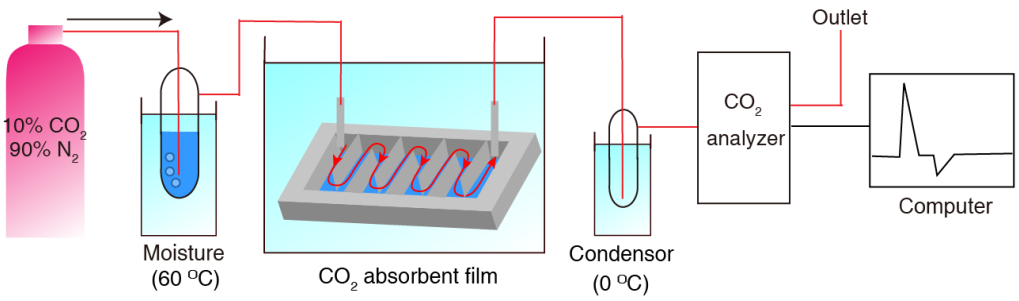

Scheme 5-4. CO_2 release and capture rate measurement by CO_2 analyzer

5.3. Results and discussion

5.3.1. Preparation of GPs with different size

Size of the series of GP-D5-L was measured by DLS, and the result was shown in figure 5-1a. Purple, blue, green and red represent the GPs prepared in the presence of 0.2 mM, 0.4 mM, 0.8 mM and 2.5 mM surfactant CTAB respectively. As expected size of GPs increased with decreasing concentration of CTAB. Figure 5-1b showes the swelling ratio of the GPs are comparable to each other. The blue one showes a lower LCST than others due to some unknown reason. In the following study CTAB 0.2mM was used as general protocol to prepare D5-L.

Figure 5-2 showed a linear relationship between $\log(D_{(50\,°C)})$ and $\log(c_{(CTAB)})$. This

result is in accordance with the previous report[3] and can be applied to preciously design GP with specific diameter.

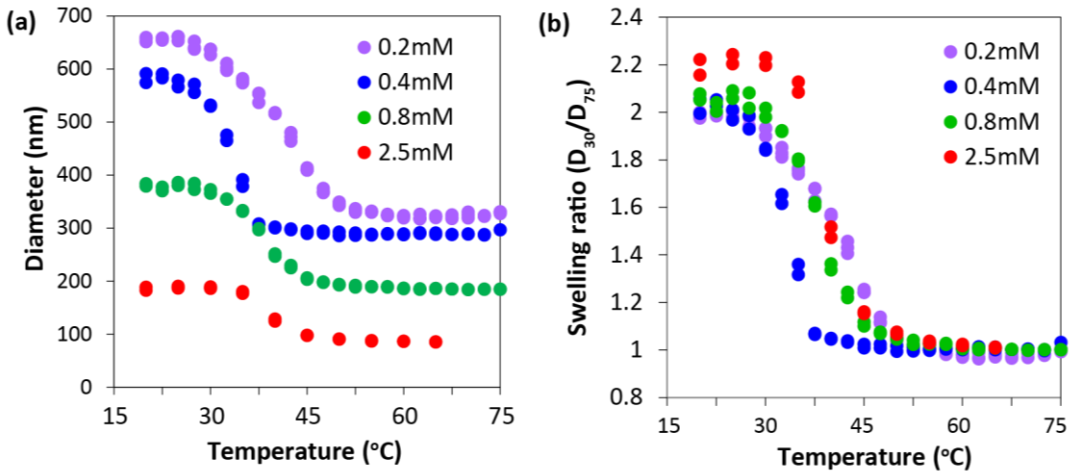

Figure 5-1. (a) Size and (b) swelling ratio of the series of D5-L synthesized with different CTAB concentration.

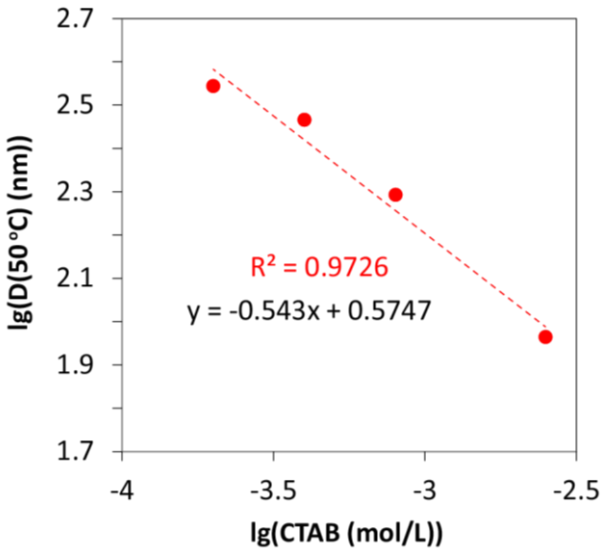

Figure 5-2. Relation between GP diameter at 50 °C and CTAB concentration

5.3.2. Preparation of fluorescent GPs

Well dispersed GP-D5 of larger diameter copolymerized with 0.01% MTRh or 0.01% AFA were successfully achieved. Figure 5-3c showed DLS data of the D5-L

(blue), D5-large-AFA0.01 (green) and D5-large-MTRh0.01 (red). The two kinds of fluorescent GPs exhibited similar diameter, but larger than the GPs without fluorescence.

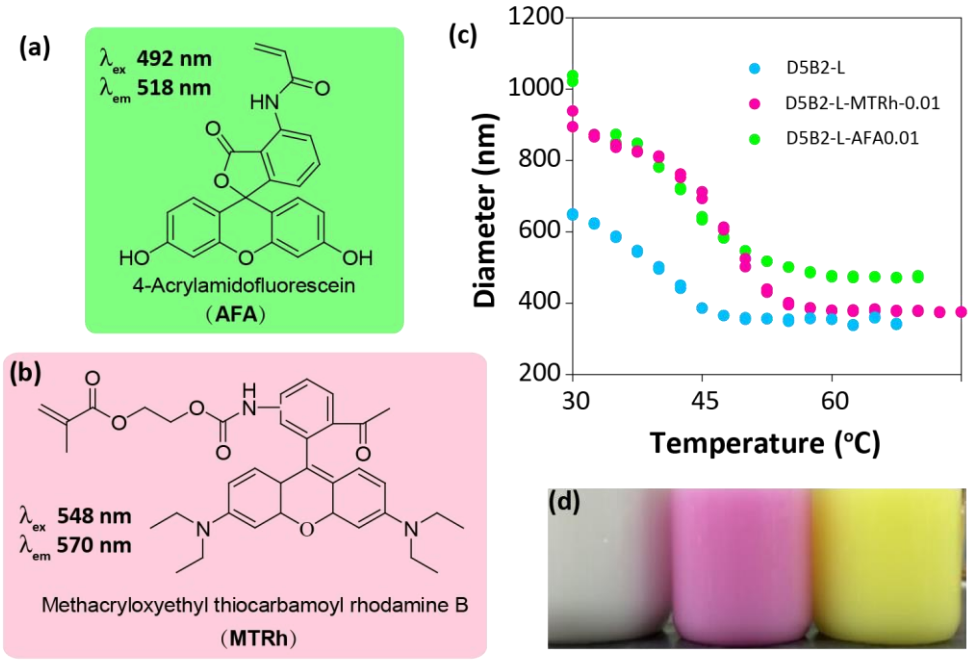

Figure 5-3. (a) and (b): Molecule structure of AFA and MTRh respectivelly and their corresponding wavelength of exciting light and emission light. (c) Temperature dependent diameter of GP-D5-L, GP-D5-L-MTRh0.01 and GP-D5-L-AFA0.01. (d) Photographs of GP-D5-L (white), D5-L-MTRh0.01 (pink) and D5-L-AFA0.01 (yellow).

5.3.3. Mobility of GPs in GP film after moisture absorption

To observe the mobility of GPs after moisture capture, the 2-layer GP film was kept absorbing 75 °C moisture for 40 min, during which water drops was observed on the glass bottom and the 2-layer GP film turned white. Then the film was dried by a drier and inner structure was observed by LSCM.

From the LSCM image shown in figure 5-5, a clear 2-layer structured GP film

was successfully prepared. However, after moisture capturing, the structure of the 2-layer GPs didn't change, indicating GPs do not diffusion in the GP films during moisture absorbing process, which is different from our expectation.

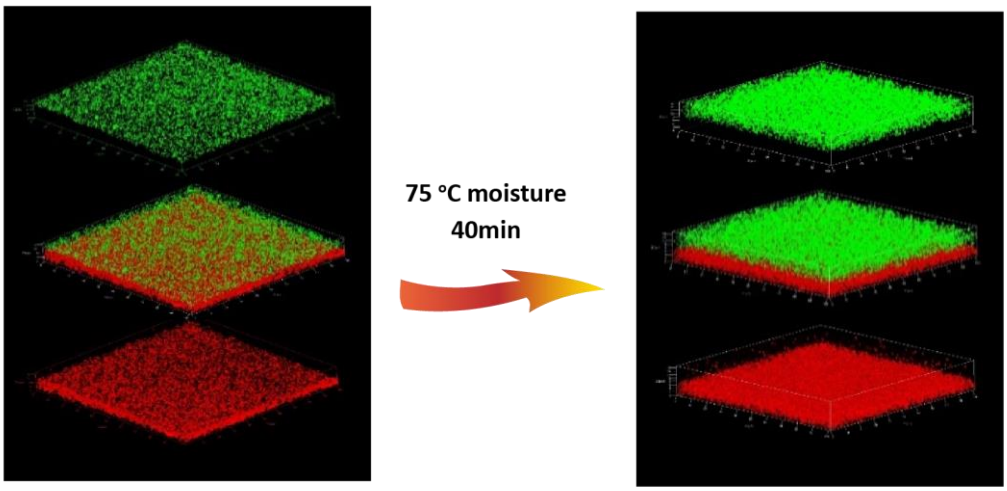

Figure 5-5. LSCM images of 2-layer fluorescent-labeled GP films before and after moisture absorption

5.3.4. Homogeneous gel and pudding gel film preparation

Homogeneous gel films and plum-pudding gel films were obtained as expected. The homogeneous gel is transparent due to the homogeneous inner structure (see figure 5-4), while the plum-pudding gel is semi-transparent~white, as a result of the incorporation of 30 wt% of GPs. The films did not change obviously after reversible CO_2 capture and release.

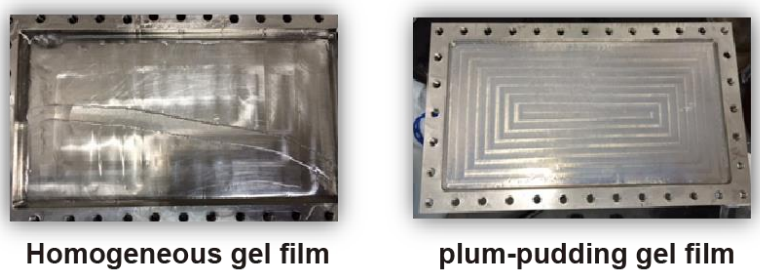

Figure 5-4. Photograph of homogeneous gel film and plum-pudding gel film.

5.3.5. Effect of flow rate of 10% CO_2 gas and void volume of quantification system on CO_2 release/capture rate

The effect of 10% CO_2 flow rate on the CO_2 release/capture rate of the CO_2 absorbent films is shown in figure 5-6a. When the flow rate increased from 100 mL/min to 200 mL/min, the CO_2 release/capture rate also increased. However when the flow rate increased from 200 mL/min to 300 mL/min, the CO_2 release/capture rate was not influenced, indicating the effect of void volume of the measurement system can be exclude by increasing the CO_2 flow rate.

The same result can also be seen from figure 5-6b. The CO_2 release/capture rate of the same film was measured by using the container of larger void volume (height = 5mm) and the container of smaller void volume (height = 2mm), respectively. By increasing CO_2 flow rate throng 5mm-height container (300 mL/min), the same release/capture rate with 2mm-height container (100 mL/min) was observed, indicating the effect of void volume of the quantification system can be exclude by increasing the CO_2 flow rate.

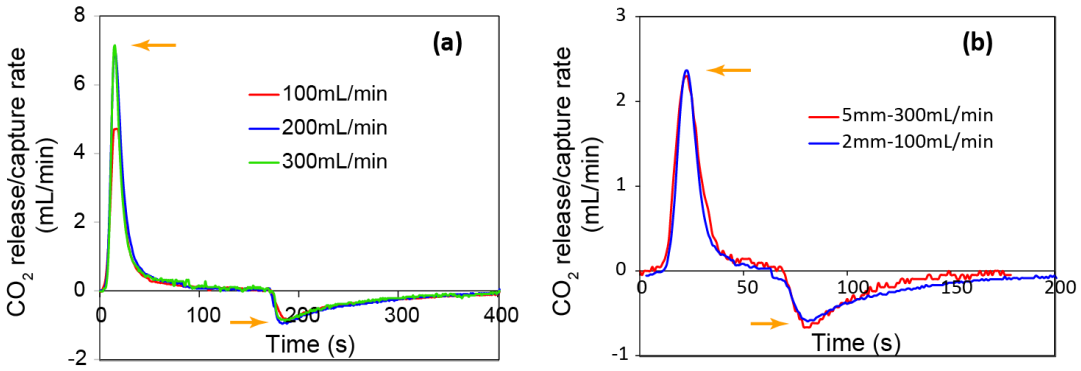

Figure 5-6. (a) CO_2 release and capture rate of the same GP film when applying different 10% CO_2 flow rate. (b) CO_2 release and capture rate of the same GP film when using film container with different void volume.

In order to exclude the effect of void volume of the container in the kinetics study, different flow rate of CO_2 feed gas was used. The CO_2 capture/release rate was accepted when the value doesn't increase with faster CO_2 flow rate.

5.3.6. Effect of inner structure of gels on the CO_2 release rate of the gel film

In this study, the top of CO_2 release/capture peak (the arrows in figure 5-6) was recorded as the CO_2 release/capture rate of the film absorbent.

Films with different thickness were prepared, and CO_2 release/capture rate of the films were measured. The thickness dependent CO_2 release flux of the films with different inner structure were shown in figure 5-7a. As revealed in figure 5-7a, in the reaction-limited range where CO_2 release rate is linearly proportional to film thickness, GPs shows faster release rate than pudding gel and homogeneous monolith gel. In the diffusion-limited range where CO_2 release rate is independent of film thickness, GP-D5-L exhibited faster release rate than GP-D5. Homogeneous monolith gel film release CO_2 slowest and pudding gel film showed obviously faster CO_2 release rate than homogeneous monolith gel film. We focused on the diffusion-limited range in this study.

This can be interpreted by the hypothesis as described in figure 5-7b. When removing the container from 30C to 75C (above VPTT 38 °C) water bath to release CO_2, the GP-D5 (black) shrink rapidly and meshes are formed among the collapsed hard GP spheres with a high Young's modulus[10]. The meshes provide easier pathways for mass diffusion, resulting in faster CO_2 release rate of GP-D5 macroscopically. With increasing GP diameter, the size of meshes increases simultaneously, expediting the mass transport furthermore, as a result a faster CO_2 release rate of GP-D5-L is observed (red). In contrast, accompanying removal

of the container of homogeneous monolith gel film from 30 °C water bath to 75 °C, a dense collapsed skin-layer is always formed on the gel surface because surface layers shrinks more rapidly than the internal gel.[4] This skin layer acts as a barrier to prevent not only the release of internal water but also the diffusion of CO_2, hugely delaying the shrinking process and CO_2 release rate (blue). In the case of pudding gel film, the incorporation of GPs into the gel network overcame the problems associating with the formation of dense skin layer by providing hydrophobic patches throughout the gel which would nucleate the collapse process and by pulling the network chains that pass through them together by the collapsed GPs and thus the entire gel showed faster responsibility to surrounding temperature change and prevented the formation of dense skin layer, leading to faster CO_2 release rate of pudding gel film (green) than homogeneous monolith gel film. However the CO_2 release rate of pudding gel film containing 30wt% of GP-D5-L is still slower than GP-D5-L films, because there are not meshes for easier diffusion though dense skin layer was inhibited.

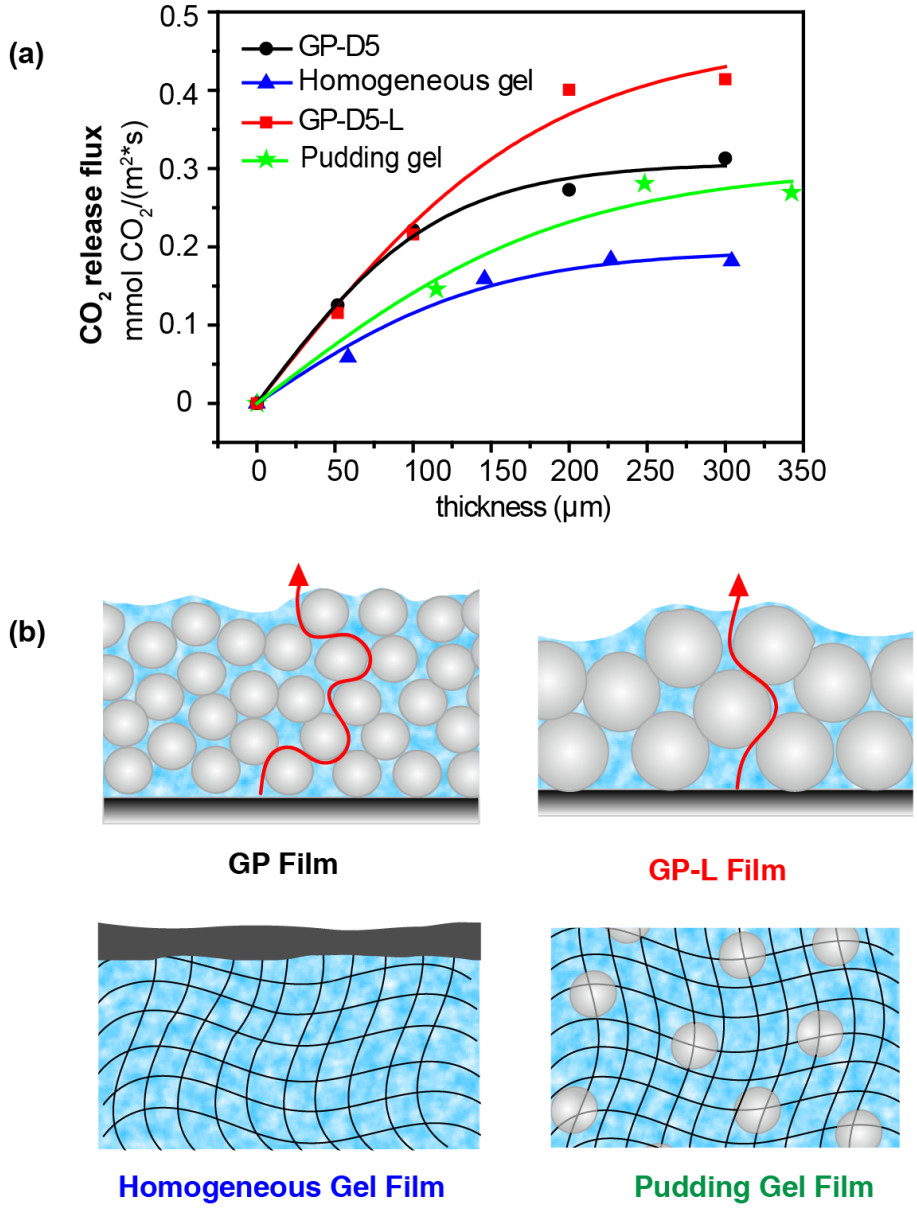

Figure 5-7. (a) CO_2 release flux as a function of the film thickness. GP film (black cycle), film of larger GPs (red square), homogeneous gel film (blue triangle) and pudding gel film were used. (b) Proposed molecule diffusion in the gels with different structure in CO_2 release process at 75 °C.

5.3.7. Effect of inner structure of gels on the CO_2 capture rate of the gel film

CO_2 capture rate of the gel films was displayed in figure 5-8a. Different from CO_2 release rate profile, the four kinds of gel films showed same capture kinetics

in both reaction-limited range and diffusion-limited range.

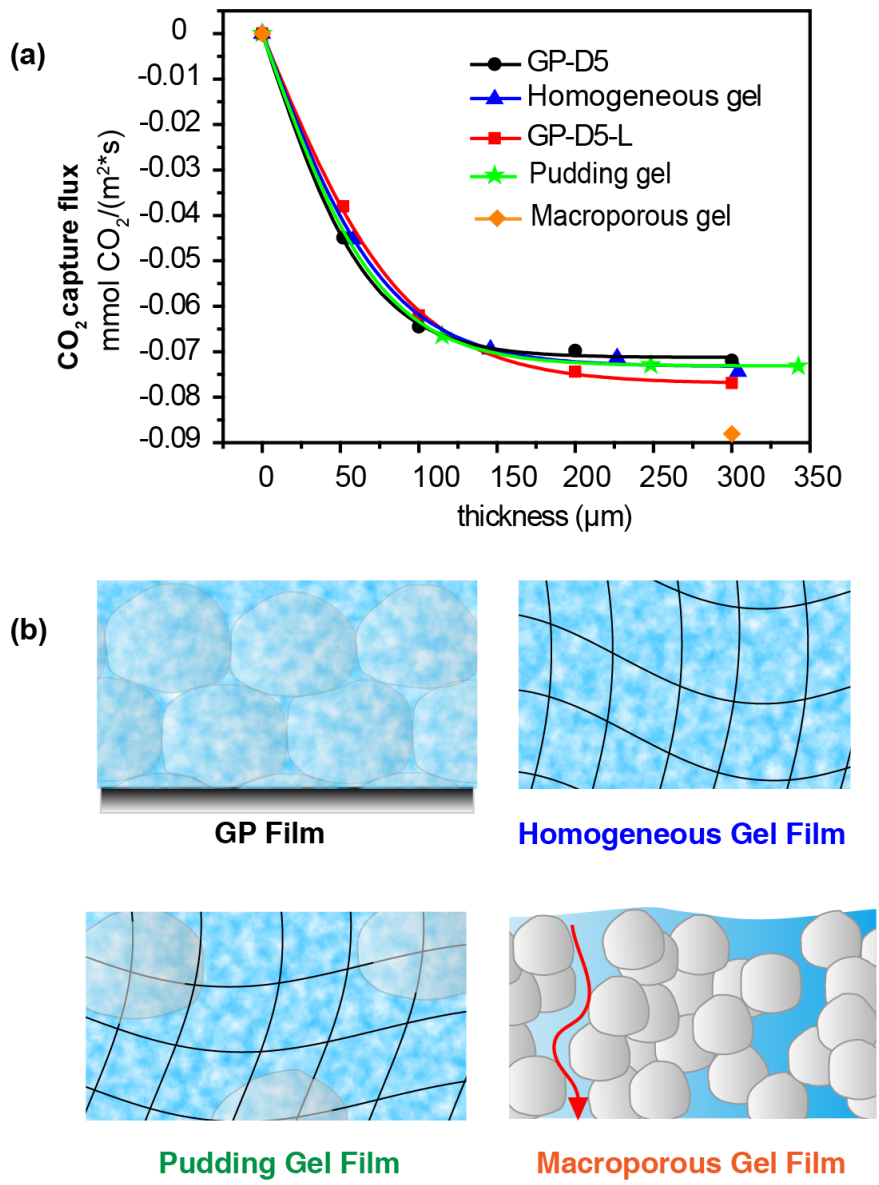

Figure 5-8. (a) CO_2 capture flux as a function of the film thickness. GP film (black cycle), film of larger GPs (red square), homogeneous gel film (blue triangle) and pudding gel film were used. (b) Proposed molecule diffusion in the gels with similar structure in CO_2 capture process at 30 °C.

It's reported that re-swelling kinetics of homogeneous monolith gel is much faster than the de-swelling kinetics.[5],[11] It's hypothesized that on returning the

container from 30 °C water bath to 75 °C, all the gel films swollen rapidly. The meshes among GPs dramatically diminished because the highly swollen GPs are too soft to maintain their spherical shape.[10] The deformation of the GPs resulted in the inner structure of the gel film comparable to homogeneous gel film and pudding gel film, as represented in figure 5-8b. As a matter of course, same CO_2 capture rate was acquired from the films with similar inner structure.

In order to see the importance of inner large pores to the CO_2 capture rate of the gels, a highly crosslinked macroporous gel (20 mol% Bis) was prepared. The macroporous gel film, which was expected to maintain parts of macropores at swollen state showed obviously faster capture rate than others (figure 5-8a), indicating the inner pores of the gel film also improve the capture kinetics.

5.4. Conclusion

In conclusion, the effect of inner gel structure on the CO_2 capture and release kinetics of the gel films are investigated in this study. Briefly, the large inter-GP pores and the fast responsibility of the GP films promoted the CO_2 release rate of GP films. The large inner pores also facilitated the CO_2 capture rate.

This study provided a guidance to design a gel film with fast CO_2 capture and release kinetics.

5.5. References

[1] A. Olah, A. Geoppert, G. K. S. Prakash, *Beyond Oil and Gas: The Methanol Economy*, Wiley-VCH: Weinheim, Germany, 2009.

[2] M. Yue, Y. Hoshino, Y. Ohshiro, K. Imamura, Y. Miura, *Angew. Chem., Int.*

Ed. **2014**, *53*, 2654-2657.

[3] X. Wu, R. H. Pelton, A. E. Hamielec, D. R. Woods, W. McPhee, *Colloid. Polym. Sci.* **1994**, *272*, 467-477.

[4] I. Lynch, K. A. Dawson, *J. Phys. Chem. B* **2003**, *107*, 9629-9637.

[5] X. S. Wu, A. S. Hoffman, P. YAGER, *J. Polym. Sci., Part A: Polym. Chem.* **1992**, *30*, 2121-2129.

[6] R.-X. Zhuo, W. Li, *J. Polym. Sci., Part A: Polym. Chem.* **2003**, *41*, 152-159.

[7] J.-T. Zhang, S.-X. Cheng, S.-W. Huang, R.-X. Zhuo, *Macromol. Rapid Commun.* **2003**, *24*, 447-451.

[8] S.-X. Cheng, J.-T. Zhang, R.-X. Zhuo, *J. Biomed. Mater. Rese. Part A* **2003** *67*, 96-103.

[9] C. Sayil, O. Okay, *Polymer* **2001**, *42*, 7639–7652.

[10] S. Schmidt, M. Zeiser, T. Hellweg, C. Duschl, A. Fery, H. Möhwald, *Adv. Funct. Mate.* **2010**, *20*, 3235-3243.

[11] J. Wang, D. Gan, L. A. Lyon, M. A. E. Sayed, *J. Am. Chem. Soc.* **2001**, *123*, 11284-11289.

Chapter 6. Summary

In chapter 2, hydrogel films composed of temperature-responsive microgel particles (GPs) containing amine groups work as stimuli-responsive carbon dioxide absorbent with a high capacity of approximately 1.7 mmol/g. Although the dried films did not show significant absorption, the reversible absorption capacity dramatically increased by adding a small amount of water (1 mL/g). The absorption capacity was independent of the amount of added water beyond 1 mL/g, demonstrating that the GP films can readily be used under wet conditions. The amount of CO_2 absorbed by the GP films was proportional to their thickness up to 200-300 μm (maximum capacity of about 2 L/m^2). Furthermore, the films consisting of GPs showed faster and greater absorption and desorption of CO_2 than that of monolithic hydrogel films. These results indicated the importance of a fast stimulus response rate of the films that are composed of GPs in order to achieve long-range and fast diffusion of bicarbonate ions. Our study revealed the potential of stimuli-responsive GP films as energy-efficient absorbents to sequester CO_2 from high-humidity exhaust gases

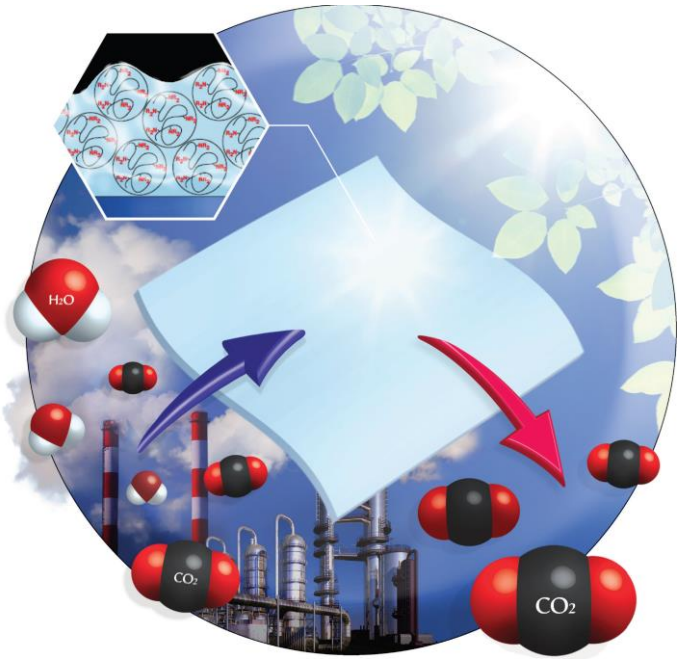

In chapter 3, inspired by the efficient CO_2 transport mechanism of hemoglobin in blood known as Bohr effect, here we revealed the design rationale of amine-functionalized thermo-responsible gel particles (GPs) films that reversibly capture

and release large amount of CO_2 efficiently from a model exhaust gas of fire power plants in a small temperature change (30 °C -75 °C). pK_a value of ammonium ions in the GPs at both CO_2 capture temperature (30 °C) and release temperature (75 °C) is found to be the primary factor responsible for the stoichiometry of reversible CO_2 capture by the amines in the GP films. The pK_a values can be tuned by the properties of GPs such as volume phase transition temperature (VPTT), the size, the swelling ratio and the imprinted microenvironment surrounding the amines. The optimal GP obtained according to the design rationale showed high capture capacity (68 mL CO_2/g GPs, 3.0 mmol CO_2/g GPs) that is comparable to most of solid sorbents though the regeneration temperature is as low as 75 °C. We anticipate that GPs films that can reversibly capture other acidic and basic gas can be achieved by the same strategy inspired by the Bohr effect of hemoglobin.

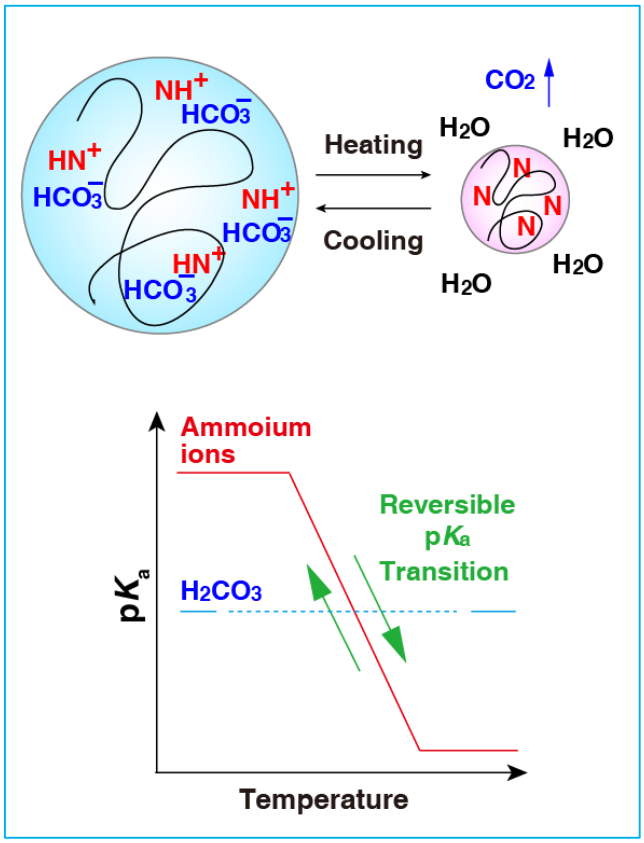

In chapter 4, the Me, i-Pr and t-Bu modified PVAm with different modification ratio were used as CO_2 capture absorbents. The CO_2 capture stoichiometry of the copolymers can be improved by the "spacing effect" of the modification groups, the larger modification groups usually show

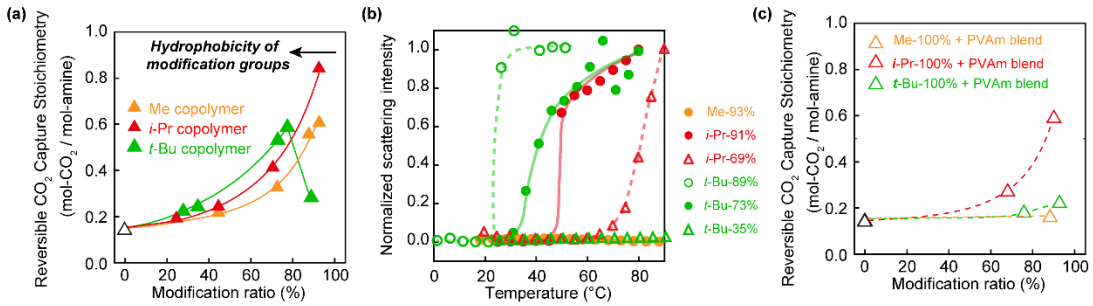

stronger "spacing effect". Phase separation behaviour of the copolymers can also facilitate the CO_2 capture stoichiometry if the LCST is above and close to 30 °C. However excessively modified copolymer with LCST below 30 °C show significantly low CO_2 capture stoichiometry. LCST of the copolymers can be decreased by increasing the hydrophobic modification ratio or by using more hydrophobic modification groups. Besides, the copolymers showed larger CO_2 capture stoichiometry than the polymer blends at the same modification ratio, indicating the intra-polymer interaction between amine groups and hydrophobic modification groups are essential for the CO_2 capture.

In chapter 5, the effect of inner gel structure on the CO_2 capture and release kinetics of the films were revealed by comparing gel films with different inner structure: the film consisting of larger GPs (GP-big film) and smaller GPs (GP-small film), the gel film with uniform structure (Hompogeneous gel film), the gel film with GPs embedded

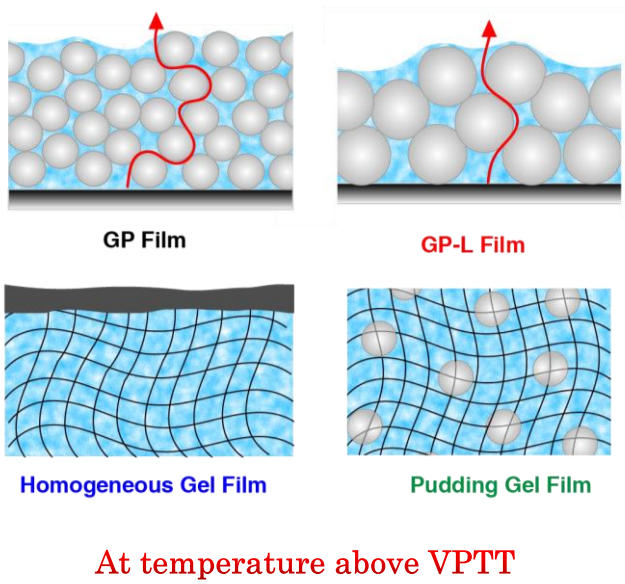

(pudding gel film), and the gel film with macropores (Macroporous gel film). It is found that the large inter-GP pores formed between the rigid collapsed GPs facilitated the molecule diffusion in the CO_2 release process at 75 °C (above VPTT 38 °C). The fast thermal responsibility of IPN gel film also improved the molecule diffusion in the film by preventing the formation of dense skin layer. The inner pores of the gel film also improve the capture kinetics in the CO_2 capture process at 30 °C (below the VPTT 38 °C), however the pores of slightly crosslinked gels will significantly diminish at their swollen state. This study provided a guidance to design a gel film with fast CO_2 capture and release kinetics.

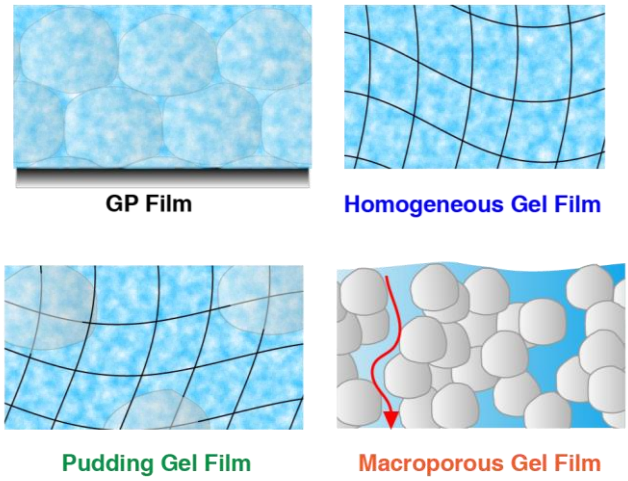

At temperature below VPTT

Acknowledgement

First of all, I would like to express my deepest appreciation to Prof. Hoshino Yu, who is a talented, kind and responsible instructor in my research. He shows us how exciting and rigorous a scientist can be, and how kind and patient a teacher can be. This thesis is accomplished with his significant guidance and support.

I would also like to thank Prof. Miura Yoshiko for giving me this change to study the advanced knowledge in her laboratory. She is a very smart and kind professor, who always considers from the standpoint of students, and has given me a lot of assistance both in research and in life.

I am grateful to Prof. Kishida Masahiro and Prof. Fukai Jun for reviewing this thesis, and for the great contribution in improving the quality of this thesis.

Thanks Prof Goto Masahiro for the support of microscope experiment.

Thanks Dr. Seto Hirokazu and Dr. Lee Haejoo for their kind guidance.

Thanks all the laboratory members, especially Nakamoto, Yamashita, Takara and Ogata for the kind teaching in the initial stage in my research, Watanabe, Nakamoto, Yamashita, Imamura, Ohshiro, Hamasaki for their collaboration in this research.

Additionally, thanks for the financial support from Chinese government during my 4 years' study in Japan.

Last, I would like to thank my families and my friends for their accompaniment and backing, that created a harmonious environment for me to develop the research smoothly.